INVESTIGATION OF HARMONICS EXTRACTION TECHNIQUES FOR ACTIVE POWER FILTER IN LOW VOLTAGE DISTRIBUTION NETWORK

M.Eng. PROJECT

BY

UWAGBOE JULIUS OMORODION
(19PGBD000063)

DEPARTMENT OF ELECTRICAL AND INFORMATION ENGINEERING,

LANDMARK UNIVERSITY, OMU ARAN.

AUGUST, 2021

INVESTIGATION OF HARMONICS EXTRACTION TECHNIQUES FOR ACTIVE POWER FILTER IN LOW VOLTAGE DISTRIBUTION NETWORK

BY

UWAGBOE JULIUS OMORODION

(19PGBD000063)

A DISSERTATION SUBMITTED TO THE DEPARTMENT OF ELECTRICAL AND INFORMATION ENGINEERING, COLLEGE OF ENGINEERING,
LANDMARK UNIVERSITY, OMU ARAN, NIGERIA.
IN PARTIAL FULFILMENT OF THE REQUIREMENT FOR THE AWARD OF THE DEGREE OF MASTER OF ENGINEERING (M.ENG.) IN ELECTRICAL POWER AND MACHINE.

AUGUST, 2021

DECLARATION

I, **JULIUS OMORODION UWAGBOE,** a master student in the Department of Electrical and Information Engineering, Landmark University, Omu-Aran, hereby declare that this dissertation entitled "Investigation of Harmonics Extraction Techniques for Active Power Filter in Low Voltage Distribution (LVD) Network", was written, implemented and submitted by me is based on my original work. Any material(s) obtained from other sources or work done by any other persons or institutions have been duly acknowledged.

Student's Full Name and Matriculation number

Signature and Date

CERTIFICATION

This is to certify that this dissertation has been read and approved as meeting the requirements of the Department of Electrical and Information Engineering, Landmark University, Omu-Aran, Nigeria, for the Award of master Degree.

_____	_____
Dr. Oghenewvogaga Oghorada (Supervisor)	Date
_____	_____
Dr. Bukola B. Adetokun (Co-Supervisor)	Date
_____	_____
Prof. M. Oki (Head of Department)	Date
_____	_____
(External Examiner)	Date

DEDICATION

This work is dedicated to God Almighty, the most gracious, the most merciful, the beginning and the end for His love, strength, wisdom and grace He granted me throughout the course of this project. To Him be all the Glory and Praise forevermore. Also to my wife and children for their support.

ACKNOWLEDGEMENT

I acknowledge God's extravagant grace over my life throughout the course of this work, to Him alone be glory, honour and adoration.

My appreciation goes to my supervisor Dr. Oghenewvogaga Oghorada and co supervisor Dr. Bukola B. Adetokun for their mentorship, guidance, and invaluable contribution toward the successful completion of this work. I also want to appreciate all the lecturers and the entire staff of the Department of Electrical and Information Engineering, Landmark University, Omu-Aran, Nigeria.

Finally, my appreciation goes to my Wife, Mrs. Uwagboe Joy. A. and my children Uwa, Isoken, and Oghomwen for being a pillar of support and a channel of God's blessings.

ABSTRACT

The continuous use of electricity as a means of powering industrial machines for the production of goods, as well as the use of semi-conductor dependent devices in the distribution network, such as diode controlled power units, has led to a high demand for electrical power around the world. Semiconductor devices cause network distortions. Harmonics distortion on low voltage distribution line deteriorates the power quality, in terms of waveform, network reliability, system efficiency and network stability.

The goal of this study is to improve the extraction unit's transient and steady-state response of the APF to reduce harmonics distortion on LVD line to the bare minimum. This research used a power system network analyzer called 'Circutor' on Landmark University (LMU) LVD network, to obtain the harmonics current present in the university environment. Current harmonics dataset obtained revealed the presence of harmonics. The LVD network was model in MATLAB-Simulink environment using a three-phase thyristor rectifier load. This investigation considered the transient and steady-state response of first and second LPF and HPF and BSF implemented in the extraction unit of Active Power Filter (APF).

The result obtained show that the harmonics present at PCC before compensation was significantly removed after compensation. The steady-state performance also revealed a low level of steady-state error, which is due to the delay in the extraction unit and the current controller unit. The transient response of each of the filter circuit implemented in the extraction unit of the APF showed that the settling time of BSF is the smallest at 0.00014seconds. The difference in THD before and after implementation showed that BSF is effective in stopping specific harmonics content across the firing angles.

A key contribution of the investigation of the extraction unit of the APF is the superiority of BSF to other filter in the extraction unit since the BSF has the least settling time and rise time, which means that the steady-state is attained faster. The investigation was able to achieve less than 5% recommended by IEEE-519 standard for current harmonics THD up to the 37^{th} order harmonics.

TABLE OF CONTENTS

DECLARATION ii

CERTIFICATION iii

DEDICATION iv

ACKNOWLEDGEMENT v

ABSTRACT vi

LIST OF ABBREVIATIONS xv

SYMBOLS xvi

CHAPTER ONE 1

INTRODUCTION 1

1.1 Background of the Study 1

1.2 Statement of the Problem 2

1.3 Aim of the Study 3

1.4 Objectives of the Study 3

1.5 Research Questions 3

1.6 Scope of the Study 3

1.7 Significance of the Study 3

1.8 Organization of the Work 4

CHAPTER TWO 5

LITERATURE REVIEW 5

2.1 Conceptual Issues 5

2.1.1 Power Quality Issues (PQI) 5

2.1.2 Harmonics in Power System 7

2.1.3 Total Harmonic Distortion 8

2.1.4 Effect of Harmonics on Distribution Network 8

2.1.5 Current Harmonics Standards 9

2.1.6 Harmonic Producing Loads 9

2.1.7 Impacts of Harmonics on Appliances 10
2.2 Harmonic Mitigation Techniques 11
2.2.1 Passive Harmonic Filters 11
2.2.2 Active Harmonic Filters 11
2.2.3 Differences between Active and Passive Filters 12
2.3 Active Power Filters 12
2.3.1 Series Active Power Filter 15
2.3.2 Shunt Active Power Filter 17
2.3.3 Hybrid Active Power Filter 18
2.4 Theoretical Review 19
2.4.1 Static VAR Compensator Transformer 21
2.4.2 Static Synchronous Compensator (STATCOM) 21
2.4.3 Thyristor Controlled Series Capacitor (TCSC) 22
2.4.5 Static Synchronous Series Compensator (SSSC) 22
2.4.6 Unified Power Flow Controller (UPFC) 23
2.5 Review of Methodological Approaches 23
2.6 Research Gap Identified in Literature 25
CHAPTER THREE 27
METHODOLOGY 27
3.1 Research Layout 27
3.2 Data Collection 28
3.3 Research Methodology 28
3.3.1 Current Harmonics Extraction Unit 30
3.3.1.1 Low Pass Filter Implementation 31
3.3.1.2 High Pass Filter Implementation 32
3.3.1.3 Band Stop Filter Implementation 34
3.3.2 Current Control Unit 35

3.3.3 Pulse Width Modulated H-Bridge Converter....36
3.4 Research Design Tools....37
3.5 Software Configuration Setup....37
CHAPTER FOUR....39
RESULTS AND DISCUSSION....39
4.1 Current Harmonic Data....39
4.2 Simulation Setup....41
4.3 Low Pass Filter Implementation....43
4.3.1 First Order LPF Implementation....43
4.3.1.1 PCC Current without Compensation....44
4.3.1.2 PCC Current with Compensation....45
4.3.1.3 Transient Response of First order LPF....47
4.3.1.4 Steady-State Performance....47
4.3.2 Second Order LPF Implementation....48
4.3.2.1 Second Order LPF PCC Current with Compensation....48
4.3.2.2 Transient Response of Second order LPF....50
4.3.2.3 Second Order LPF Steady State Error....50
4.4 High Pass Filter Implementation....51
4.4.1 First Order HPF Implementation....51
4.4.1.1 PCC Current with Compensation....51
4.4.1.2 Transient Response of First order HPF....53
4.4.1.3 First Order HPF Steady State performance....53
4.4.2 Second Order HPF Implementation....54
4.4.2.1 PCC current with compensation....55
4.4.2.2 Transient Response of Second Order HPF....55
4.4.2.3 Second HPF Steady State performance....56
4.5 BSF Implementation....56

4.5.1 PCC Current with Compensation 57
4.5.2 Transient Response of BSF 59
4.5.3 BSF Steady State Performance 59
4.6 Comparative Analysis 60
4.6.1 Transient performance 60
4.6.2 Steady State performance 61
4.6.3 Comparison of THD between Extraction Unit and PCC Current 63
4.6.4 Comparison of THD After compensation 63
CHAPTER FIVE 66
CONCLUSION AND RECOMMENDATIONS 66
5.1 Conclusion 66
5.2 Recommendation for Further Work 66
5.3 Contribution to Existing Knowledge 67
REFERENCE 68
Appendix A2 SIMULINK block model 89
Appendix B1 Steady State performance of LPF, HPF and BSF at $\boldsymbol{\alpha = 0°}$ 89
Appendix B2 Steady – State Performance of LPF, HPF and BSF at $\alpha = 30^0$ 89
Appendix B3 Steady – State Performance of LPF, HPF and BSF at $\alpha = 60^0$ 89
Appendix B4 THD Error Analysis between Extraction Unit and PCC Current after Compensation 90

LIST OF TABLES

Table 2.1: IEEE 519-2014 Current Distortion Limits (<69kV).....9
Table 2.2: Comparison of Active Power Filter and Passive Filter 12
Table 2.3: classification of facts devices 21
Table 2.4: Summary of Gap Identified in Literature 26
Table 3.1: Simulink specification. 38
Table 4.1: APF system parameters 43
Table 4.2: PCC current before and after compensation for 1st order LPF 47
Table 4.3: steady-state response of LPF. 48
Table 4.4: PCC current before and after compensation for 2nd order LPF 49
Table 4.5: Second order LPF steady-state error.....51
Table 4.6: PCC current before and after compensation for first order HPF 52
Table 4.7: first order HPF steady-state error 54
Table 4.8: PCC current before and after compensation for 2nd order HPF. 55
Table 4.9: Second order HPF steady state error 56
Table 4.10: PCC current before and after compensation for 2nd order BSF. 59
Table 4.11: BSF steady-state Analysis 60
Table 4.12: Transient performance 60
Table 4.13: THD PCC current during Compensation.....64

LIST OF FIGURES

Figure 2.1: Block Diagram of Power Quality Issues 5
Figure 2.2: Generalized Block diagram of APF 14
Figure 2.3: Series Based VSI APF Configuration 16
Figure 2.4: (a) 1 -ϕ Equivalent circuit of SAPF (b) Fundamental equivalent circuit and (c) Equivalent harmonics circuit 16
Figure 2.5: Shunt based VSI Active Power Filter 17
Figure 2.6: Hybrid APF Configuration 18
Figure 2.7: Block Diagram of Active power filter unit 20
Figure 2.8: Static VAR Compensator 21
Figure 2.9: Static Synchronous Compensator (STATCOM). 22
Figure 2.10: Thyristor Controlled Series Capacitor 22
Figure 2.11: Static Synchronous Series Compensator 23
Figure 2.12: Unified Power Flow Controller 23
Figure 3.1: Research methodology block diagram 27
Figure 3.2: APF Control Configuration 29
Figure 3.3: Current harmonics extraction unit. 30
Figure3.4: LPF implementation block diagram 31
Figure 3.5: LPF Bode plot 31
Figure 3.6: Second order LPF Bode plot 32
Figure 3.7: HPF implementation block diagram 33
Figure 3.8: First order HPF Bode plot 33
Figure 3.9: Second Order HPF Bode plot 34
Figure 3.10: Band stop filter implementation block diagram 34
Figure 3.11: BSF 5^{th} harmonic Bode plot 35
Figure 3.12: (a) APF block diagram and (b) phasor diagram. 36
Figure 3.13: Three phase PWM configuration 37
Figure 4.1: Current THD in a typical day across three phases 39
Figure 4.2: current harmonics (a): in phase 1, (b) in phase2, (c) in phase 3 for 24hours 41
Figure 4.3: Power system simulation configuration 42
Figure 4.4: LPF implementation block diagram. 43
Figure 4.5: PCC current without compensation. 44

Figure 4.6: PCC current without compensation. (a) current waveform at $\alpha = 0°$, (b) current waveform spectrum $\alpha = 0°$, (c) current waveform at $\alpha = 30°$, (d) current waveform spectrum $\alpha = 30°$, (e) current waveform at $\alpha = 60°$ and (f) current waveform spectrum $\alpha = 60°$.....45
Figure 4.7: PCC current with compensation. (a) current waveform at $\alpha = 0°$, (b) current waveform spectrum $\alpha = 0°$, (c) current waveform at $\alpha = 30°$, (d) current waveform spectrum $\alpha = 30°$, (e) current waveform at $\alpha = 60°$ and (f) current waveform spectrum $\alpha = 60°$. 46
Figure 4.8: Transient Response of first order LPF 47
Figure 4.9: PCC current with compensation. (a) current waveform spectrum at $\alpha = 0°$, (b) current waveform at $\alpha = 0°$, (c) current waveform spectrum at $\alpha = 30°$, (d) current waveform at $\alpha = 30°$, (e) current waveform spectrum at $\alpha = 60°$ and (f) current waveform at $\alpha = 60°$. 49
Figure 4.10: Second order LPF Transient Response 50
Figure 4.11: HPF implementation block diagram.....51
Figure 4.12: first order HPF PCC current with compensation. (a) current waveform at $\alpha = 0°$, (b) current waveform spectrum $\alpha = 0°$, (c) current waveform at $\alpha = 30°$, (d) current waveform spectrum $\alpha = 30°$, (e) current waveform at $\alpha = 60°$ and (f) current waveform spectrum $\alpha = 60°$. 52
Figure 4.13: first order HPF transient response 53
Figure 4.14: Second order HPF PCC current with compensation. (a) current waveform at $\alpha = 0°$, (b) current waveform spectrum $\alpha = 0°$, (c) current waveform at $\alpha = 30°$, (d) current waveform spectrum $\alpha = 30°$, (e) current waveform at $\alpha = 60°$ and (f) current waveform spectrum $\alpha = 60°$. 55
Figure 4.15: Second order HPF transient response.....56
Figure 4.16: (a) BSF implementation block diagram, (b) cascaded BSP, (c) BSF Bode plot. 57
Figure 4.17: Second order BSF PCC current with compensation. (a) current waveform at $\alpha = 0°$, (b) current waveform spectrum $\alpha = 0°$, (c) current waveform at $\alpha = 30°$, (d) current waveform spectrum $\alpha = 30°$, (e) current waveform at $\alpha = 60°$ and (f) current waveform spectrum $\alpha = 60°$. 58
Figure 4.18: BSF Transient Response 59
Figure 4.19: Transient performance of LPF, HPF and BSP 61

Figure 4.20: Steady State performance of LPF, HPF and BSF (a) percentage THD (b) at $\alpha = 0°$, (c) at $\alpha = 30°$ and (d) at $\alpha = 60°$. 62
Figure 4.21: THD Analysis between extraction unit and PCC current after Compensation 63
Figure 4.22: Comparison of THD after Compensation 64
Figure 4:23: Cascaded Band Stop Filter 64
Figure 4.24: BSF response at $\alpha = 60°$ (a) FFT plot (b) waveform 65

LIST OF ABBREVIATIONS

AC	Alternating Current
APF	Active Power Filter
BSF	Band Stop Filter
DC	Direct Current
FACTs	Flexible AC Transmission System
HAPF	Hybrid Active Power Filter
HPF	High Pass Filter
IGBTs	Insulated Gate Bipolar Transistor
LMU	Landmark University
LPF	Low Pass Filter
LVD	Low Voltage Distribution
MMCC	Modular Multilevel Cascaded Converter
MOSFET	Metal Oxide Semiconductor Field Effect Transistor
PCC	Point of Common Coupling
PQI	Power Quality Issue
PQP	Power Quality Problem
SAPF	Shunt Active Power Filter
SCADA	Supervisory Control and Data Acquisition
SRF	Synchronous Reference Frame
SSSC	Static Synchronous Series Compensator
STACOM	Static Compensator
SVC	Static VAR Compensator
TCSC	Thyristor Controlled Series Capacitor
TDD	Total Demand Distortion
THD	Total Harmonics Distortion
UPFC	Unified Power Flow Controller
VSC	Voltage Source Converter

SYMBOLS

Ma	Amplitude modulation index
i_c	Compensated current
V_c	Converter voltage
I_h	Current harmonic
ξ	Damping ratio
C_{DC}	DC capacitor voltage
i_d	Direct axis current component
i_{h_d}	Direct axis current harmonics component
M_f	Frequency modulation index
i_L	Load current
i_q	Quadrature axis current component
i_{h_q}	Quadrature axis current harmonics component
V_{ref}	Reference voltage
Ts	Sampling interval
Is	Source current
Vs	Source voltage
fs	Switching frequency
i_{abc}	Three phase current
V_f	Voltage harmonics

CHAPTER ONE

INTRODUCTION

1.1 Background of the Study

The increase in urban cities across the world due to high human population and technological advancement has led to the high demand for electrical power; continuous use of electricity as a means of powering industrial machines for production of goods and dependence of domestic consumers in their respective homes (Huang, 2018). The conventional power generator sources are those that emit greenhouse gases which are harmful to human health and environment hence, fossil fuel-dependent technology is being replaced by a distributed generation which is mainly renewable and power electronics dependent (Chishti et al., 2021; Kumar et al., 2020; Suslov & Stepanov, 2015). The resultant effect of having increased semi-conductors dependent devices in the power distribution network, such as diode controlled power unit etc. are undesirable and it causes power quality problems (PQP) (Al-Ogaili et al., 2020; Kalair et al., 2017; Khan et al., 2018; Klaić et al., 2020; Mishra et al., 2018; Rusinaru & Merfu, 2014). The most common PQP associated with non-linear load is that of current harmonics on the low voltage distribution line (Taiwo et al., 2017). In addition to other PQP on the network, is the imbalance created by grid-connected three-phase inverter from distributed generators (Al-Ogaili et al., 2020).

Harmonics distortion on low voltage distribution line deteriorate the power quality available for use by consumers, in terms of the waveform, network reliability, system efficiency, and network stability (Pandurangan et al., 2021; Wang & Kang, 2019). Others are current and voltage imbalance which are significant during a fault condition in low voltage distribution line (Taiwo et al., 2017). These power quality problem causes the sensitive device to malfunction and low power factor (Akagi, 1999).

Distortion on the High Voltage line has been suppressed with the use of flexible AC Transmission System (FACTs) devices, which use power electronics circuitry (Huang, 2018). These devices do not only control grid voltage, as well as the system overall power, but they also effectively suppress the harmonic content on the grid. They include phase-shifting transformer, capacitor bank and mechanically switched inductors(Huang, 2018; Moeini et al., 2020). FACTs devices are limited in use because of their switching problems with age, high cost of transformer and capacitor bank only

provide fixed compensation and cannot be used in a dynamic environment (Mahanty, 2014; Varshney et al., 2021).

Harmonics constitute a major challenge in low voltage distribution network, due to the effect it has on voltage and current sensitive equipment (Jacob et al., 2014; Patel & Makwana, 2020; Suslov & Stepanov, 2015). Passive filters are primarily used for harmonic mitigation in the distribution network (Khan et al., 2018; Kumar et al., 2020; Zhilin & Prasol, 2020). Passive filtering techniques offer limited function since it is frequency-specific and suffer from an aging deficiency in the turning circuit, it also has low bandwidth hence cannot accommodate a large range of frequencies (Ebadian et al., 2015). The limitation associated with the passive filters used in harmonics mitigation gave rise to further research (Al-Ogaili et al., 2020). Researchers then applied an Active power filter (APF) circuit, that is able to detect harmonics current on the network and inject a signal capable of canceling the harmonics on the line (Ni et al., 2020). Although APF successfully addressed the limitations of passive filter, it is however slow in response (Mishra et al., 2018). The extraction unit of the APF is of special importance because the accuracy of the current and voltage harmonics extraction unit affects the entire APF harmonics mitigation configuration (Vardar & Akpinar, 2011). The APF has challenges in the extraction unit, making the APF configuration inadequate in total harmonics mitigation (Jacob et al., 2014; Moeini et al., 2018).

In this study, various filter circuit will be implemented in the extraction unit of APF to investigate their transient and steady-state behavior.

1.2 Statement of the Problem

Fourier series analysis extraction method is based on frequency domain in which signals of importance are selected to reconstruct signal in the time domain. Signals in the frequency domain are converted to signal in the time domain given as a formula.

As a result of the high computational complexity involved in the use of the Fourier series method of harmonic extraction and the long processing period required to obtain a result, coupled with the complex mathematical algorithm and selective specification extraction of specific harmonic components. There is a need to solve the problem of slow extraction rate and individual harmonic extraction in order to reduce cost and complexity. Also most common extraction techniques for detection of current harmonics in the extraction units of the active power filter involves the use of a first-

order low-pass filter, first-order high - pass filter and Notch filters. These filters are unable to extract all the harmonics content at the extraction unit.

1.3 Aim of the Study

The aim of this research is to improve the transient and steady state response of the extraction unit of the active power filter.

1.4 Objectives of the Study

The objectives of this research are to:

i. Investigate current harmonic contents present in a typical LVD network;
ii. Use (i) to model a LVD network in MATLAB SIMULINK environment;
iii. Investigate the transient response of first and second order low pass filter (LPF), high pass filter (HPF) and band stop filter (BSF);
iv. Investigate the steady state response of first and second order LPF, HPF and BSF;
v. Evaluate and analyze the influence of the various extraction techniques on the performance of the APF for harmonic mitigation.

1.5 Research Questions

The purpose of this research is to provide answers to the following questions as it relates to the investigation of harmonics extractions techniques for APF, using Landmark University (LMU) as a case study.

i. What are the various types of current harmonics present on the LMU LVD line?
ii. What are the causes of the various current harmonics presents on the distribution system?
iii. What is the most effective method of current harmonics extraction unit for APF in LVD network?
iv. What is the transient and steady state response of the current harmonic extraction unit for APF?

1.6 Scope of the Study

This research is limited to the investigation of LPF, HPF and BSF in the extractions unit of the active power filter for harmonic mitigation on LVD network.

1.7 Significance of the Study

This study sought to improve the extraction unit of APF current harmonics mitigation technique. The investigation will also be useful to other researchers that are interested

in shunt active power filter extraction algorithm, the transient and steady-state behavior of Low Pass Filter (LPF), High Pass Filter and Notch Filter which is a special type of Band Stop Filter.

1.8 Organization of the Work

The second chapter contains the review of related literature while chapter three discusses the methodology adopted in the investigation, the research layout and the design of filter circuit implemented in the extraction unit of APF. Chapter four contains current harmonic data obtained through real-time measurement from Landmark University LVD with a power network analyzer it also covers the system implementation and analysis of LPF, HPF, and Band Stop Filter in the extraction unit of APF and the comparative analysis of their transient and steady-state experimental outcome in MATLAB/SIMULINK. Chapter five discusses the findings by giving a summary of the investigation, and a conclusion. Finally, it provides future study recommendations.

CHAPTER TWO

LITERATURE REVIEW

This chapter discusses the concept of power quality issues (PQI) in power system, the concept of harmonics, causes of harmonics, and effect of harmonics on the consumer connected on the LVD network and the utility company. This chapter also discusses relevant literature in the study of current harmonics extraction techniques, active power filtering methods of mitigating current harmonics due to load current and explain various APF components employed in harmonics mitigation.

2.1 Conceptual Issues

Harmonic distortions occur when the waveform of voltage or current assumes a non-sinusoidal shape with different phase and magnitude produced by frequencies that are multiples of fundamental frequency (Srinivas et al., 2020). These distortions constitute what is referred to as Power Quality Issue (PQI).

2.1.1 Power Quality Issues (PQI)

Mikkili & Panda (2018) reported that PQI is a problem resulting from voltage, a current deviation that results in equipment breakdown or failure. Mamdouh et al., (2014) defined PQI as deviation from standard current, voltage and frequency values, waveform. PQI results in equipment failures both to domestic consumers and the industry (Somasundaram, 2016). Figure 2.1 shows common PQI in power system.

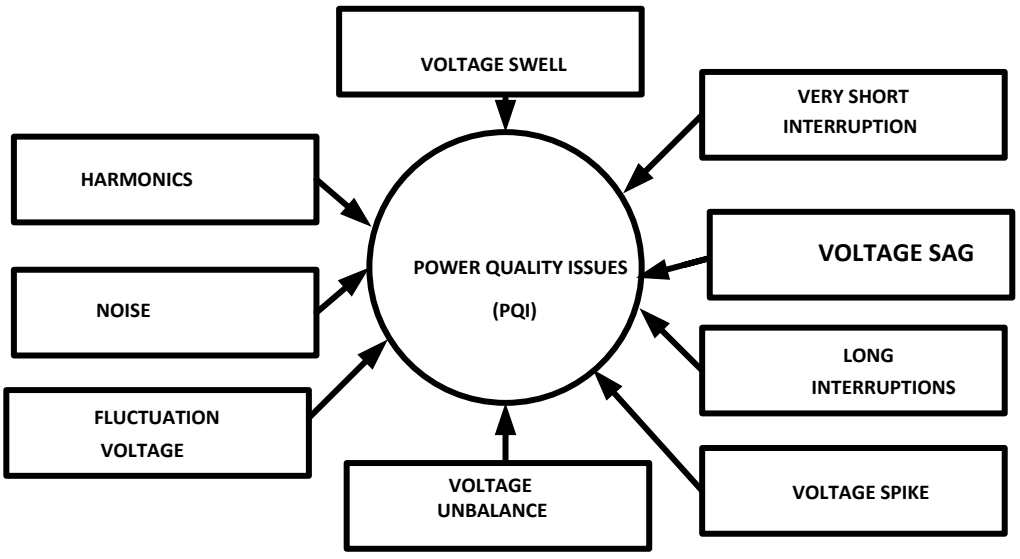

Figure2.1: Block Diagram of Power Quality Issues

Voltage Swell occur in LVD network when RMS voltage increases above the nominal tolerance for a period of 0.5 cycles to 1minute. Voltage swell is caused by poorly regulated switching from utility supply (Singh & Jain, 2020). It destroys sensitive equipment if the voltage exceeds the nominal tolerance. Harmonic Distortion occurs when a waveform of voltage or current assumes non-sinusoidal shape with different phases and magnitude produced by frequencies that are multiples of fundamental frequency (Kumarpandey, 2017). They are caused by an electric motor working above its magnetic saturation (knee magnetization) and non-linear load. Harmonic distortion causes overheating in cables, equipment, overload of neutral in three-phase system, electromagnetic interference in a communication network, unwanted tripping in the thermal protection system, etc. (Mikkili & Panda, 2018). Voltage Fluctuation occurs when there is an oscillation of the nominal voltage value, in amplitude by frequency of 0 to 30Hz (Dubey et al., 2021). It is caused by frequent start/stop of the electric machines and Arc furnaces. Voltage Spike occurs when there is a very fast variation in nominal voltage value for several microseconds to a few millisecond voltage spikes is caused by lighting, instantaneous switching, and discontinuation of heavy load. Long Interruption occurs in LVD network when there is a total interruption of electrical supply for a period greater than 1 to 2seconds (Mikkili & Panda, 2018). Very Short Interruptions occur when there is a total interruption of electrical supply for a period of few milliseconds to one second. It is usually due to the opening and recloses of protective devices when isolating a fault section of a network (Karimi-Ghartemani et al., 2004). Noise occurs when there is a superimposition of high-frequency signals on the waveform. It is caused by radiation from a welding machine, arc furnace, and improper grounding (Verma et al., 2016). Voltage unbalance occur when there is a variation in nominal voltage of three-phase power system such that the phase angle voltage magnitude is not equal, it is caused by large single-phase load, improper distribution of load in a three-phase system (Singh & Jain, 2020).

Joseph Fourier is recorded to have been the first scientist that developed the concept of harmonics in the 19th century. Fourier proposed that, all periodic non-sinusoidal signals can be illustrated by the indefinite series of sinusoids with discontinuous frequencies (Hu et al., 2020), as given in the equation 2.1.

$$i(t) = I_o + \sum_{h=1}^{a} I_h \cos(hwt + \phi_h) \quad 2.1$$

Where I_o is the direct current component, I_h is the harmonics component and ωt is the frequency components. The initial term of the aggregate with the index h=1 represent the coordinate of the signal.

2.1.2 Harmonics in Power System

In any electrical power network, harmonics is often a voltage or current generated by the operation of nonlinear loads (Li et al., 2020; Zare et al., 2017). Nonlinear load include rectifiers, discharge lights, or saturated magnetic equipment at a multiple of the rated fundamental frequency of the network (Jacob et al., 2014). Harmonic frequencies in transmission and distribution network are a common causes of power quality issues (Ogheneovo, 2016). Harmonics in distribution networks result in increased heating in the machinery and conductors, malfunctioning of variable speed drives, and torque pulsations in motors (Sanjan et al., 2020). Nonlinear loads produce harmonics in distribution networks, other examples of nonlinear loads include semiconductor equipment such as transistors, Insulated Gate Bipolar Transistor (IGBTs), Metal-oxide-semiconductor field effect transistors (MOSFETs), diodes, etc (Huang, 2018; Kanjiya et al., 2015; Mamdouh et al., 2014). Popular office electrical appliances, such as computers and printers, fluorescent lamp, phone chargers and even adjustable speed drives, are also regarded as examples of nonlinear loads(Li & Klontz, 2017; Yousfi et al., 2020).

Nonlinear loads are the major causes of current harmonics (Suslov & Stepanov, 2015). When nonlinear load devices like a rectifier circuit are connected to LVD network, the rectifier circuit draws current that is not really inherently sinusoidal. Osman et al., (2019); Ebadian et al., (2015); Nivetha & Karunakaran (2016) in their work on "Development of active power filter using rectifier boost technique" reveal that, depending on the type of equipment and its ability to interact with other elements of the network, the current waveform becomes distorted and can also become very complex. Voltage harmonics component are often caused by current harmonics, because of input impedance, the voltage provided by the voltage source will be influenced by current harmonics. Whereas if sources voltage impedance remains small, only very small voltage harmonics can be induced by current harmonics. Relative to current harmonics, it is usually the case that voltage harmonics are always minimal. For this reason, the signal waveform of such voltage could indeed generally be

approximated by its voltage fundamental frequency (Rameshkumar & Indragandhi, 2020).

2.1.3 Total Harmonic Distortion

Total harmonic distortion (THD) is the ratio of the RMS of the harmonic content to the RMS value of the quantity expressed as a percentage of the fundamental quantity.

$$\%THD_V = \sqrt{\frac{\sum_{h=2}^{\infty} V_h^2}{V_1}} \quad 2.2$$

$$\%THD_I = \sqrt{\frac{\sum_{h=2}^{\infty} I_h^2}{I_1}} \quad 2.3$$

Harmonic content in the waveform are mostly visible when observed at the point of common coupling (PCC).

Total demand distortion [TDD] on the other hand, is based on the load current I_L over a given period.

$$TDD = \sqrt{\frac{\Sigma_{h=2}^{\infty} I_h^2}{I_L}} \quad 2.4$$

Where I_L is the peak demand loads current. The metering point of the consumer is usually the PCC and gives the maximum demand of the consumer. The high current demand when compared to the standard current reveals a significant distortion of the waveform (Moeini et al., 2018, 2020; Osman et al., 2019).

2.1.4 Effect of Harmonics on Distribution Network

The increase in the use of nonlinear load in low voltage distribution network (LVD) produces unwanted sinusoidal waveform contrary to the acceptable standard required for the effective operation of consumers' equipment (Chishti et al., 2021; Huang, 2018). Because nonlinear loads are connected to the distribution system, voltage fluctuations resulting from the disturbance is introduced which, due to loop impedances, become more, moving from the supply to the load (Pandurangan et al., 2021; Yaghoobi et al., 2018). For the most part, real distortions are triggered by loads. Also linear loads can produce nonlinear currents if the waveform of the supply voltage is distorted considerably (Mamdouh et al., 2014; Srinivas et al., 2020).

Harmonics cause sensitive electrical electronics devices to fail, it also result in overheating of transformers, distribution lines and causes breakers to trip (Ogheneovo, 2016; Rajput et al., 2021; Taiwo et al., 2017)

2.1.5 Current Harmonics Standards

The Institute of Electrical and Electronics Engineers. IEEE regulations IEEE-519 (2014) stipulated the level of current harmonics. Table 2.1 shows a section of the document, showing the maximum limit of harmonic current that the consumer connected on LVD line can inject into the distribution network.

Table 2.1: IEEE 519-2014 Current Distortion Limits (<69kV)

Maximum Harmonic Current Distortion (% of I_L)						
Individual Harmonic Order (Odd Harmonics)						
$I_{SC}a/I_Lb$	$3 \leq h \leq 11$	$11 \leq h \leq 17$	$17 \leq h \leq 23$	$23 \leq h \leq 35$	$35 \leq h \leq 50$	TDD[c]
< 20	4.0	2.0	1.5	0.6	0.3	5.0
20 < 50	7.0	3.5	2.5	1.0	0.5	8.0
50 < 100	10.0	4.5	4.0	1.5	0.7	12.0
100 < 1000	12.0	5.5	5.0	2.0	1.0	15.0
>1000	15.0	7.0	6.0	2.5	1.4	20.0

a: I_{SC}= maximum short-circuit current at PCC

b: I_L= maximum demand load current (fundamental frequency component) at the PCC under normal load operating conditions

TDD[c] = Total Demand Distortion (Huang, 2018).

2.1.6 Harmonic Producing Loads

To properly comprehend the process through which harmonic currents are induced in the power distribution network, there is a need to know the basic harmonic inducing loads. There are two loads classifications namely; the linear and nonlinear loads (Sanjan et al., 2020).

Previous studies showed that transformers and rotating machines which are examples of linear load, were the main sources of the alterations in waveform because they adopt the use of magnetic materials that are operated often in the nonlinear region for economic considerations (Kanjiya et al., 2015; Kumar et al., 2020; Li & Klontz, 2017; da Silva et al., 2020).

With the advancement in research, factors contributing to harmonic distortions have been expanded to include;

i. Heating materials/ Furnaces

ii. Wind and solar-powered DC/AC converters. These applications prompt harmonic distortion as a result of their activities which basically involve energy conversion and control.

iii. Non-linear loads such as large computer systems, Supervisory Control and Data Acquisition (SCADA) systems, Universal Power Supply systems (UPS), switch-mode power supplies (SMPs in TV sets), battery chargers, cyclo converters, twelve-pulse, and six-pulse to mention just but a few.

iv. Controlling activities of electronic applications like inverters, choppers, etc. are responsible for causing variations in power systems resulting in harmonic distortion.

v. The direct connection of electric metal-melting arc furnaces with power absorption level of tens of megawatts to power system networks.

vi. Electrical lightning ballasts.

vii. Solid-state rectifiers.

viii. Arc welders. (Somasundaram, 2016).

2.1.7 Impacts of Harmonics on Appliances

The adverse effect of harmonics distortions on a power system network are continually on the increase as new challenges posed by harmonic distortion continue to emerge. Some of the practical problems that are encountered by power distribution networks include, but not limited to the once listed below according to (Amamra et al., 2020; Deokar & Waghmare, 2011; Klaić et al., 2020; Zhilin & Prasol, 2020), they are:

a. Increase of the current within power system.

b. Malfunctions of circuit breakers and other protective devices.

c. Reactive power and Resonance problem.

d. Overheating of apparatus, such as transformers and generators.

e. Inaccuracy of measuring equipment.

f. The malfunction of a control electronics and microprocessors.

g. Long power factor requiring transformer kVA upsizing or neutral upsizing.

2.2 Harmonic Mitigation Techniques

Harmonic filters are devices that extract or attenuate harmonics signal to considerable levels. They are used to deplete harmonic distortion to the levels contained in IEEE 519. The IEEE standard 519, is the approved practice and requirements acceptable globally for harmonic regulation in Electrical Power Systems. Dubey et al., (2021); Kumar et al., (2020); Salam et al., (2006); Sanjan et al., (2020) reported that harmonic filters help to reduce alterations to fundamental signal by filtering out harmonic components in the LVD line. Harmonic filters are categorized into two namely;

i. Passive and

ii. Active filters. (Annapoorani & Samikannu, 2017).

2.2.1 Passive Harmonic Filters

Passive filters consist of passive components like capacitors, resistors, and inductors which have no amplifying elements (Zhilin & Prasol, 2020). Capacitor, inductors, and resistor are arranged in such a way that the resultant circuit is able to remove the harmonics contents (Anandh et al., 2017; Kumar et al., 2020). The conventional method employed to suppress harmonics on the power network is a passive filter, which consists of capacitance, inductance, and resistance elements (Anandh et al., 2017). According to Hoon et al., (2019) the passive filtering method is frequency-specific and becomes ineffective in removing harmonics contents in an environment with changing frequencies, which imposes limitations on its use. Gurguiatu et al., (2011); Osman et al., (2019); Al-Ogaili et al., (2020) reported that the advancement in the field of power electronics led to further interest in APF design as a way of mitigating harmonics distortion on distribution lines.

2.2.2 Active Harmonic Filters

Active power filter was developed in the 70s and has been a unique solution for PQI (Mamdouh et al., 2014; Osman et al., 2019; Sanjan et al., 2020). Although active filters combine other passive elements like resistors and capacitors, it however, does not use the inductor in their design (Izadian, 2019), active filters normally adopt operational filters attributes. Active filters are commonly classified into the following hinged on the method of configuration or connections to the power grid;

i. Series Active Power Filters (series APF)

ii. Shunt Active Power Filters (SAPF)

iii. Hybrid Active Power Filters (HAPF)

Though bearing the unique merit zero resonate with the system and can execute autonomously with regards to the system intransigence attributes, active filters are novel types of applications for removing harmonics currents (Al-bakry et al., 2018; Mohammad et al., 2015; Suleiman et al., 2017). These filters depend on power electronic components and are deemed to be exorbitant than passive filters. They are used in complex situations where passive filters do not deploy triumphantly due to resonance problems and interfere with other components stationed in the power system (Mishra et al., 2018; Zhang et al., 2019).

2.2.3 Differences between Active and Passive Filters

Electronic filters are circuits that execute the job of processing electrical signals with the basic goal of removing redundant frequency components from the signal, to facilitate the movement of wanted frequency element (Khan et al., 2018; Yousfi et al., 2020). Table 2.2 contain the differences between active power filter and passive filter configuration.

Table 2.2: Comparison of Active Filter and Passive Filter

Active Filter	Passive Filter
1. Can suppress current harmonics and reactive current	Can suppress only harmonic current
2.They do not cause harmful resonance with L V D network	It causes harmful resonance with L V D network
3. It results in high frequency noise causing electromagnetic interference [E M I] in L V D network.	It do not result in electromagnetic interference in L V D network.
4. Does not require inductor	It requires inductor
5. They are more expensive	Relatively cheaper
6. Requires extra power to supply unit	Depends only on signal input
7. Combine active element and passive element (OP-Dump, resistor, capacitor)	Combine passive elements (capacitor, inductor and resistor)

2.3 Active Power Filters

Kanjiya et al., (2015); Muhammad Kashif et al., (2020) in their research describe APF as power electronics devices designed for the purpose of improving the quality of electrical energy and the efficiency of use. They reported that APF operation is based

on its ability to produce a particular current value that will cancel out the harmonics currents components produced by the non-linear load connected on the LVD line.

Hoon et al., (2019) reported that APF has proved to be the most effective method for compensating harmonics distortion due to nonlinear loads. Shunt APF configuration is reported to have been the most frequently applied topology. They reported that Shunt APF is connected in parallel with the load. The fundamental use of Shunt APF configuration is the cancellation of current harmonics generated by the non-linear load connected on the LVD line; this load is known as harmonics current source (HCS) loads (Dubey et al., 2021; Hoon et al., 2017). Furthermore, Shunt APF is not efficient where non-linear load produces Voltage harmonics also known as harmonics Voltage Source (HVS) load (Kanjiya et al., 2015; Yousfi et al., 2020). For this purpose, Series Configuration is used, in which the APF is connected in series with the load (Annapoorani & Samikannu, 2017; Ebadian et al., 2015). In the event where APF configuration either in series or Shunt composition with the load current and is unable to effectively produce harmonic cancellation for both HCS and HVS, the combination of both Shunt and Series topologies with active and passive filter is used, this combination is called hybrid filter (Baliyan et al., 2021; He & Li, 2013).

A Typical APF System connection is shown in Figure 2.2

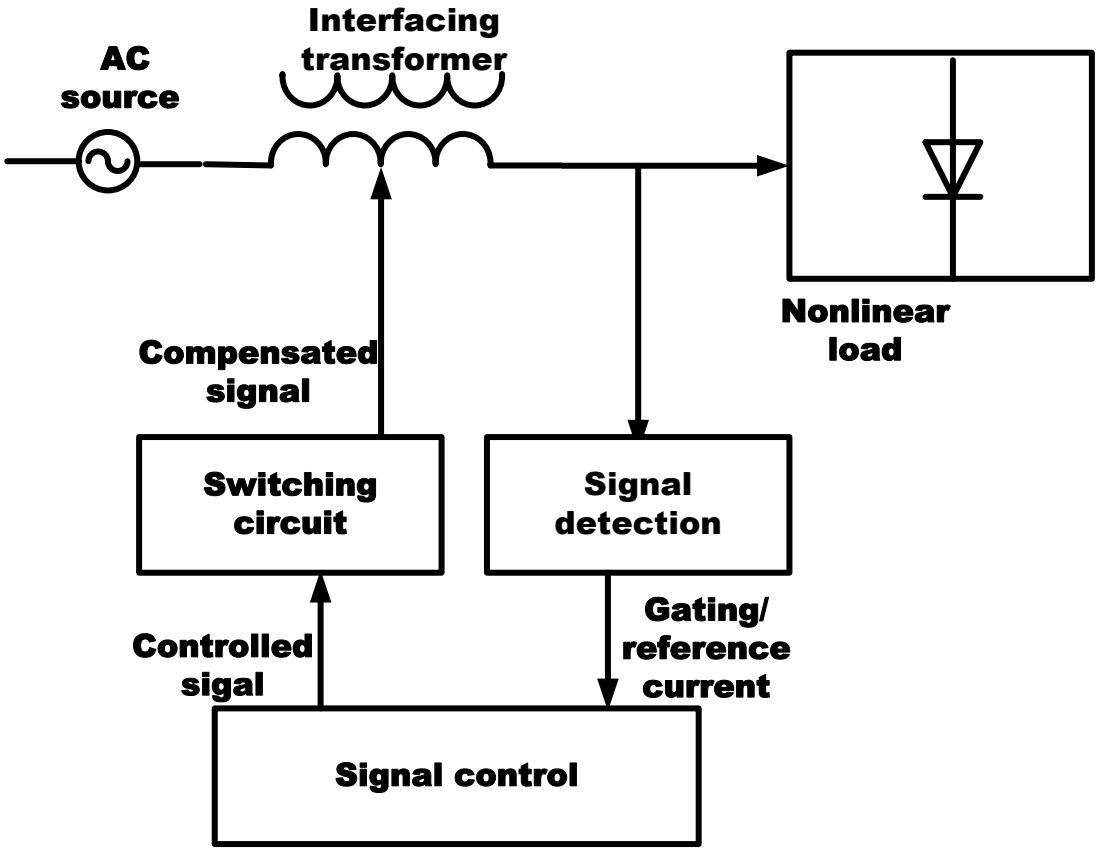

Figure 2.2: Generalized Block diagram of APF

The generalized block diagram of APF shows that the compensated reference signal from the estimator circuit control or drives the entire system controller. The signal eventually generates the control signal for the gating signal generator. The output signal from the gating signal generator controls the power network through a suitable interface (Liu et al., 2017; Sanjan et al., 2020). From the block diagram, the power circuit is either connected in series, parallel, or series/parallel arrangement depending on the interfacing transformer used. APF circuit is sometimes considered as a compensator for harmonics in power system LVD network (Dubey et al., 2021; Zainuri et al., 2018). APF mainly consists of three stages which are the signal conditions unit, derivation of compensating signal, and gating signal generator unit. While the signal conditioning detector senses the harmonics in the LVD line, as shown in Figure 2.2, the reference signal processed by the controller is the main component that determines the accuracy of the operation of APF. The reference signal estimator unit initiates the detection of vital current/voltage signals needed to collect accurate system information. AC and DC bus voltage of the APF is used to detect the variable current/voltage signal. Based on

the variable of interest, system variables feedbacks, reference signal estimators in terms of current/ voltage levels are determined either in time-domain or frequency domain.

According to Tiwari & Sharma, (2017) the derivation is the next stage of compensating signal from the resultant disturbance waveform, which is composed of harmonic contents and the fundamental components. Time domain and frequency domain techniques are two approaches used in signal detection (Al-Ogaili et al., 2020; Mamdouh et al., 2014), reported that frequency domain uses algorithms such as Fourier transform (FT), Fast Fourier Transform (FFT) etc. While time-domain uses a different algorithm, such as Synchronous–Reference frame theorem, Synchronous detection theorem, instantaneous reactive power theorem, etc.

The gating signal generation stage for harmonic cancellation is the last stage (Annapoorani & Samikannu, 2017; Lahare et al., 2020; Sanjan et al., 2020). Many control techniques have been developed and used by various researchers which includes space vector PWM, repetitive control, sliding mode control, fuzzy control, artificial neutral network method etc (Agrawal et al., 2017, 2018; Srinivas et al., 2020; Kryltcov et al., 2021; Kumar et al., 2020; Mai, 2020; Mamdouh et al., 2014; Musa et al., 2017; Yousfi et al., 2020). These algorithms have been used in many configurations of the active power filter. The gate signal generated in the general block diagram of APF is used for this purpose.

2.3.1 Series Active Power Filter

Series APF Configuration is shown in Figure 2.3. The main goal of the series APF is to locally rectify the grid. It is evaluated as a harmonic voltage source tasked with removing the voltage perturbations triggered by the grid (Khan et al., 2018). In their study, Ebadian et al., (2015); Ni et al., (2020) provided a basic diagrammatic description of a series active power filter as configured to the distribution line. Series APF is connected in series with the distribution line via a transformer (Annapoorani & Samikannu, 2017).

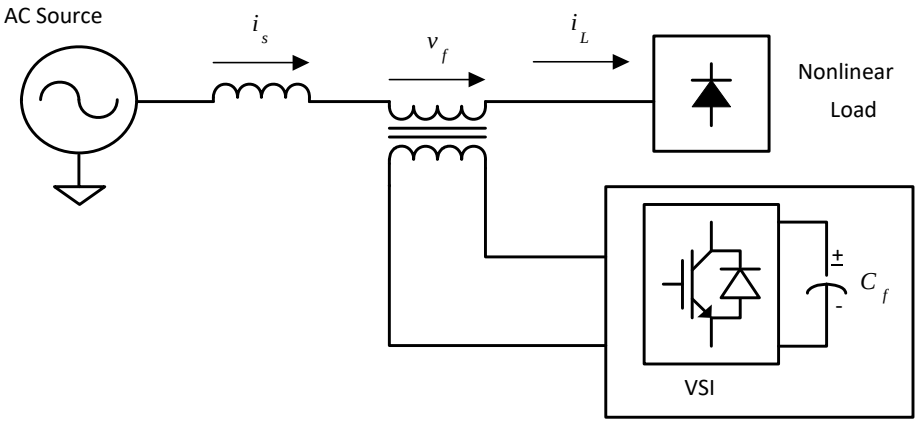

Figure 2.3: Series Based VSI APF Configuration

Often voltage source inverter is employed as the control source, thereby making the operation of Series APF is primary on the cancellation of harmonics disturbance between the AC supply Source and the nonlinear load (Annapoorani & Samikannu, 2017; Baliyan et al., 2021). This is obtained through the injection of voltage harmonic (V_f) from the interfacing transformer. V_f is then added or subtracted depending on the source voltage, so as to maintain the original sinusoidal Waveform of the supply Voltage across the nonlinear load (Annapoorani & Samikannu, 2017). Ebadian et al., (2015) showed that, Series APF functions as a harmonic isolator, by appearing as a resistor having an infinite impedance. Because harmonics is able to flow from the source to the nonlinear load and vice versa as illustrated in Figure 2.4 (a), (b), and (c).

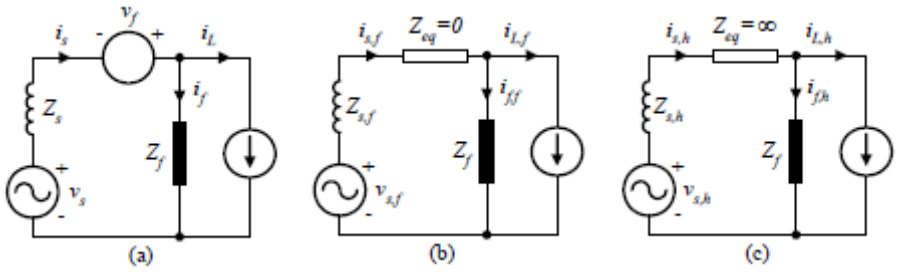

Figure 2.4: (a) 1 -ϕ Equivalent circuit of SAPF (b) Fundamental equivalent circuit and (c) Equivalent harmonics circuit.

Series APF is commonly used to protect sensitive electrical devices that require pulse sinusoidal voltage waveform for effective operation (Annapoorani & Samikannu, 2017), hence it is more suitable for improving the quality of voltage in LVD line. However, the main disadvantage of Series APF is, the need to provide high capacity load current, resulting in the increased current rating which leads to increase I^2R losses

especially on the secondary side of the interfacing transformer (Ebadian et al., 2015; Ni et al., 2020).

2.3.2 Shunt Active Power Filter

Shunt APF is often used in the detection and cancellation of current harmonics on the LVD lines. To ensure that nonlinear load receives pure sinusoidal waveform. It is also used for reactive power compensation (Shembekar & Deshmukh, 2015; Yousfi et al., 2020). Shunt AFP configuration is based on voltage source inverter (VSI) principle, Figure 2.5 shows a circuit of Shunt Active power filter. In their studies, Srinivas et al., (2020); Hoon et al., (2017); Kanjiya et al., (2015); Yousfi et al., (2020), asserted that the operational rule of shunt active power filters can be regarded as exemplary source current injecting harmonics and a reactive component of load current at the point of common coupling (PCC). Their findings described the Active shunt power filters as a device deployed to attenuate the distortions caused in the sinusoidal waveform by nonlinear loads. Figure 2.5 shows how a shunt active power filter is connected to the voltage source.

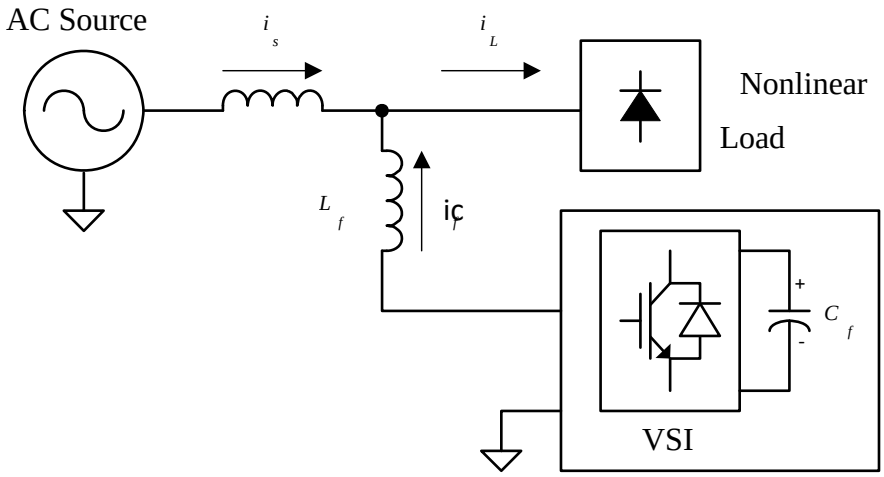

Figure2.5: Shunt based VSI Active Power Filter

The purpose of Shunt APF is to cancel the load currents harmonics on LVD network. Shunt APF consist of the main voltage source, a power electronics switch, a capacitor *(C_f)* and an inductor (L_F). The shunt APF based on VSI is the most commonly used for compensating current harmonics resulting from nonlinear loads (Büyük et al., 2019; Zhilin & Prasol, 2020). In operation, Shunt APF inject current that is of equal magnitude to the distorted current harmonics, hence, canceling the generated current harmonics on the distribution network (Hoon et al., 2019). The purpose of installing Shunt APF is to create an alternating source current from the algebraic evaluation of

VSI compensated current (i_c) and the measured load current ($i_{L)}$. This relationship is expressed as

$$i_s = i_L + i_c \quad 2.5$$

If the load current is written as the sum of the current harmonics i_{Lh} and the fundamental current component i_{Lc}

$$i_L = i_{Lc} + i_{Lh} \quad 2.6$$

then compensated injected current by the Shunt APF becomes :

$$i_c = -i_{Lh} \quad 2.7$$

the resultant source current is given as :

$$i_s = i_L - i_c = i_{Lc} \quad 2.8$$

Equation (2.8) is the resultant current content containing the fundamental component of the load current and hence supplying pure sinusoidal waveform devoid of harmonics content.

2.3.3 Hybrid Active Power Filter

Hybrid APF (HAPF) configuration is the combination of Shunt, and Series APF topology (Kumar et al., 2020). Majority of the limitation inherent in SAPF and Shunt APF necessitated the need for improvement. (Chishti et al., 2021; Hoon et al., 2019; Li & Klontz, 2017) reported that Shunt APF is not useful where the load generate voltage harmonics because Shunt APF acts as a current source used to compensate current harmonics emanating from nonlinear loads, on the other hand, Series APF has been used for cancellation of voltage harmonics (Agrawal et al., 2018; Kumar et al., 2020). To adequately eliminate both voltage and current harmonics present on the distribution network, hybrid HAPF topology is implemented as shown in Figure 2.6.

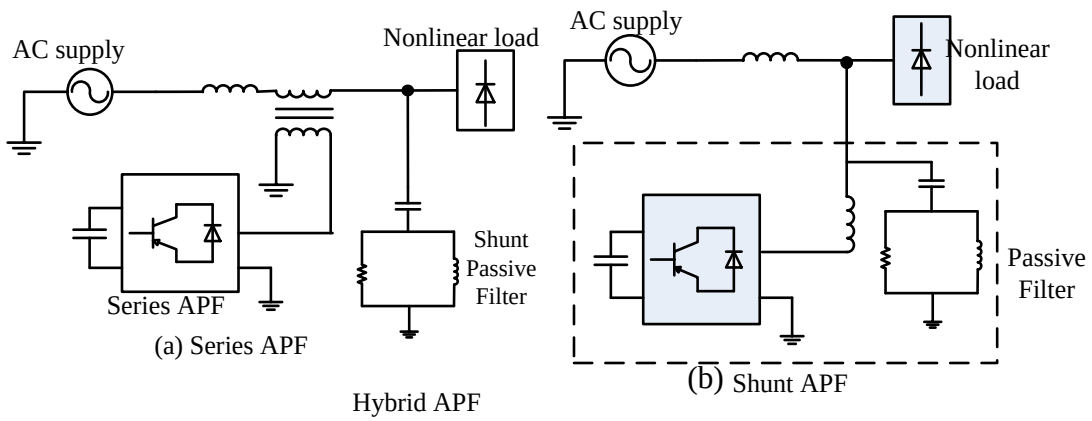

Figure 2.6: Hybrid APF Configuration

The configuration of HAPF is shown in Figure 2.6 helps to reduce the electromagnetic interference (EMI) and switching losses with improved performance and lower cost. According to Schwanz et al., (2016); Subramaniam et al., (2019); Zare et al., (2017), many types of research use HAPF as a means of achieving lower cost because of the limitations of signal drift associated with APF. Xie et al., (2019); Zhang et al., (2019) reported that fast switching power electronic device used in APF circuit results in noise-free harmonics appearing after the filtering process. However, the switching frequency requires a separate filtering circuit to overcome EMI (Kumar et al., 2020; Subramaniam et al., 2019). These inherent disadvantages associated with APF techniques are largely reduced with the use of HAPF, in addition to the advantages of both SAPF and Shunt APF and Passive Filter, HAPF is an improvement in terms of reduction in the level of EMI and noise associated with switches (Subramaniam et al., 2019; Zare et al., 2017). The most commonly applied HAPF in literature is shown in Figure 2.6. Both Shunt APF and SAPF are frequently used by researchers.

In Figure 2.6 (a), the topology shows a hybrid Series APF, which consists of a Series APF/ coupled to the LVD line by transformer and a Shunt passive filter having one or more single-turned (LC) high pass filter circuits. By injecting a controlled voltage harmonics signal, the hybrid series APF acts as a harmonic isolator between the supply and the nonlinear load connected to the distribution network. This configuration is controlled at fundamental frequency to offer zero impedance and high impedance at any unwanted harmonics frequencies. This restricts the load current harmonics to flow through the least resistive part which is the passive filter, thereby isolating the nonlinear load from the supply at all frequencies except at fundamental frequency (Mamdouh et al., 2014). Figure 2.6 (b) shows the system configuration of a hybrid shunt APF, it consists of shunt APF, a passive filter circuit, and a nonlinear load connected in parallel with the passive filter. It perform two functions mainly: the cancellation of lower order harmonics using shunt APF and the filtering of higher order frequencies harmonics by the passive high pass filter. This configuration is a modification of the existing shunt APF.(Kumar et al., 2020; Yousfi et al., 2020).

2.4 Theoretical Review

Harmonics mitigation in LVD network is resolved traditionally with the use of the passive filter, line reactor and DC chokes, phase shift transformers, and active power filter (Moeini et al., 2018; Salam et al., 2006; Sanjan et al., 2020; Yaghoobi et al.,

2018). Zhang et al., (2019) reports that the main limitation of the passive *LC* filter is that it provides only fixed compensation, hence cannot be used in an environment with changing harmonics content of interest. Additionally, the components required for the turning circuit are of large size and suffer from aging. The use of a thirty-degree phase shift transformer is limited because the circuit is complex, leading to a high cost of production (Nwobu et al., 2015). The line reactor is less effective in mitigating harmonics in general but finds applications in mitigating harmonics associated with variable speed drives (Li & Klontz, 2017; Patel & Makwana, 2020). To solve the problems associated with the harmonics mitigation techniques listed above, the Active Power Filter (APF) is used. Active filter employs a power electronics control circuit, which injects suitable anti-phase harmonics contents to cause harmonics cancellation (Xie et al., 2019; He et al., 2014; Merabet et al., 2013; Wang & Kang, 2019). The APF mitigation process is shown in Figure 2.7. It consists of the extraction unit that detects the harmonics content in the load current and current controller circuit which generates the reference voltage that is then used as input into the PWM modulators.

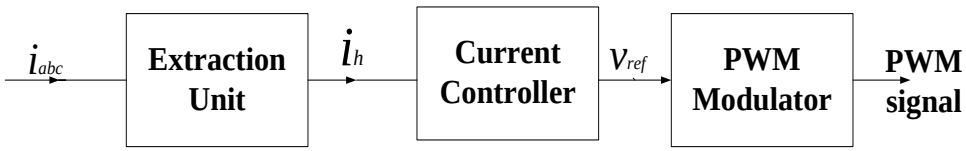

Figure 2.7: Block Diagram of Active power filter unit

Furthermore, Flexible AC transmission system (FACTS) devices are used for high voltage transmission line (Huang, 2018). FACTS application is installed at a critical point on the power network due to the need for flexibility, FACTS devices was improved from initial phase–shifting transformer, Capacitor, and mechanical switched inductors to three groups consisting of series or parallel connected devices with a power system to improve quality (Huang et al., 2018, 2021; Nwobu et al., 2015).

Table2.3: classification of facts devices (Source: Huang 2018)

Series –Connected	Parallel – Connected	Generation
Thyristor controlled Series Capacitor (TCSC)	Static VAR compensator (SVC)	1st generation
Static synchronous Series compensator (SSSC)	Static synchronous Compensator (STATCOM)	2nd generation
Unified power Flow controller (UPFC)		3rd generation

2.4.1 Static VAR Compensator Transformer

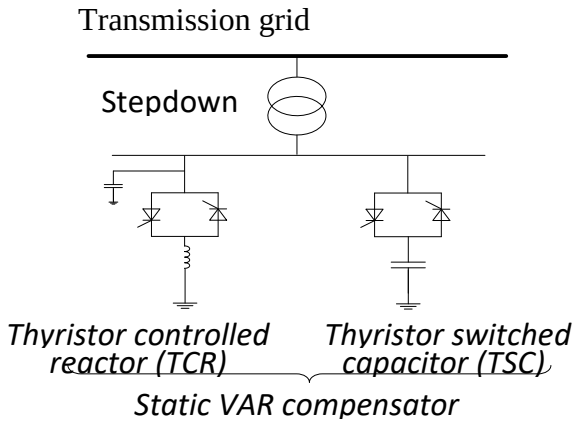

Figure 2.8: Static VAR Compensator
(Source Huang 2018).

Figure 2.8 showed that both SVC and TCSC of the first generation FACTS devices are simple in design and inexpensive but requires a tedious calculation of the switch-in and off capacitors and inductors at every instance of time, TCSC does not produce harmonics, however, the capacitor's charging current when switched on is difficult to control (Huang, 2018; Kryltcov et al., 2021; Yaghoobi et al., 2018).

2.4.2 Static Synchronous Compensator (STATCOM)

STATCOM technology became popular in the 1990s. It consists of a voltage source converter (VSC), DC energy storage device (capacitor) and a control Circuit. STATCOM is connected in parallel with the AC line usually through a step-down transformer (Kumar & Kumar, 2019; Kumar et al., 2020; Nwobu et al., 2015; Oghorada et al., 2021) as can be seen in Figure2.9.

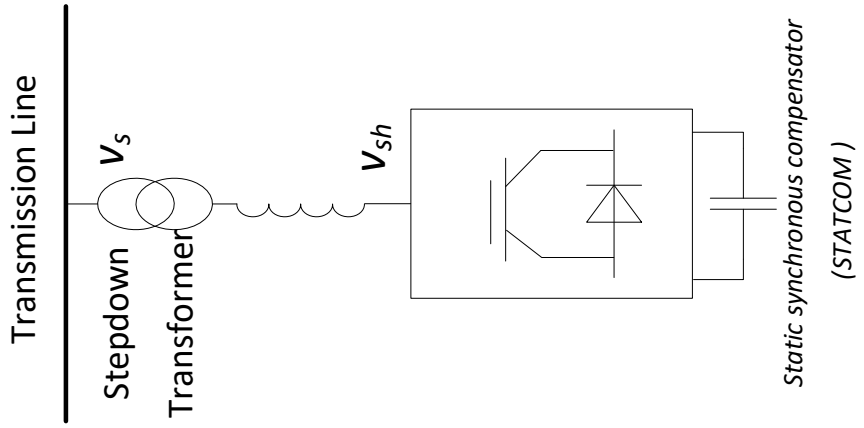

Figure 2.9: Static Synchronous Compensator (STATCOM) (Source: Huang, 2018).

2.4.3 Thyristor Controlled Series Capacitor (TCSC)

Rajput et al., (2021); Wu et al., (2020) reported that TCSC is installed between two points on high voltage transmission line as a means of controlling line reactance. It consist of reactors and Thyristor controlled capacitor as shown in Figure 2.10.

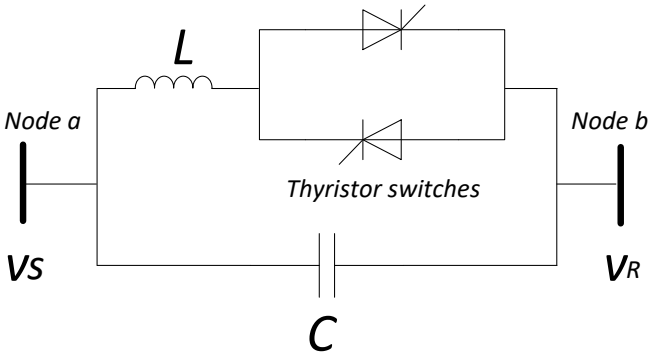

Figure 2.10: Thyristor Controlled Series Capacitor

2.4.5 Static Synchronous Series Compensator (SSSC)

It consists of a DC source and Voltage Source Converter connected in series with the transmission grid (Vadirajacharya et al., 2007), as shown in Figure 2.11.

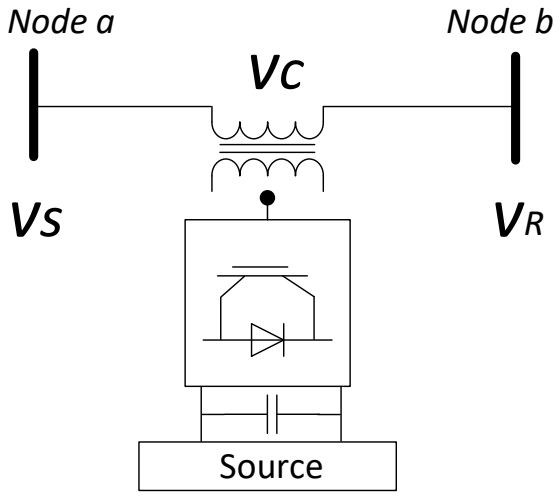

Figure 2.11: Static Synchronous Series Compensator

2.4.6 Unified Power Flow Controller (UPFC)

UPFC was describe as the combination of SSSC and STATCOM technique according to (Huang et al., 2021; Ni et al., 2020)**.** It is the most improved FACTS.as seen in Figure 2.12.

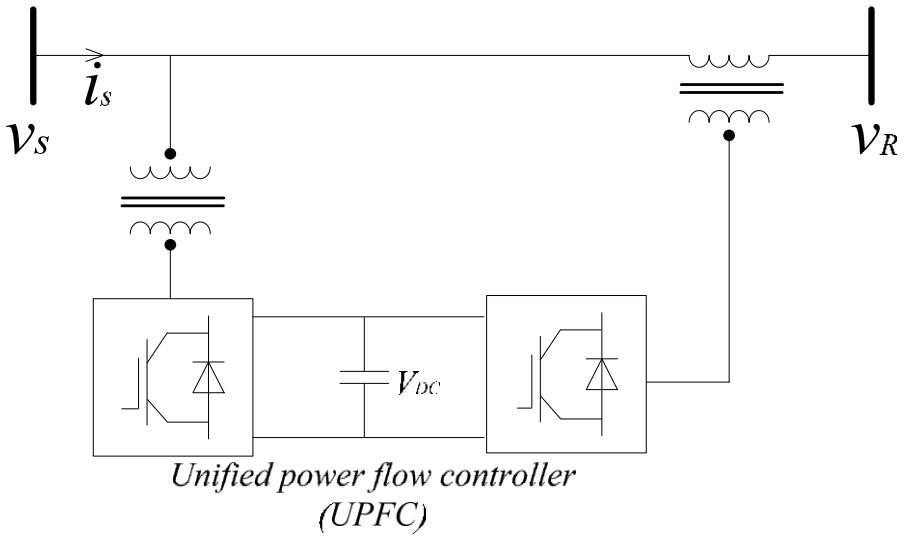

Figure 2.12: Unified Power Flow Controller

2.5 Review of Methodological Approaches

The APF scheme are implemented in either frequency or time domain Al-Ogaili et al., (2020); Kashif et al., (2020); Neelima et al., (2020). Frequency domain techniques include Fourier transform, Fast Fourier transform, Kalman filter; wavelet transform and Discrete Fourier transform according to Dubey et al., (2021); Liu et al., (2017); Sengar & Kumar, (2019). The time domain techniques are based on mathematical derivation which include instantaneous real power (p), and reactive power (q), denoted as *pq*-theory**,** cross vector theory, *p-q-r* theory, synchronous reference frame which could be

in form of filtered signal and moving average, synchronous detection and adaptive interference cancellation techniques.

Determining harmonics content in load current is a crucial part of APF controller, this involves the extraction of harmonics content of the load current with appropriate control mechanism with power electronics interface, so as to cancel the resultant harmonics in the load current (Mamdouh et al., 2014; Xie et al., 2019).

Researchers have used different method in current harmonics extraction scheme. Xie et al., (2019) in their work on Fast Selective Harmonic Extraction, employed multiple second-order comb filter in the extraction unit. They discovered that there was slow transient and steady-state response. Kashif et al., (2020) in their study based on current harmonics extraction improvement for APF proposed a novel extraction technique called structure turning that uses low pass filter ,tracks the load current, analyze frequency and the magnitude of the other remaining component of the waveform. They also discovered that it was cheaper to employ first order Low Pass Filter to obtain the reference current in the extraction unit, than second order low pass filter but at a higher cost, however, LPF has a limitation of slow response when the signal involvers multiple frequencies of interest, LPF causes phase shift to the fundamental during sudden load change and it has low bandwidth due to its low gain.

Huang, (2018); Huang et al., (2019), (2021); Nwobu et al., (2015); Oghorada et al., (2020); Oghorada et al., (2021); Oghorada & Zhang, (2019) although their work did not actually concentrate on the extraction unit of the APF, they were interested in tracking the reference current at the current controlled unit by using Modular Multilevel Cascaded Converter (MMCC). Neelima et al., (2020); Srinivas et al., (2020) in their research work paid less attention to the reference current generating unit, their focus was on the reference current tracking. They also employed the first order LPF in the extraction unit of APF in order to generate the reference current needed as input to the current control unit in their respective study.

The efficiency of the APF configuration depend on the accuracy of the current extraction unit, more researchers are focusing on how to improve the extraction unit. Hence, Dubey et al., (2021); Serrhini, (2019) employed triangular orthogonal theory and a second order LPF circuit in the extraction unit to obtain reference signal from the load current, this study of harmonics extraction only considered the transient response of the applied filter in the extraction unit. LPF based extraction unit technique with

Hybrid APF was used for current harmonics mitigation by (Kashif et al., 2020). In a dedicated network with peculiar need, Neelima et al., (2020) applied passive filter on the line to mitigate the current harmonics contents on the network. This also did not concentrate on the extraction unit.

2.6 Research Gap Identified in Literature

Sundaram & Venugopal, (2016) employed first order LPF in extraction unit of shunt APF for current harmonics extraction technique, they implemented three phase shunt APF by converting *abc*. Stationary reference frame to *d-q* rotating frame. However the study was able to detected few dominant harmonics and reduces the THD below 5% in line with IEEE-519 standard. To be able to mitigate more harmonics present on the network, this investigation will expand attempt to mitigate up to the 17^{th} harmonics by considering other filter design in the extraction unit.

Huang, (2018); Huang et al., (2019) deployed cascaded BSF in the APF extraction unit for current harmonics and reactive power compensation. The prevalent harmonics around the fundamental was successful extracted but was only able to eliminate few dominant content up to the 11th harmonics. Srinivas et al., (2020) employed a second order LPF in the Current Harmonic extraction unit for the Reduction of Source Side harmonics by using ANN Controller, this study did not consider transient and steady state response. Hu et al., (2020) considered in their research the use of notch filter in the extraction unit of for the load current Harmonics cancellation. The study emphasis was on harmonics associated with the pulse width modulation output signal and proposed a novel method of coupling the PWM signal to LVD network for APF in unbalanced three phase four wire system. The study did not consider the transient and steady state behavior of the filter circuit applied in the extraction unit.

The need to improve the performance of the APF current harmonic extraction unit due to the limitation associated with the use of LPF and BSF, from the reviewed literature is the focus of this work. This investigation shall investigate the use of first and second order LPF, HPF and Band Stop Filter used in the current extraction unit of APF, this study will consider the transient and steady state response of listed filter under a balanced network.

Table 2.4: Summary of Gap Identified in Literature

S/N	TITLE OF WORK	AUTHOR	APPLIED METHOD	LIMITATIONS
1	Electrical Power and Energy Systems On design and implementation of three phase three level shunt active power filter for harmonic reduction using synchronous reference frame theory	(Sundaram & Venugopal, 2016)	They employed first order LPF in extraction unit of shunt APF for current harmonics extraction	The study was able to detected few dominant harmonics due to LPF limited bandwidth.
2	Analysis and Control of Modular Multilevel Cascaded Converter-Based Flexible AC Transmission Systems and Analysis and Control of a Modular Multilevel Cascaded Converter-based Unified Power Flow Controller	(Huang, 2018; Huang et al., 2019)	This study was focused on the reference current control scheme, but considered BSF in the APF extraction unit for current harmonics.	It could only eliminate few dominant harmonics
3	Current Harmonic Reduction on Source Side by using ANN Controller	(Srinivas et al., 2020)	They deployed a second order LPF in the extraction unit of Current Harmonic Reduction on Source Side by using artificial neural network techniques for the current Control.	This study did not consider transient and steady state response. But brought improvement of Hysteresis controller based APF with neural network logic controller

4	Research on three-phase four-wire active power filter based on LCLCL coupling structure.	(Hu et al., 2020)	This study considered in their research the use of notch filter in the extraction unit of for the load current Harmonics cancellation. The study emphasis was on harmonics associated with the pulse width modulation output signal and proposed a novel method of coupling the PWM signal to LVD network for APF in unbalanced three phase four wire system.	The study did not consider the transient and steady state behavior of the filter circuit applied in the extraction unit.

CHAPTER THREE

METHODOLOGY

This chapter discusses the research layout in five stages. It also presents the method used to obtain harmonic current data at Landmark University. A power system network analyzer called 'Circutor' is used to measure the harmonics and its data will be stored in the Secure Digital (SD) card. The method adopted for the current harmonics extraction unit for APF and how it will be implemented was also discussed. The implementation circuit of first and second-order lowpass, high pass filter and second-order band stop filters used in the extraction unit of the active power filter is presented. The relationship between the transfer function for each filter and the cutoff frequency is also discussed. The research tool and the software configuration setup used for the investigation is also discussed.

3.1 Research Layout

This research methodology involves the following stages:

i. A power network analyzer will be used in obtaining the harmonic current data from a substation in Landmark University.

ii. The obtained data will be used in modelling a power system network in MATLAB SIMULINK environment.

iii. First and second order low pass, high pass, band stop and band pass filters will be designed.

iv. These filters will be implemented in the extraction unit of the active power filter.

v. Obtained results form (iv) will be used to ascertain the transient and steady state response of the selected extraction techniques on the APF.

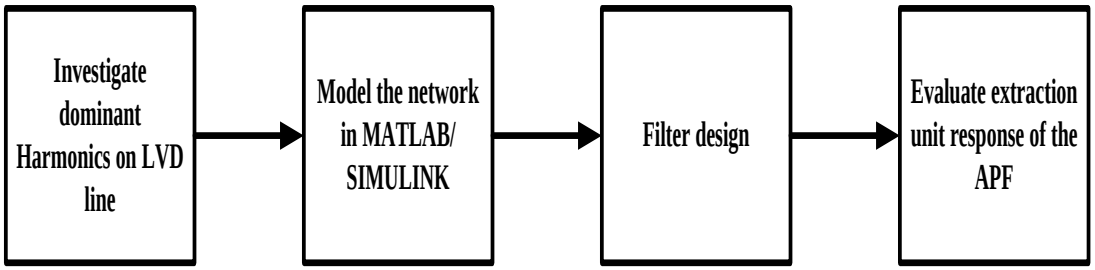

Figure 3.1: Research methodology block diagram

Research methodology block diagram consist of identification of the current harmonic available in Landmark university LVD network, modelling of the network in MATLAB/SIMULINK environment followed by filter implementation stage, as shown in Figure 3.1

3.2 Data Collection

Landmark University low voltage distribution substation is supplied by Ibadan electricity Distribution Company (IBEDC), the expected harmonics value permitted should be less than 5% THD (Dubey et al., 2021). The current harmonics obtained from LMU distribution network however reveal the presence of high percentage current harmonics. The current harmonics was obtained through the use of power system network analyser called 'Circutor'. The Circutor is a gap-less device that captures details of power quality parameters during measurement and store its data on secure digital (SD) card. The Circutor was deployed at various locations within LMU to measure the current harmonics present. The recorded data was extracted through an interface software called Power Vision Plus and presented in excel sheet.

3.3 Research Methodology

This section discusses the method employed in achieving the objectives of current harmonics extraction techniques of the active power filter (APF).

The APF configuration diagram consist of a three phase voltage sources v_{sa}, v_{sb} and v_{sc}, load current i_{la},i_{lb} and i_{lc} connected to the extraction unit, where the current harmonics are extracted, this serve as the reference signal for the current control section as seen in Figure 3.2, the reference voltage obtained from the current control unit serves as input signal for the pulse width modulation unit (PWM unit). The shunt APF (i.e. inverter) is coupled to the line (i.e. the point of common coupling) via a line filter.

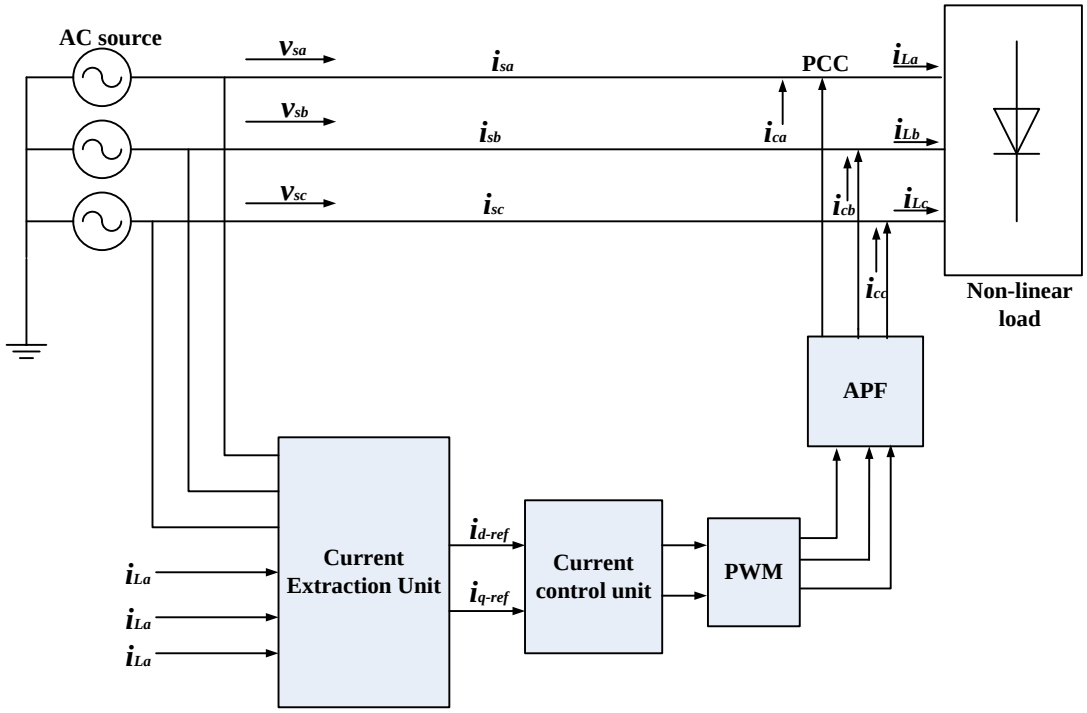

Figure 3.2: APF Control Configuration

Figure 3.2 is an illustration of shunt active power filter connected at the point of common coupling in between a non-linear load and the AC source. The circuit current and source voltage at PCC are given as;

$$i_s(t) = i_L(t) + i_c(t) \quad 3.1$$

$$v_s = v_{sm} \sin \omega(t) \quad 3.2$$

Where

$i_{s(t)}$= source current

$i_{L(t)}$ =Load current

$i_{c(t)}$ = Compensated current

v_s =Source voltage and

v_{sm}= peak value of source voltage

The extraction unit consist of synchronous reference frame algorithm that convert the alternating three phase voltage from *abc* to *dq* quantity. According to (Al-Ogaili et al., 2020; Kashif et al., 2020; Rameshkumar & Indragandhi, 2020) Synchronous reference frame *(dq)* method is a time base current transformation technique based on Park transformation, which involves the transformation of *abc* stationary reference frame to a *dq* synchronously rotating reference frame as show in equation 3.3. *dq* reference frame technique has the advantage of being used in unbalance network compared to the

pq theory (Dubey et al., 2021; Hu et al., 2020; Lahare et al., 2020; Shembekar & Deshmukh, 2015).

Applying Park transformation, the rotating reference frame is given as;

$$\begin{matrix} i_d \\ i_q \end{matrix} = \sqrt{\frac{2}{3}} \begin{bmatrix} \cos\theta & \cos\left(\theta - \frac{2\pi}{3}\right) & \cos\left(\theta + \frac{2\pi}{3}\right) \\ -\sin\theta & -\sin\left(\theta - \frac{2\pi}{3}\right) & -\sin\left(\theta + \frac{2\pi}{3}\right) \end{bmatrix} \begin{bmatrix} i_a \\ i_b \\ i_c \end{bmatrix} \quad 3.3$$

Where θ is the angle of the rotation of the dq axis, $\theta = wt$ and ω is the angular frequency and i_d, i_q are the active and reactive current components.

The active and reactive components of current contain the fundamental and higher order harmonics as expressed in Equation 3.4.

$$i_d = I_d + i_{h\_d} \quad 3.4a$$

$$i_q = I_q + i_{h\_q} \quad 3.4b$$

Where $I_d$and I_q denote the fundermental component while i_{h_d} and i_{h_q} denote the higher order harmonic components of *dq* current.

The harmonics are obtained as shown in Figure3.3, the three phase load current i_{La}, i_{Lb}, i_{Lc}, are converted to direct and quadrature axis (Hoon et al., 2016). It consist of i_d and i_q the direct axis component and the quadrature axis which represents the active and reactive power components.

3.3.1 Current Harmonics Extraction Unit

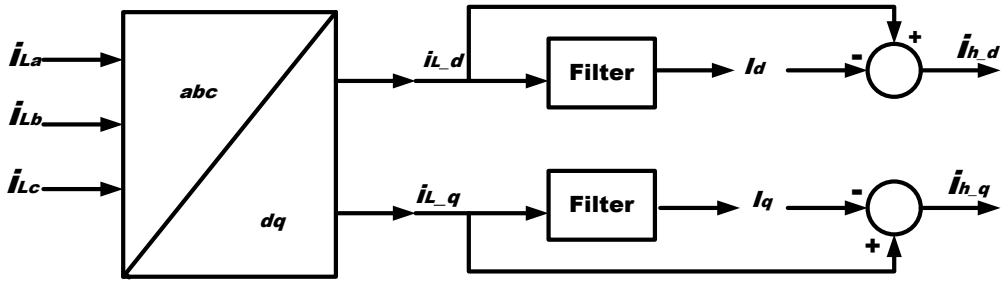

Figure 3.3: Current harmonics extraction unit.

The method adopted at Current harmonics extraction unit for the generation of reference signal is the Synchronous Reference Frame (SRF) as shown in figure3.3. SRF configuration circuit transforms three phase *(abc)* signal into *dq* frame, i_{h_d} and i_{h_q} are the harmonics current present in the active and reactive power components of the filtered signal, the filtered signal is applied to the current controller unit. Effective separation of the fundamental signal from the harmonics signal is achieved with this configuration, appropriate selection of the filter parameter such as transfer function, cut-off frequency and damping ratio representing low pass filter, high pass filter, and

BSF filter, will be implemented in the extraction unit to remove the current harmonics signal present in the load current.

3.3.1.1 Low Pass Filter Implementation

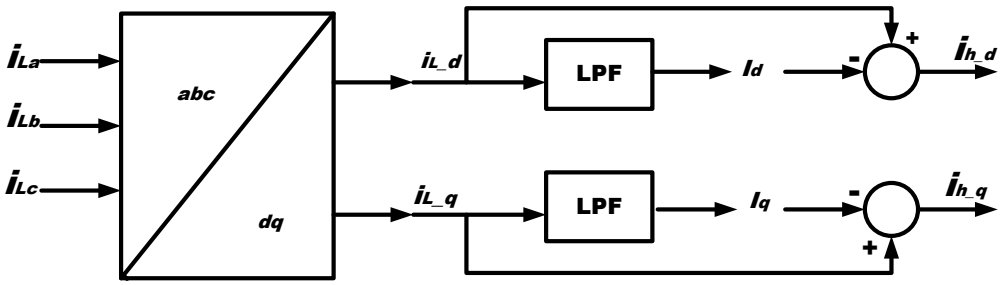

Figure3.4: LPF implementation block diagram

Implementation of LPF in the extraction unit block diagram is designed to filter out the current harmonic in load current as shown in Figure 3.4. By using a LPF, the distorted load current i_L is transformed into direct and quadrature axis i_{L_d} and i_{L_q}, this is based on Park transformation equation in Equation (3.3). The resultant i_{L_d} and i_{L_q} contains the fundamental and harmonics component. The harmonics component is obtained subtracting LPF output from i_{L_d} and i_{L_q} signal. LPF response with various frequencies is given in Figure 3.5

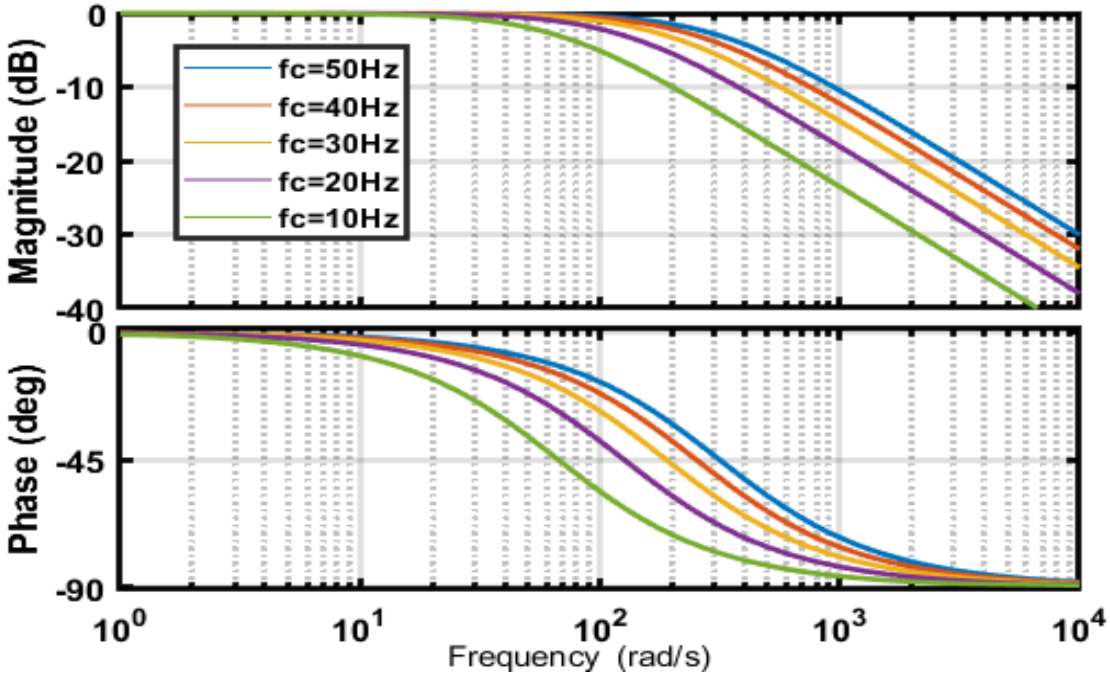

Figure 3.5: LPF Bode plot

The frequency of 50Hz represented by blue line gives a better steepness. To maintain the system requirement a cut off frequency of 50Hz is implemented for the LPF.

The transfer function (TF) for a first order LPF is given as:

$$\text{T f(s)LPF} = \frac{\omega_0}{S+\omega_0} \quad 3.5$$

Where ω_0 is the frequency component given as $2\pi f_c$ and f_c is the cutoff frequency. This investigation is also implemented in second order LPF with transfer function given as

$$TF_{(s)LPF} = \frac{{\omega_0}^2}{s^2+2\xi\omega_0 s+{\omega_0}^2} \quad 3.6$$

Where $2\xi\omega_0 = \frac{W_0}{Q} = B$

ξ is the damping factor, Q is the quality factor while B is the bandwidth.

Second order LPF steepness is by $40\,\frac{dB}{dec}$

Generally, the higher the order of the filter, the faster the roll off or steepness. The zeta value chosen was obtained by checking the response of the system with different ξ values.

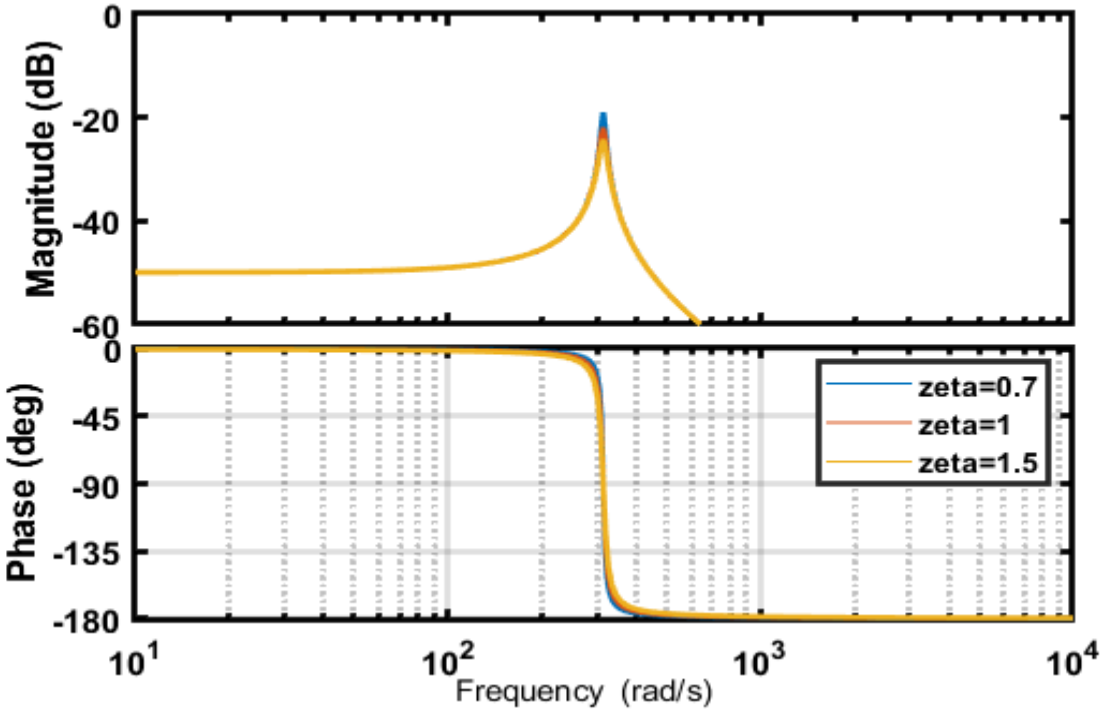

Figure 3.6: Second order LPF Bode plot

Figure 3.6 shows that at ξ = 0.7 the system has a better roll-off rate. Hence, the response of the second order filter is better than the response from first order filter.

3.3.1.2 High Pass Filter Implementation

High Pass filter implementation block diagram shown in Figure 3.7, is the applied input signal into the extraction unit and the three-phase load current.

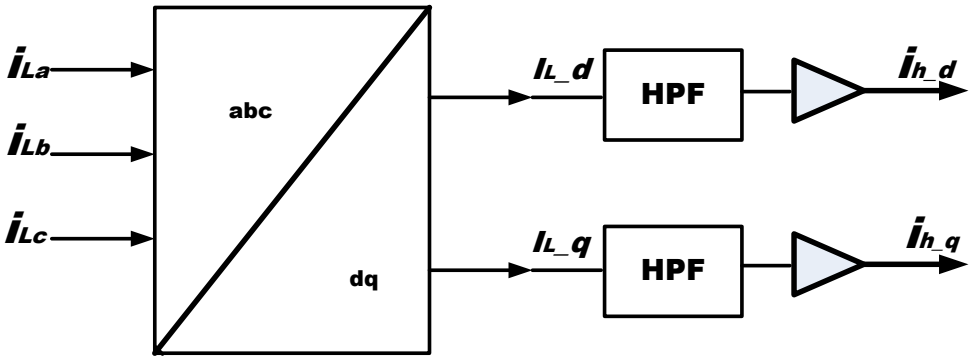

Figure3.7: HPF implementation block diagram

The high pass filter circuit attenuate signal below the cutoff frequency f_c and allow the multiple frequency signal above the f_c that account for the harmonics to pass through. The transfer function of first order HPF implemented in this investigation is given as

$$\mathrm{TF}_{(s)\mathrm{HPF}} = \frac{s}{S+\omega_0} \qquad 3.7$$

The cut-off frequency needed to achieve maximum extraction from HPF was selected by making a Bode plot with different frequencies. The result obtained when f_c of 50Hz, 40Hz, 30Hz, 20Hz and 10Hz were implemented indicated that better roll-off with 50Hz cutoff frequency as shown in Figure 3.8.

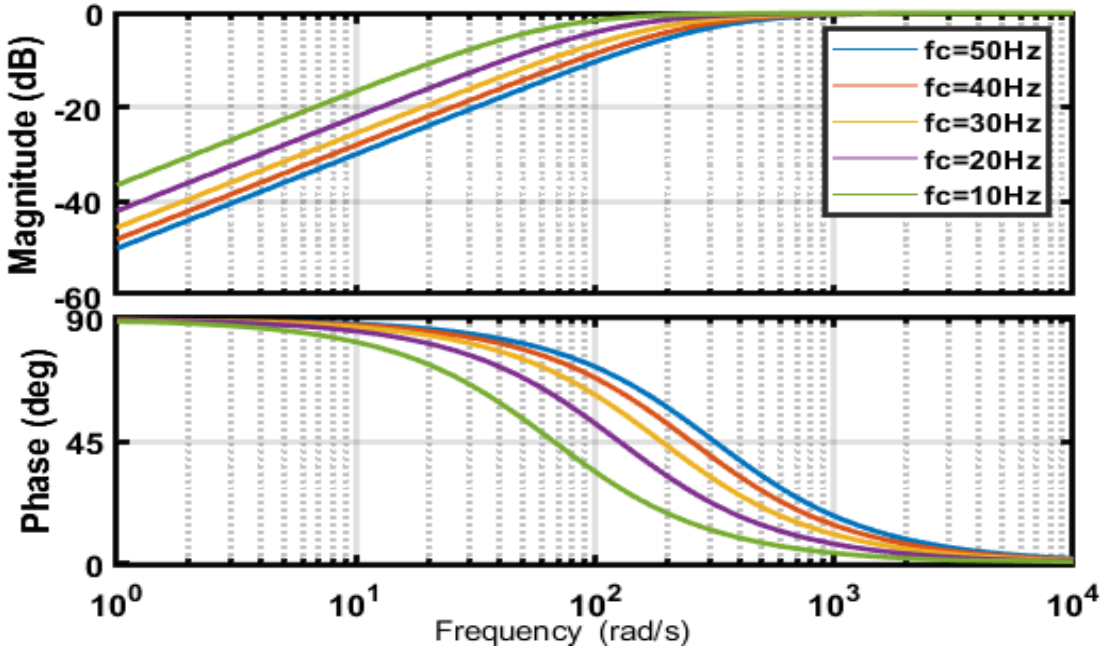

Figure 3.8: First order HPF Bode plot

The transfer function for the second order high pass filter implemented in the extraction unit of APF is given as

$$TF_{(s)HPF} = \frac{s^2}{s^2+2\xi\omega_0 s+{\omega_0}^2} \qquad 3.8$$

where ξ is the damping factor, ω_0 is the frequency component, for 50Hz cut off frequency, to extract the 3rd harmonics for example, the implementation is represented during simulation as $\omega_0 \geq 2\pi \times 150$ rad/s. The damping ratio is inversely proportional to the quality factor and determine the roll-off rate.

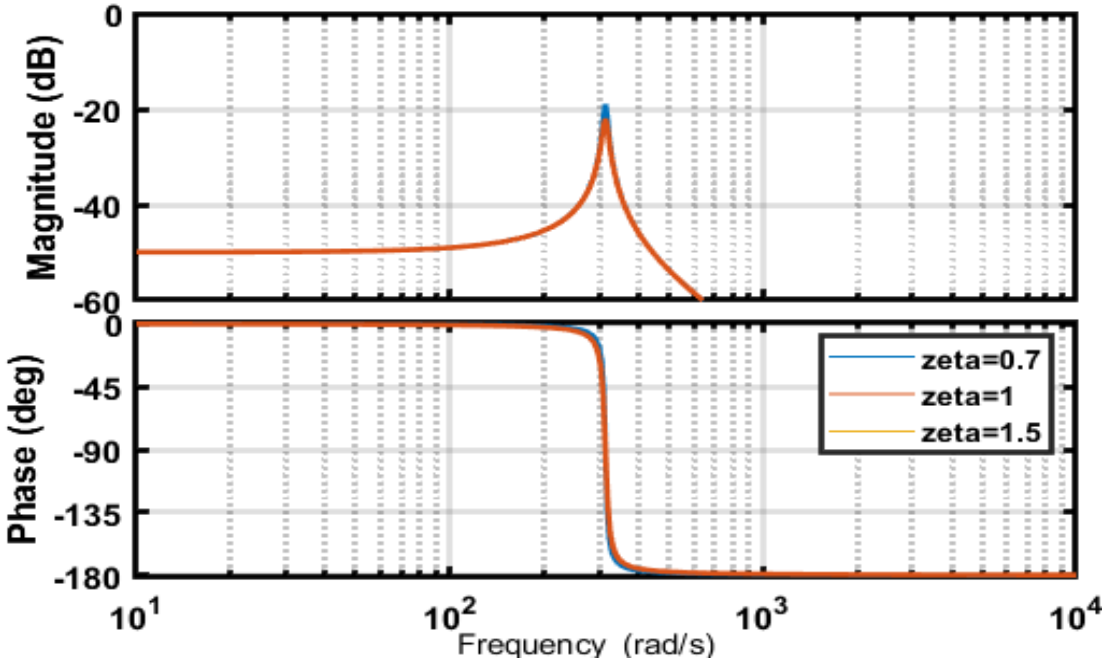

Figure 3.9: Second Order HPF Bode plot

The peak of the second order bode plot occur at ξ =0.7, corresponding to the system maximum response as shown in figure 3.9

3.3.1.3 Band Stop Filter Implementation

Band Stop Filter (BSF) block diagram implemented in the extraction unit of the APF is shown in Figure 3.10.

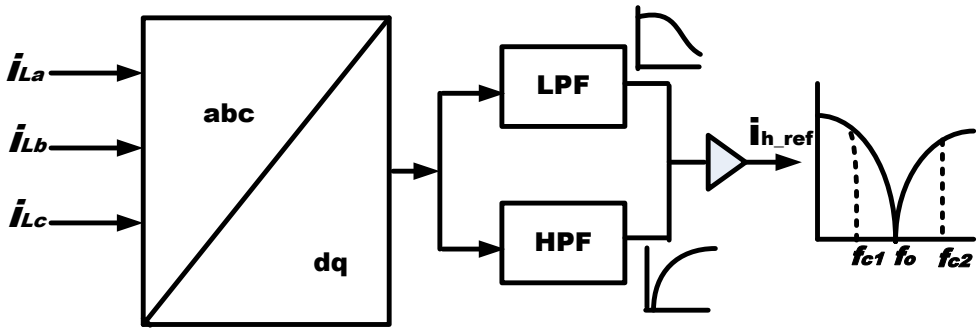

Figure 3.10: Band stop filter implementation block diagram

BSF consists of LPF connected in parallel with HPF. The LPF allow signal $\leq f_{c1}$, to pass through and attenuate others while the HPF attenuate signal $\leq f_{c2}$. Thus, relative to cutoff frequency f_c, LPF and HPF has one cutoff frequency, while band pass filter and band stop filter have two cutoff frequencies f_{c1} and f_{c2}, the difference between f_{c1} and

f_{c2} is the bandwidth. Notch filter is a special form of Band stop filter, the response of all second order BSF filters depend on damping ratio and angular frequency.

The Transfer function (TF) for first order active band stop filter is not achievable because it is a combination of two first order filter circuit (Sengar & Kumar, 2019).

The transfer function of second order BSF is given as

$$T.F_{(s)BSF} = \frac{s^2+{\omega_0}^2}{s^2+2\xi\omega_0 s+{\omega_0}^2} \quad 3.11$$

Where ω_0 account for the cutoff frequency and ξ is the damping factor that determine the band width of the Band stop filter, for example to stop the 5th harmonics, the value of ω_0 will be $2\pi\times50$(n) rad/s, where n=5. As illustrated in Figure 3.11 the5th harmonic BSF Bode plot shows that at ω_0= 1571rad/s the logarithm magnitude tend towards infinity.

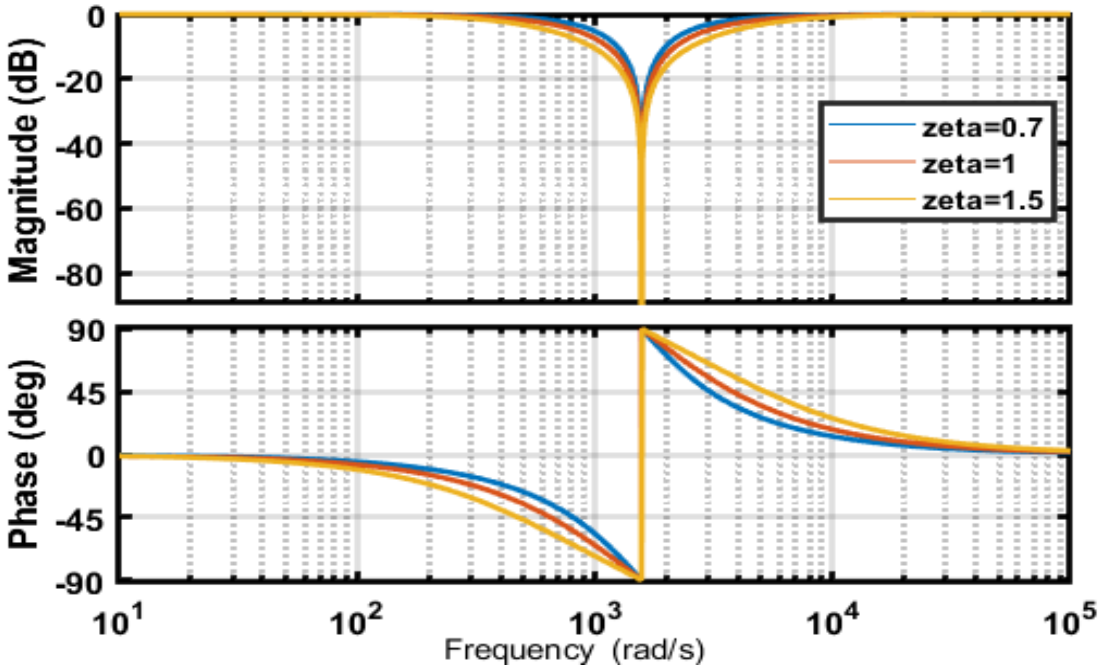

Figure 3.11: BSF 5th harmonic Bode plot

With ξ = 0.7 the Bode plot produce a steeper curve capable of attenuating the 5th harmonic.

3.3.2 Current Control Unit

Predictive current control configuration shown in Figure 3.12 (a) and (b) is a technique that uses discrete – time model to predict the future value of compensation current from the converter for each voltage generated by the inverter.

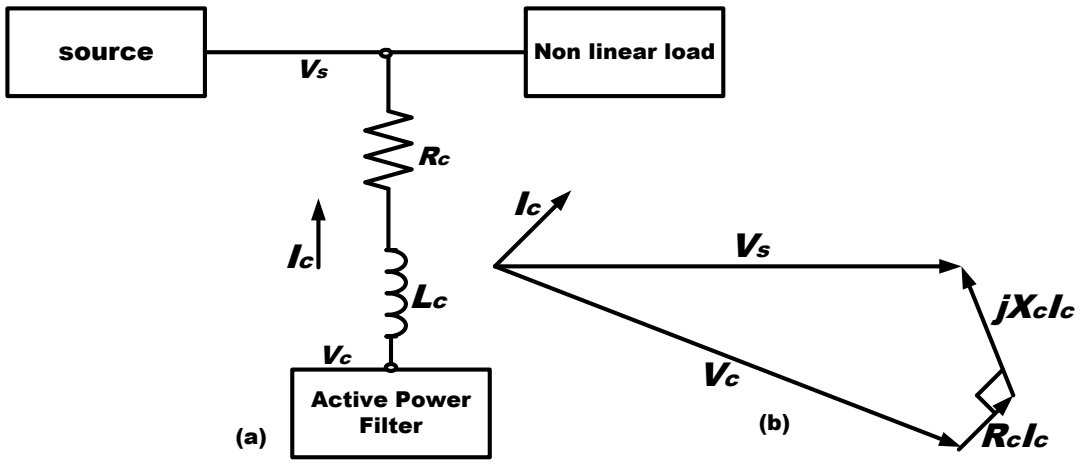

Figure 3.12: (a) APF block diagram and (b) phasor diagram.

The operation of the figure is given by the phasor diagram, showing the space vector expression.

$$\overrightarrow{V_S} - \overrightarrow{V_C} = L_C \frac{dI_C}{dt} + R_C I_C \qquad 3.12$$

Using digital implementation, with small sampling interval T_s defined over K[th] and $(K+1)^{th}$ sample interval, change in converter current i_c; becomes

$$\frac{dI_C}{dt} = \frac{\Delta I_C}{T_s} = \frac{i_c(k+1) - i_c(k)}{T_s} \qquad 3.13$$

Because the $i_c(k+1)$ cannot be obtained in advanced, then $\overrightarrow{\iota_c^*}(k)$, is used as the reference current.

Rearranging Equation (3.12) and (3.13) the next sampling period is obtained as Equation (3.14)

$$\overrightarrow{\iota_c^*}(k) = \overrightarrow{V_S}(k) - \left[\frac{L_C}{T_S}\right]\overrightarrow{\iota_c *} + \left[\frac{L_c}{T_s} - R_c\right]\overrightarrow{\iota_c(k)} \qquad 3.14$$

State space equation from equation (3.14) is given as

$$\begin{bmatrix}\overrightarrow{V_{C-d}^*}(k) \\ \overrightarrow{V_{C-q}^*}(k)\end{bmatrix} = \begin{bmatrix}\overrightarrow{V_{s-d}}(k) \\ \overrightarrow{V_{s-q}}(k)\end{bmatrix} - \begin{bmatrix}\frac{L_c}{T_s} & 0 \\ 0 & \frac{L_c}{T_s}\end{bmatrix}\begin{bmatrix}\overrightarrow{i_{cd}^*}(k) \\ \overrightarrow{i_{cq}^*}(k)\end{bmatrix} + \begin{bmatrix}\frac{L_c}{T_s} - R_c & -wL_c \\ wL_c & \frac{L_c}{T_s} - R_c\end{bmatrix}\begin{bmatrix}\overrightarrow{\iota_{cd}}(k) \\ \overrightarrow{\iota_{cq}}(k)\end{bmatrix} \qquad 3.15$$

The value of v_c serve as the reference signal for generating PWM signals.

3.3.3 Pulse Width Modulated H-Bridge Converter

PWM configuration are commonly used for switch mode arrangement that applies Voltage Source Inverter (VSI) (Mamdouh et al., 2014; Moeini et al., 2020; Nwobu et al., 2015; Subramaniam et al., 2019; Tandekar et al., 2019; Yousfi et al., 2020). The output of the predictive current controller is compared with a triangular carrier signal at a high frequency. The purpose of the inverter circuit is to produce a sinusoidal output signal with desired voltage magnitude and frequency (Kumar et al., 2020a; Zhilin &

Prasol, 2020). The two major parameter in the sampling are the amplitude modulation Index (M_a) and the Frequency Modulation ratio (M_f) (Moeini et al., 2018; Nwobu et al., 2015; Tandekar et al., 2019). M_a is the ratio of the magnitude of reference signal to the triangular carrier signal magnitude while M_f is the ratio of the frequency of carrier signal to the frequency of the reference signal, in this case is 50Hz. A three phase voltage source inverter was applied in realizing the current harmonics mitigation techniques for APF. Figure3.13 shows that the three phase voltage source inverter convert the reference voltage V_{ref} into a voltage of know frequency and magnitude, A, B and C are the three phase output voltages obtained. The three phase PWM inverter circuit is therefore configure to shape and control the three phase output signal in magnitude and frequency resulting from the reference voltage.

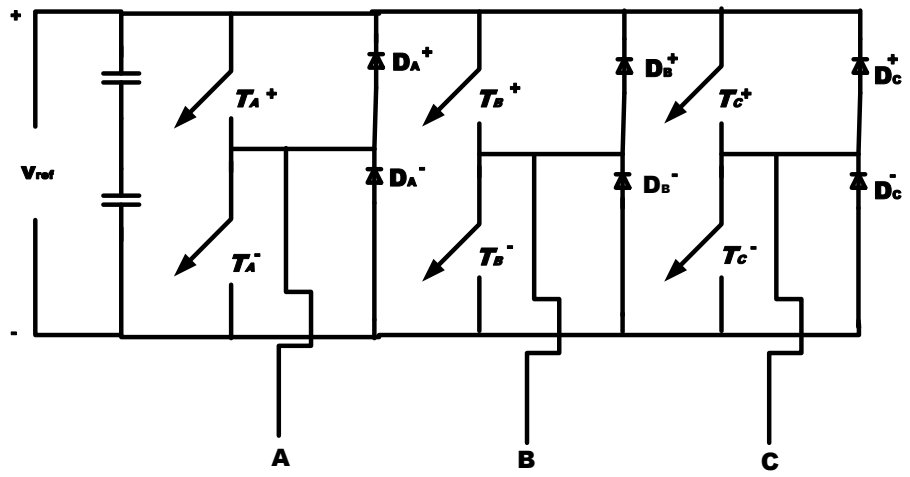

Figure 3.13: Three phase PWM configuration

3.4 Research Design Tools

Digital filter design simulated on MATLAB/SIMULINK is used to conduct this investigation. Simulink perform graphical and computational operations, tunable Simulink filter block, each using block parameters obtained from the Simulink library was simulated. For each simulation, the transfer function representing LPF, HPF and BSF is implemented to study the transient and steady state behavior of the harmonics current extraction unit for active power filter. Harmonics contents on LVD network is realized using a three phase thyristor controlled circuit with various Firing angle ranging from 0˚, 30˚and 60˚.

3.5 Software Configuration Setup

The Simulink software used in the investigation has the following specifications as shown in Table3.1.

Table3.1: Simulink specification.

Required software	Specification
Operating system (OS)	Windows 10 64 bits
MATLAB	2018
Microsoft Excel	2013
Power Vision Plus	2013

CHAPTER FOUR

RESULTS AND DISCUSSION

The results of the current harmonic data measured at Landmark University is presented in this chapter. The predominant current harmonics present in the network was utilized in selecting the network model parameters to be simulated in MATLAB/SIMULINK environment for implementation of active power filter. The transient and steady-state performance of the various filters circuits implemented in the extraction unit of APF is also presented. In addition, the influence of the various filter in the extraction units of APF harmonic mitigation is also discussed.

4.1 Current Harmonic Data

These datasets were obtained through real-time measurements using power system analyser (Circuitor). The raw data in excel sheet is attached as appendix A1 and the graph showing the various harmonics content present in the distribution network is shown below. The measured current total harmonic distortion is presented over a 24 hours.

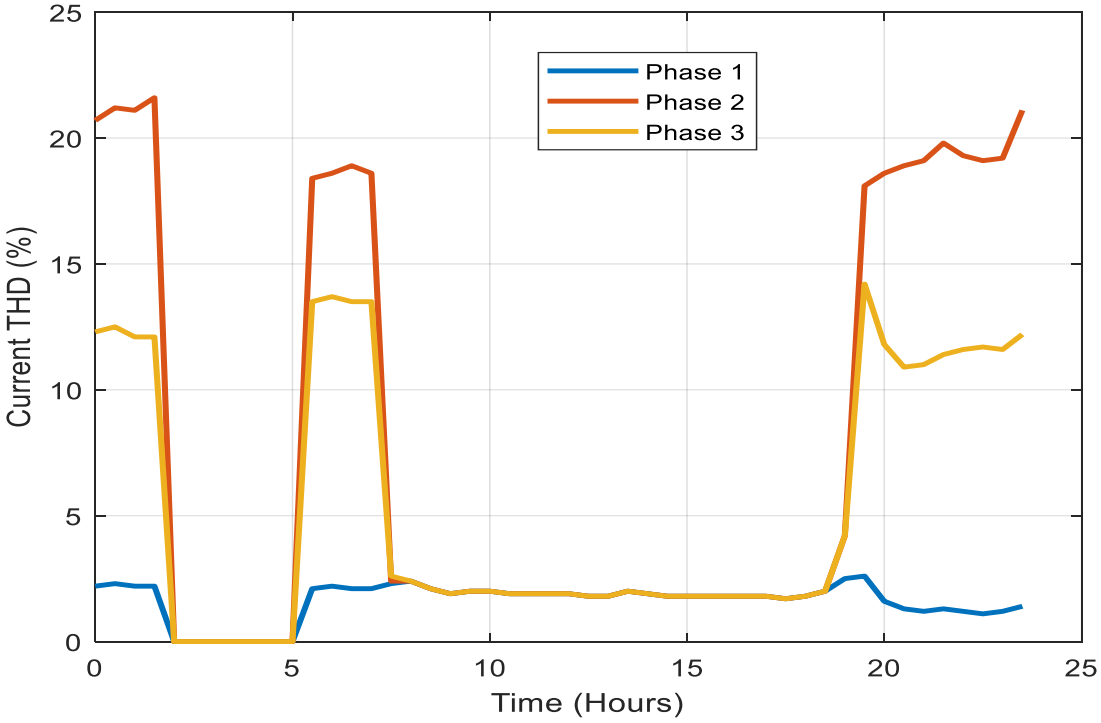

Figure 4.1: Current THD in a typical day across three phases

Figure 4.1 is a chart showing the current THD in a typical day. The data shows the presence of harmonics in each of the three phases. The figure reveals that phase 1

indicated by blue is within the recommended 5%THD limit for LVD network. However phase 2 and phase 3 contains above 5% THD limit.

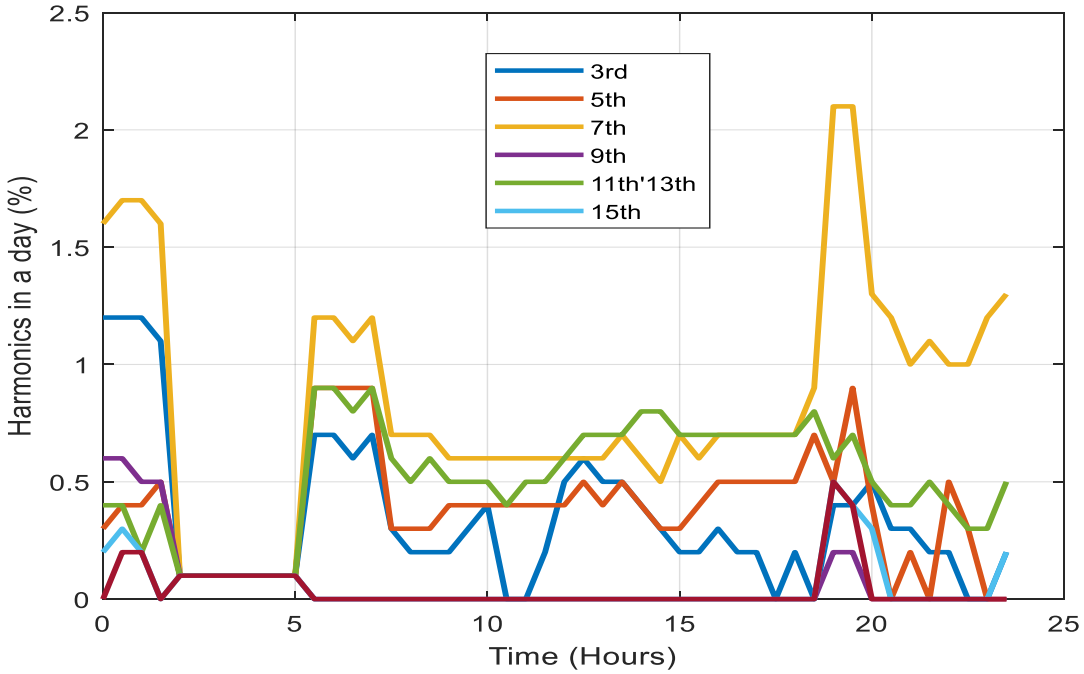

(a)

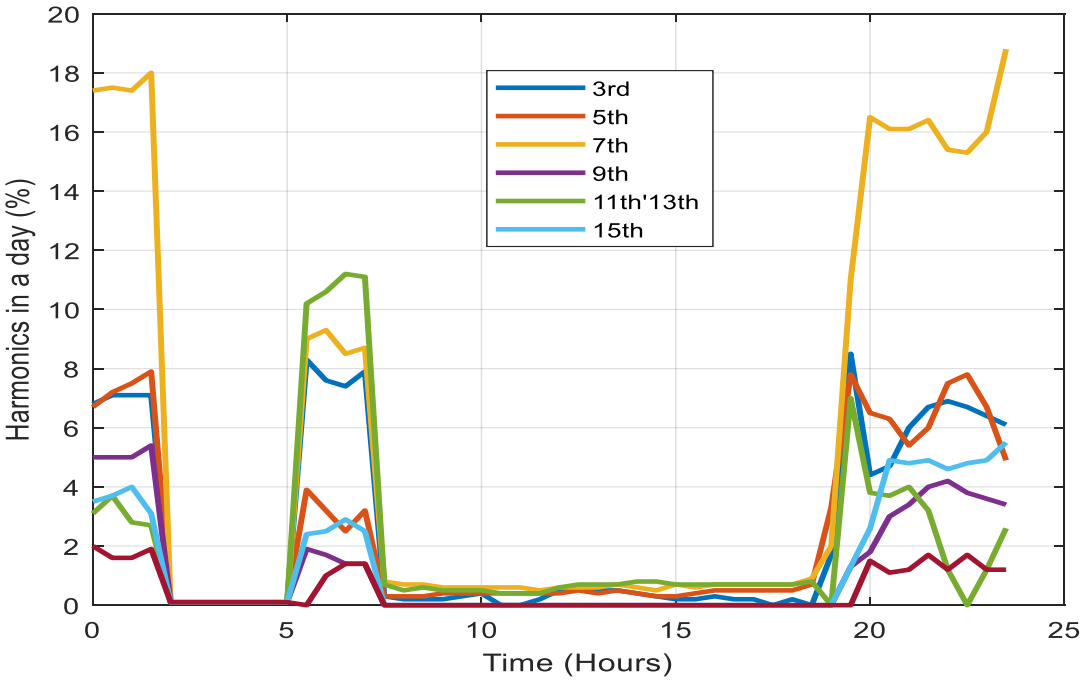

(b)

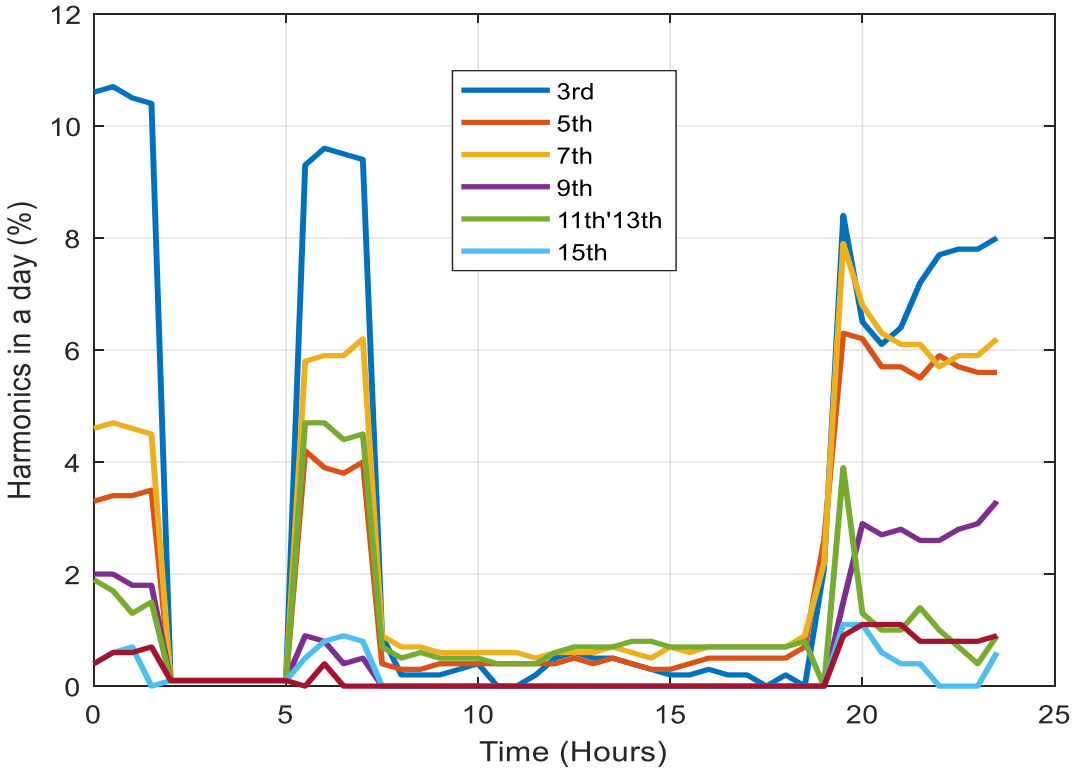

(c)

Figure 4.2: current harmonics (a): in phase 1, (b) in phase2, (c) in phase 3 for 24hours

Figure 4.2 (a)-(c) give the current harmonic in phase 1-3 of a three-phase four wire distribution line within 24 hours in LMU. Chart (b) and (c) reveal that the harmonics values are above the permitted limit of 5% THD. The current harmonics data reveal that the percentage THD values of 3rd, 5th, 7th, 9th, 11th, 13th, and 15th are above the required standard.

These results form the basis of the simulation of common load in a University environment using the results obtained from the real time measurement discussed in section 4.1, having established the predominant harmonics present on the line. The harmonics generating load is simulated in MATLAB/SIMULINK environment using three phase thyristor controlled load.

4.2 Simulation Setup

The experimental setup of current harmonic extraction unit for APF was implemented using MATLAB/SIMULINK. Figure 4.3 shows the simulation configuration of three phase balanced network and the simulation parameters are shown in Table 4.1.

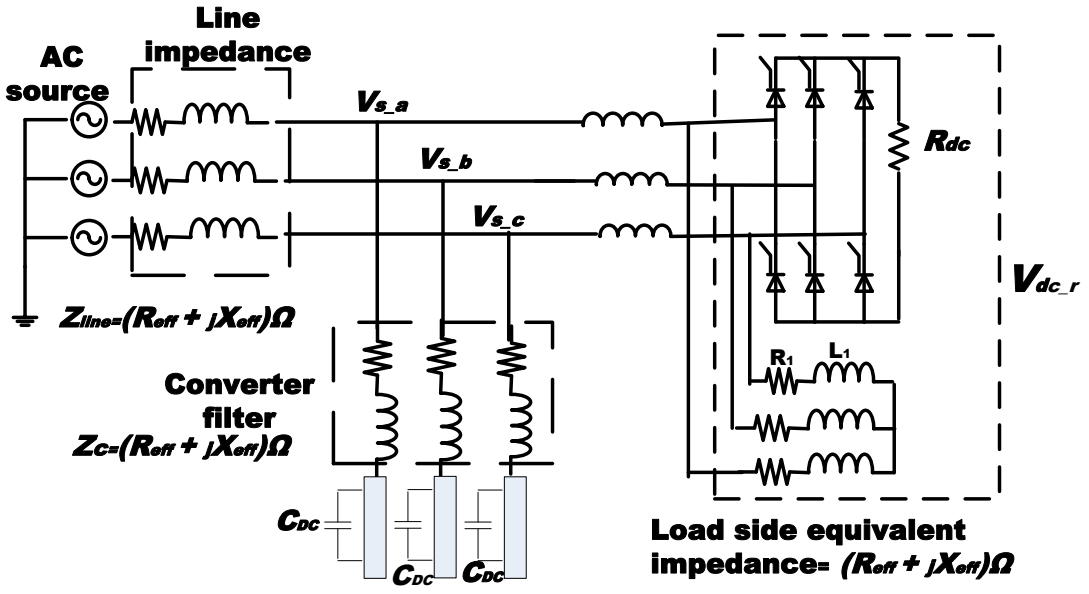

Figure 4.3: Power system simulation configuration

The power system simulation block diagram in Figure 4.3 consists of three-phase voltage source with the converter connected at the point of common connection, PCC. The distribution line parameters is represented as line impedance between the source voltage and PCC. The block diagram also contains the converter impedance Z_c. The actual system parameters used for the MATLAB/SIMULINK environment simulation is presented in Table 4.1, while the SIMULINK block model is attached as appendix A2. Table 4.1 shows the voltage at the PCC of LVD line, the load side and converter side parameters. The load side is represented by a rectifier made up of three phase thyristor controlled circuit connected in parallel with an R-L load of 0.8 power factor (pf). Thyristor firing angle is varied at 30^0 between 0˚ to 60˚. The performance of the harmonics extraction unit is studied by considering three scenarios, by firing the thyristor rectifier at different firing angles. The period for 0˚, 30^0 and 60^0 firing angles are 0 to 0.4sec, 0.4 to 0.8sec and 0.8 to 1.2sec respectively.

Table 4.1: APF system parameters

Components		**Value**
PCC Side	Source end voltage V_{S0}	240 V
Distribution Line	Aluminium PI TX line (d= 10mm, L=1.1km)	$R_{line} = 0.2\ \Omega$ $L_{line} = 3mH$
Load Side	Three Phase Thyristor Rectifier	$R_{dc\_r} = 20\Omega$ $L_{ac\_r} = 8.3mH$
	Firing angle α	$0°; 30°; 60°$
	R+L Load	$R_l = 10\Omega$ $L_l = 48mH$
Converter Side	RL Filter Cutoff frequency	$R_c = 1.59\Omega$ $L_c = 5mH$ $F_c = 50Hz$
	DC capacitor	$C_{DC} = 1.12\ mF$
	DC voltage V_{dc}	$400\ V$
	Switching frequency f_s	$4\ KHz$

4.3 Low Pass Filter Implementation

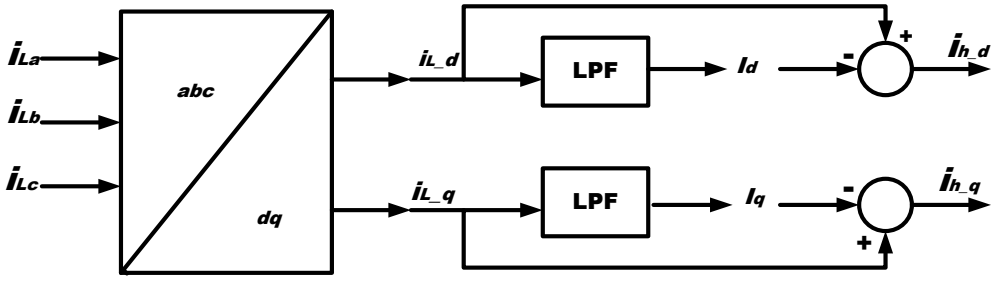

Figure 4.4: LPF implementation block diagram.

The block diagram in Figure 4.4 represents the current harmonic extraction unit using LPF. Load currents, i_{La}, i_{Lb} and i_{Lc} were transformed into i_{L_d} and i_{L_q} through park transformation. i_{L_d} and i_{L_q} contain the fundamental and harmonics signal.

4.3.1 First Order LPF Implementation

Using a first order LPF with the transfer function (TF) given as:

$$\text{T f(s)LPF} = \frac{\omega_0}{S+\omega_0} \qquad 4.1$$

The angular frequency component ω_0 is given as $2\pi f_c$ and f_c is the cutoff frequency. In LPF implementation, frequencies greater than f_c are attenuated while frequencies less than or equal to f_c will pass through the filter. The values of i_{h_d} and i_{h_q} are the resultant harmonics content present as the direct and quadrature components of load current. 50Hz cutoff frequency is applied with $\omega_0 \leq 2\pi \times f_c$ rad/s.

4.3.1.1 PCC Current without Compensation

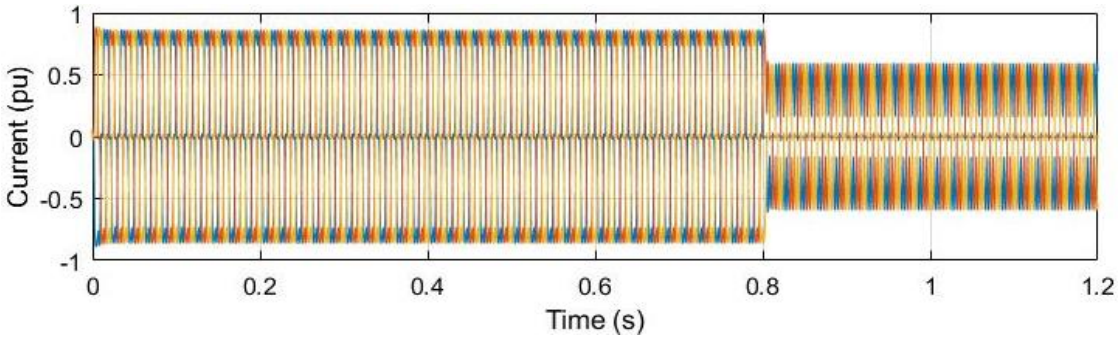

Figure 4.5: PCC current without compensation.

The PCC current without compensation is shown in figure 4.5. The uncompensated current at PCC is the same as the load current. It is the combination of α =0° , 30° and 60° firing angles. A closer look to ascertain the current harmonics level at the respective firing angle are shown in figure 4.6 (a) – (f). The signal indicates the presence of current harmonics observed as distorted waveform across the three phase.

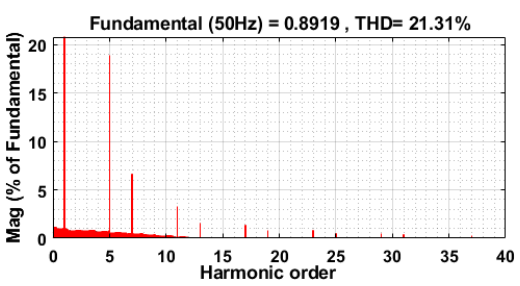

(a)

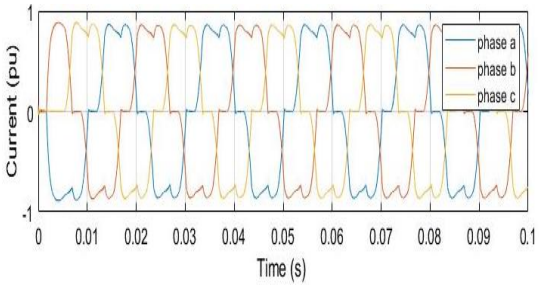

(b)

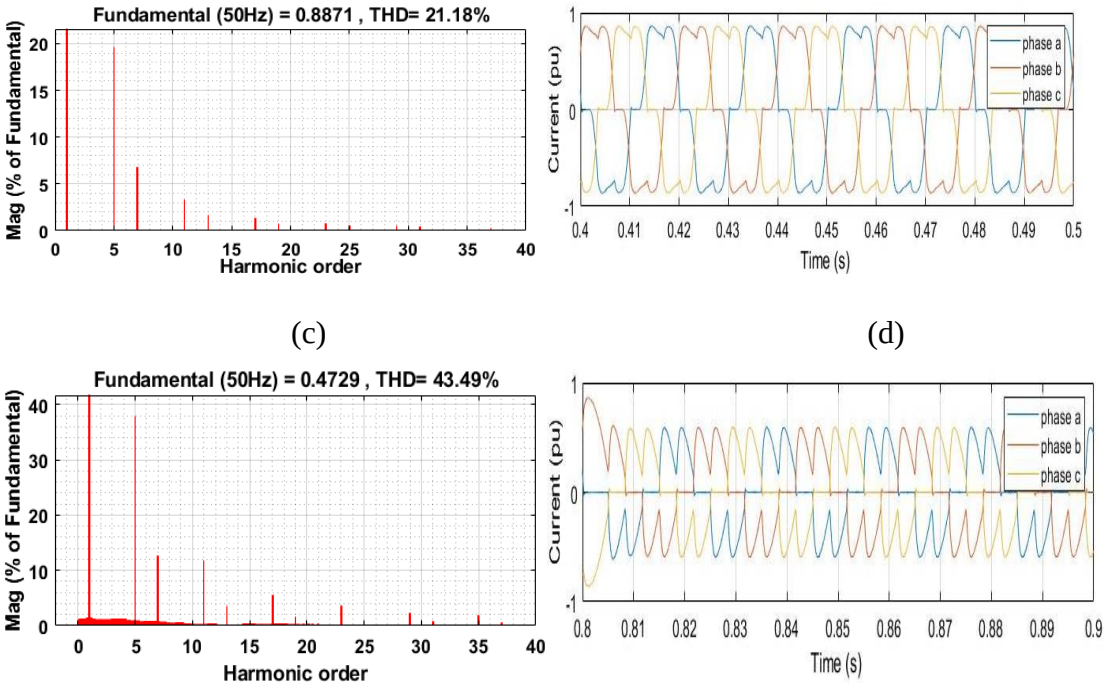

Figure 4.6: PCC current without compensation. (a) current waveform at $\alpha = 0°$, (b) current waveform spectrum $\alpha = 0°$, (c) current waveform at $\alpha = 30°$, (d) current waveform spectrum $\alpha = 30°$, (e) current waveform at $\alpha = 60°$ and (f) current waveform spectrum $\alpha = 60°$.

Figure 4.6(a), (c) and (e) are the FFT plot of the PCC current before compensation at α =0^0, $30^0$and 60^0, the current waveform are (b), (d) and (f), when α= 0^0, 30^0 and 60^0 respectively. In figure4.6 (a), (c) and (e) clearly show that 21.13%, 21.18% and 43.49% are the THD corresponding to α=0^0, 30^0 and 60^0 respectively.

4.3.1.2 PCC Current with Compensation

The effect of the first order LPF extraction scheme of the APF on the level of current harmonics before compensation is seen to have been significantly reduced. The harmonic content at PCC during compensation are shown in Figure 4.7 (a)- (f).

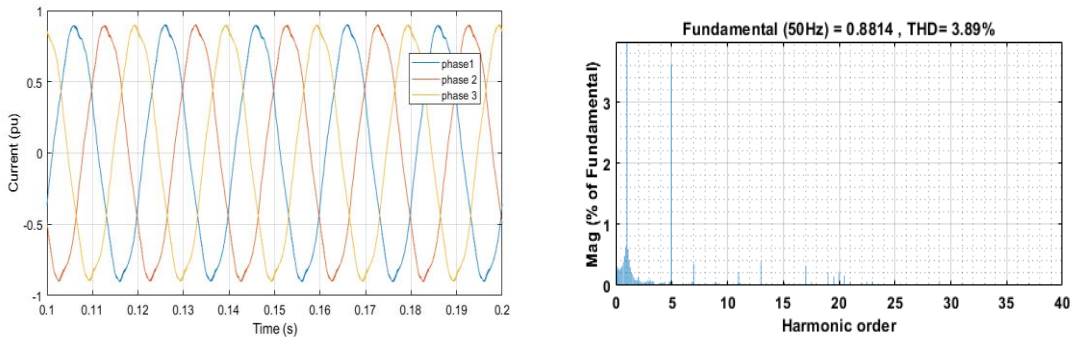

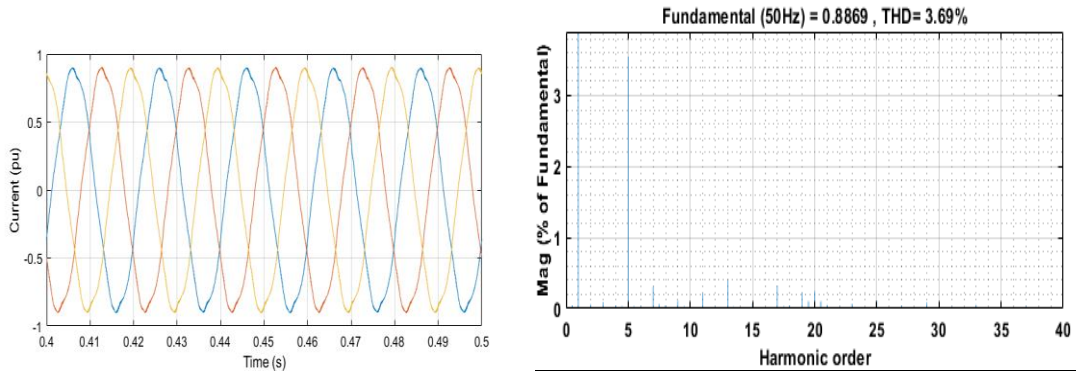

(c) (d)

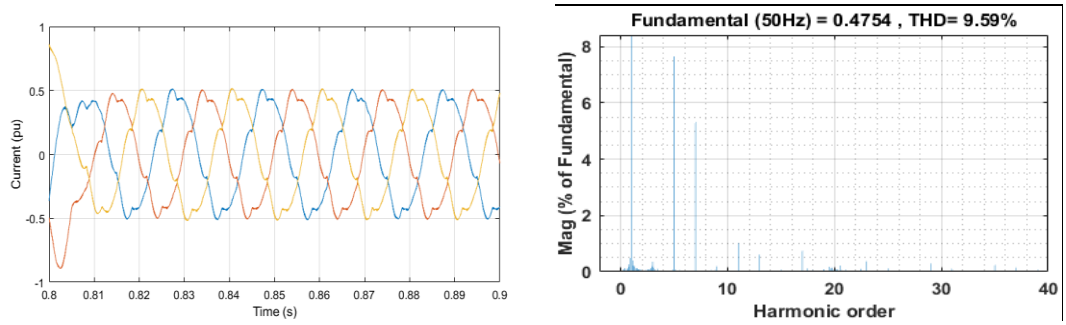

(e) (f)

Figure 4.7: PCC current with compensation. (a) current waveform at $\alpha = 0°$, (b) current waveform spectrum $\alpha = 0°$, (c) current waveform at $\alpha = 30°$, (d) current waveform spectrum $\alpha = 30°$, (e) current waveform at $\alpha = 60°$ and (f) current waveform spectrum $\alpha = 60°$.

Figure 4.7 shows that the THD at $\alpha = 0^0$, 30^0 and 60^0 has decreased from 21.31% to 3.89%, 21.18% to 3.69% and 43.49% to 9.59% respectively.

Table4.2 shows the data represented in Figure 4.6 and 4.7 respectively. It was observed that the 3rd harmonics content is absent with its multiples because in a balanced three phase network, the 3rd harmonics are canceled out.

Table: 4.2 PCC current before and after compensation for 1st order LPF

PCC current without compensation				PCC current after compensation		
Order	$\alpha = 0^0$ %	$\alpha = 30^0$ %	$\alpha = 60^0$ %	$\alpha = 0^0$ %	$\alpha = 30^0$ %	$\alpha = 60^0$ %
5^{th}	18.88	19.60	37.89	3.62	3.54	7.65
7^{th}	6.60	6.81	12.58	0.36	0.31	5.31
11^{th}	3.30	3.34	11.86	0.21	0.21	1.02
13^{th}	1.58	1.65	3.50	0.39	0.39	0.62
17^{th}	1.35	1.38	5.58	0.32	0.33	0.75
THD	21.31	21.18	43.49	3.89	3.69	9.59

4.3.1.3 Transient Response of First order LPF

The result of the transient response of first order LPF is shown in figure 4.8. The rise time and settling time of the system are 0.008 sec and 0.015 sec. No overshoot was observed since the system is a first order system.

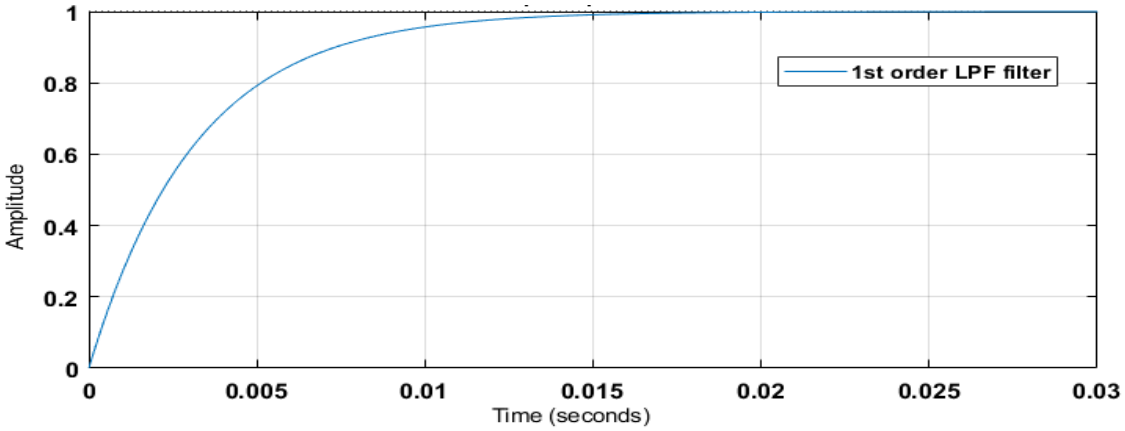

Figure 4.8: Transient Response of first order LPF

4.3.1.4 Steady-State Performance

The steady-state response of the first order LPF extraction unit is shown in Table 4.3. The steady state error represents the level of harmonic content that is present after compensation, It is seen that the steady state error has the highest and lowest values at $\alpha = 60^0$ and 30^0 with THD of 6.64% and 3.39% respectively. This however, reflect the performance of the current extraction unit.

Table 4.3 steady-state response of LPF.

Harmonics	$\alpha = 0^0$ %	$\alpha = 30^0$ %	$\alpha = 60^0$ %
5^{th}	3.19	3.19	6.25
7^{th}	1.09	1.09	1.94
11^{th}	0.27	0.28	0.97
13^{th}	0.14	0.13	0.32
17^{th}	0.07	0.07	0.32
THD	3.38	3.39	6.64

4.3.2 Second Order LPF Implementation

The results of Second order LPF implementation in the extraction unit, however, gives a better current harmonics mitigation compared with the first order LPF. Referring to the second order LPF equation in section 3.3.1, the harmonics current during compensation are presented in figure 4.9(a)- (f).

4.3.2.1 Second Order LPF PCC Current with Compensation

With a damping ratio of 0.707 and a cut-off frequency of 50Hz, the PCC current before compensation was reduced to 1.25%, 1.26% and 11.29% from 21.63%, 21.18% and 43.49% over a firing angle of 0^0, 30^0 and 60^0 respectively, as seen in figure 4.9 (a) –(f).

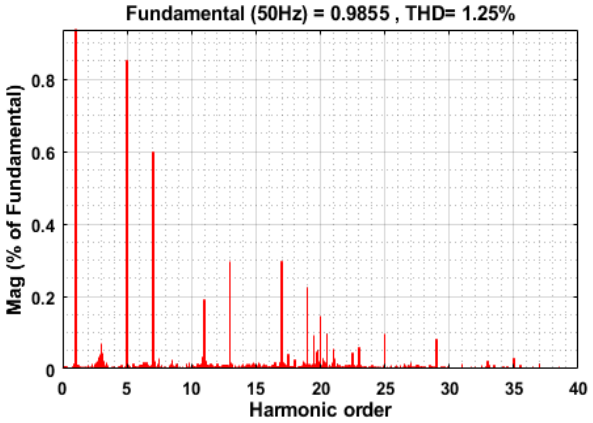

(a)

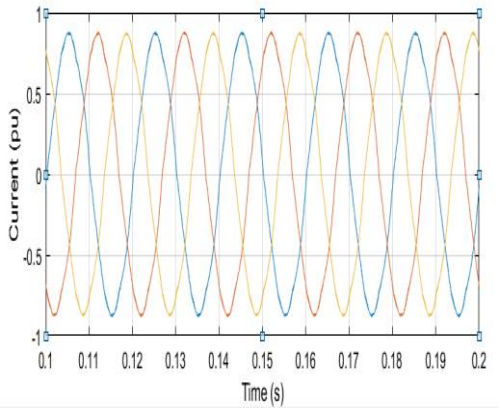

(b)

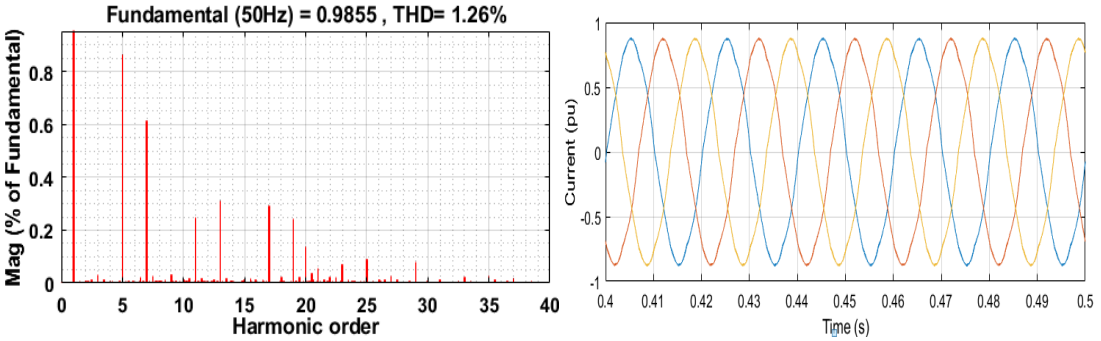

(c) (d)

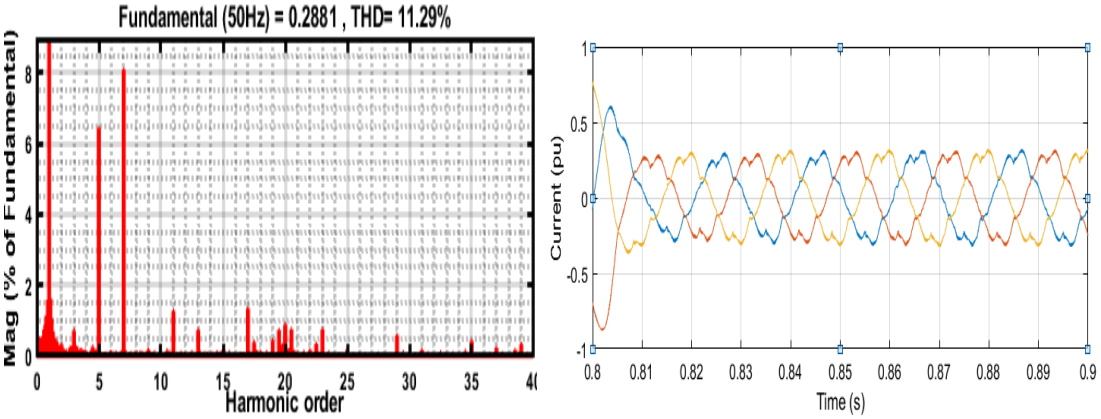

(e) (f)

Figure 4.9: PCC current with compensation. (a) current waveform spectrum at $\alpha = 0°$, (b) current waveform at $\alpha = 0°$, (c) current waveform spectrum at $\alpha = 30°$, (d) current waveform at $\alpha = 30°$, (e) current waveform spectrum at $\alpha = 60°$ and (f) current waveform at $\alpha = 60°$.

The dataset represented by the second order LPF PCC current waveform after compensation shown in figure 4.9 (a) - (f) is given in Table 4.4.

Table 4.4: PCC current before and after compensation for 2nd order LPF

PCC current Without Compensation				PCC current after Compensation		
Harmonics	$\alpha=0^0$ %	$\alpha= 30^0$ %	$\alpha=60^0$ %	$\alpha=0^0$ %	$\alpha=30^0$ %	$\alpha=60^0$ %
5th	18.88	19.60	37.89	0.86	0.87	6.44
7th	6.60	6.81	12.58	0.60	0.62	8.10
11th	3.30	3.34	11.86	0.21	0.25	1.27
13th	1.58	1.65	8.50	0.30	0.31	0.73
17th	1.35	1.38	5.58	0.30	0.29	1.34
THD	21.63	21.18	43.49	1.25	1.26	11.29

Table 4.4 shows the PCC current before and after compensation. The table shows that the second order LPF is more effective in the extraction unit compare with the first order LPF, while the former reduces the PCC current before compensation to 1.25%, 1.26% and 11.29%, the latter reduced it to 3.89%, 3.69% and 9.59% respectively.

4.3.2.2 Transient Response of Second order LPF

The transient Performance of second-order LPF harmonics extraction unit of APF configuration shows that the settling time occurs at time t =0.025 while the rise time is 0.0080sec as shown in Figure 4.10. There was an approximate overshoot of 7.14%.

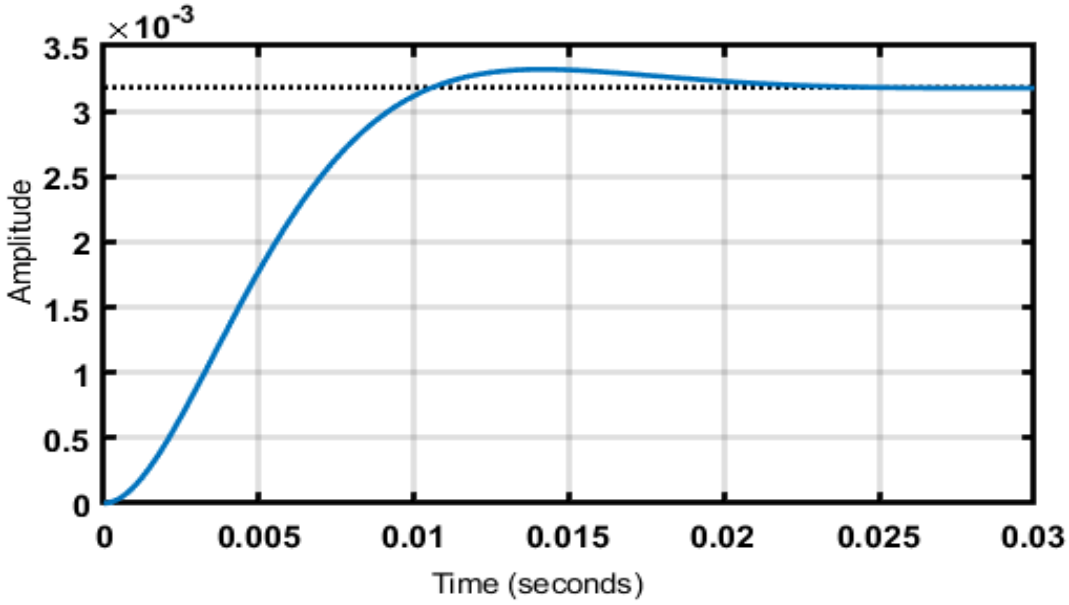

Figure 4.10: Second order LPF Transient Response

4.3.2.3 Second Order LPF Steady State Error

The steady-state performance of second order LPF of the APF extraction unit is shown in Table 4.5. The table shows considerable reduction in harmonics signal present during steady-state when compared with first order LPF.

Table 4.5: Second order LPF steady-state error

Harmonics	$\alpha = 0^0$ (%)	$\alpha = 30^0$ (%)	$\alpha = 60^0$ (%)
5^{th}	0.57	0.56	1.07
7^{th}	0.18	0.19	0.13
11^{th}	0.03	0.03	0.09
13^{th}	0.01	0.01	0.03
17^{th}	0.01	0.01	0.01
THD	0.61	0.59	1.13

4.4 High Pass Filter Implementation

The implementation block diagram of HPF consist of *abc* to *dq* conversion algorithm from the load current as shown in Figure 4.11. The reference signal is fed into the filter circuit, since HPF allows signal $\geq f_c$ to pass through and block signal less, the implemented cut-off frequency is $>$ 50Hz. Hence only the harmonic signal passes through the filter. The fundamental load current is obtained by subtracting the harmonics signal from the reference signal.

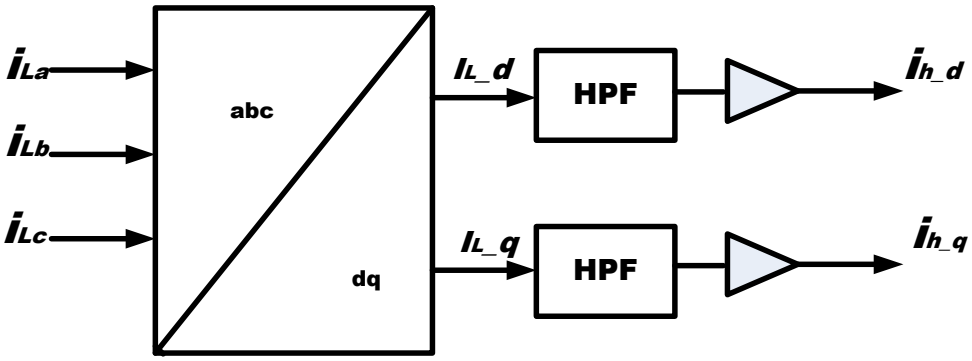

Figure 4.11: HPF implementation block diagram.

4.4.1 First Order HPF Implementation

The result obtained from the current extraction unit of the APF when first order HPF was implemented is based on the transfer function (TF) given as:

$$TF_{(s)HPF} = \frac{s}{S+\omega_0} \quad 4.2$$

4.4.1.1 PCC Current with Compensation

The same load current at the PCC is applied to the HPF in the extraction unit, the converter current tracked the harmonics content so as to suppress the detected harmonics signal, the PCC current decreases from 21.63% to 4.03% for $\alpha=0^0$, 21.18%

to 3.71% at α=30^0 and 43.49% to 9.59% at α=60^0. This is illustrated in Figure 4.12 (a)-(f).

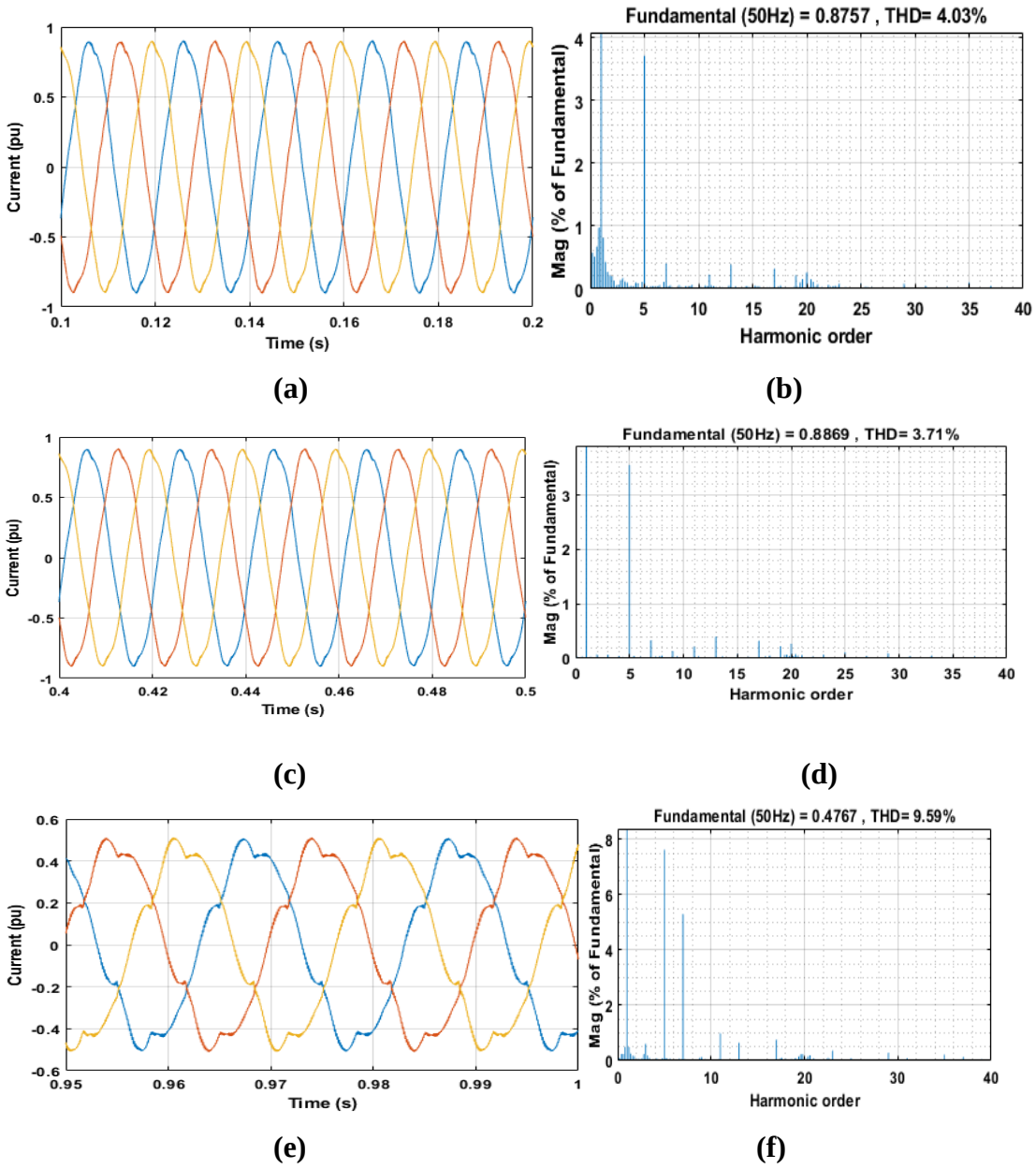

Figure 4.12: first order HPF PCC current with compensation. (a) current waveform at $\alpha = 0°$, (b) current waveform spectrum $\alpha = 0°$, (c) current waveform at $\alpha = 30°$, (d) current waveform spectrum $\alpha = 30°$, (e) current waveform at $\alpha = 60°$ and (f) current waveform spectrum $\alpha = 60°$.

From the waveform and FFT spectrum presented in Figure 4.12, the corresponding dataset relative to the fundamental are shown in Table 4.6

Table 4.6: PCC current before and after compensation for first order HPF

PCC current without compensation				PCC current with compensation		
Harmonics	$\alpha = 0^0$ %	$\alpha = 30^0$ %	$\alpha = 60^0$ %	$\alpha = 0^0$ %	$\alpha = 30^0$ %	$\alpha = 60^0$ %
5^{th}	18.88	19.60	37.89	3.72	3.55	7.63
7^{th}	6.60	6.81	12.58	0.40	0.33	5.30
11^{th}	3.30	3.34	11.86	0.23	0.21	0.99
13^{th}	1.58	1.65	8.50	0.39	0.40	0.65
17^{th}	1.35	1.38	5.58	0.32	0.32	0.76
THD	21.63	21.18	43.49	4.03	3.71	9.59

4.4.1.2 Transient Response of First order HPF

The transient response of first-order HPF shows that the settling time occurs at time t = 0.018 while the rise time is 0.006sec as shown in Figure 4.13. There was no overshoot.

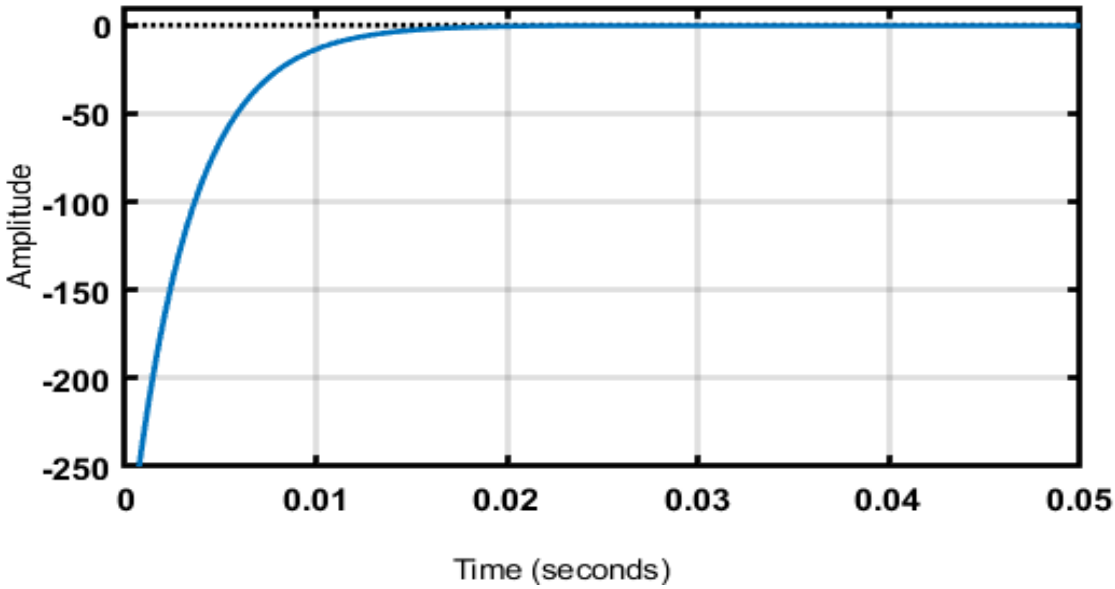

Figure 4.13: first order HPF transient response

4.4.1.3 First Order HPF Steady State performance

Steady-state performance of first order HPF harmonics extraction scheme reveal the presence of 6.63% error at $\alpha = 60^0$, 3.39% at $\alpha = 30^0$ and 3.40% at $\alpha = 0^0$ respectively as shown in Table 4.7.

Table 4.7: first order HPF steady-state error

Harmonics	$\alpha = 0^0$ (%)	$\alpha = 30^0$ (%)	$\alpha = 60^0$ (%)
5^{th}	3.19	3.20	6.25
7^{th}	1.09	1.09	1.97
11^{th}	0.26	0.28	0.97
13^{th}	0.13	0.13	0.31
17^{th}	0.08	0.07	0.32
THD	3.40	3.39	6.63

4.4.2 Second Order HPF Implementation

The current waveform and current waveform spectrum in Figure 4.14 show the PCC current for second order HPF implementation in the extraction unit of the APF during compensation. This implementation applied Equation 3.8 with $\xi = 0.6$, for $\alpha = 0°$, 30^0 and 60^0 respectively. The percentage total harmonic distortions present in the load current was observed to have been reduced from21.63%, 21.18% and 43.49% to 1.87%, 1.82% and 10.42% as seen in Figure 4.14 (a)-(f). The corresponding data for the 5^{th}, 7^{th}, 11th, 13th, and 17^{th} harmonics are presented in Table 4.8.

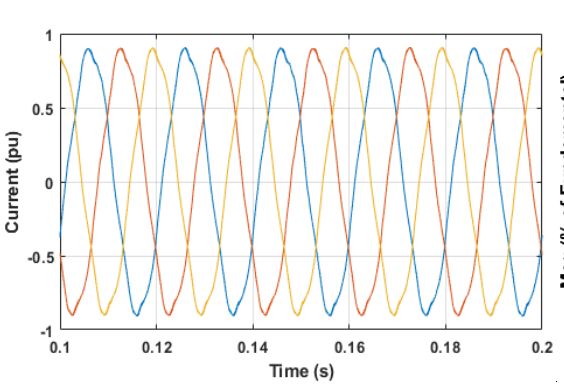

(a)

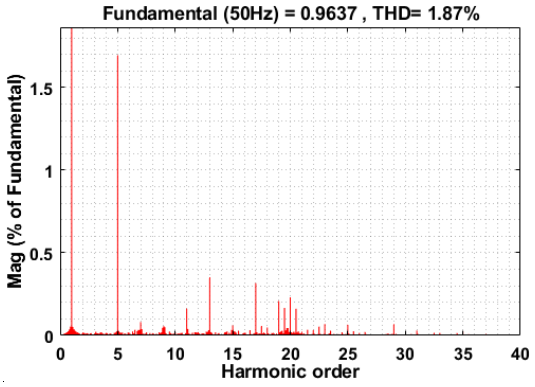

(b)

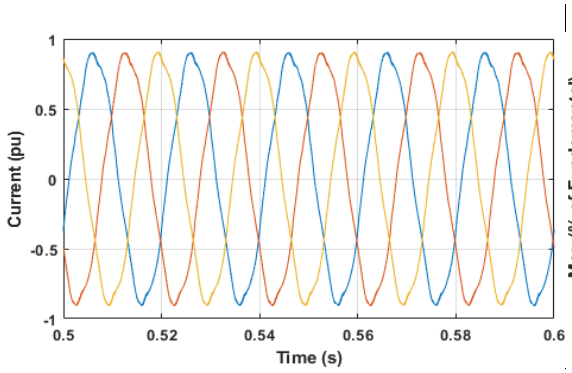

(c)

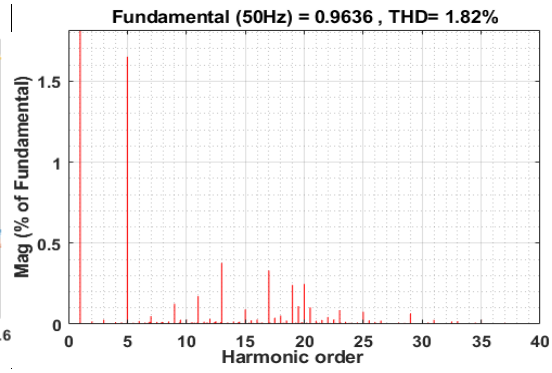

(d)

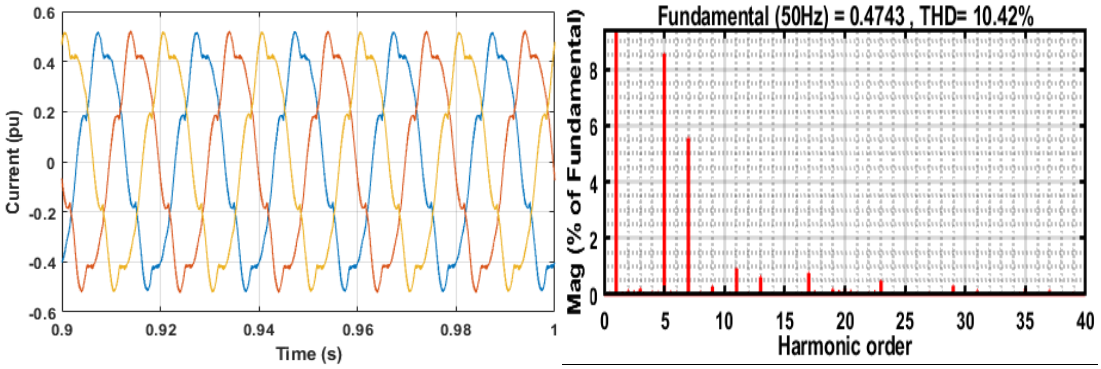

(e) (f)

Figure 4.14: Second order HPF PCC current with compensation. (a) current waveform at $\alpha = 0°$, (b) current waveform spectrum $\alpha = 0°$, (c) current waveform at $\alpha = 30°$, (d) current waveform spectrum $\alpha = 30°$, (e) current waveform at $\alpha = 60°$ and (f) current waveform spectrum $\alpha = 60°$.

4.4.2.1 PCC current with compensation

Table 4.8 shows the PCC current before and after compensation of the APF with 2nd order HPF in the extraction unit.

Table4.8: PCC current before and after compensation for 2nd order HPF.

PCC Current without compensation				PCC Current with compensation		
Harmonics	$\propto = 0°$ (%)	$\propto = 30°$ (%)	$\propto = 60°$ (%)	$\propto = 0^0$ (%)	$\alpha = 30°$ (%)	$\propto = 60^0$ (%)
5th	18.88	19.60	37.89	1.69	1.65	8.55
7th	6.60	6.81	12.58	0.03	0.05	5.55
11th	3.30	3.34	11.86	0.16	0.17	0.92
13th	1.58	1.65	8.50	0.35	0.38	0.62
17th	1.35	1.38	5.58	0.32	0.33	0.76
THD	21.63	21.18	43.49	1.87	1.82	10.42

.

4.4.2.2 Transient Response of Second Order HPF

Second-order HPF transient Performance of extraction unit of the APF shown in Figure 4.20, shows that the system attain steady-state at time t = 0.05sec while the rise time is 0.007sec. The 2nd order HPF however has a 9.5% overshoot, this can be attributed to the small damping ratio used.

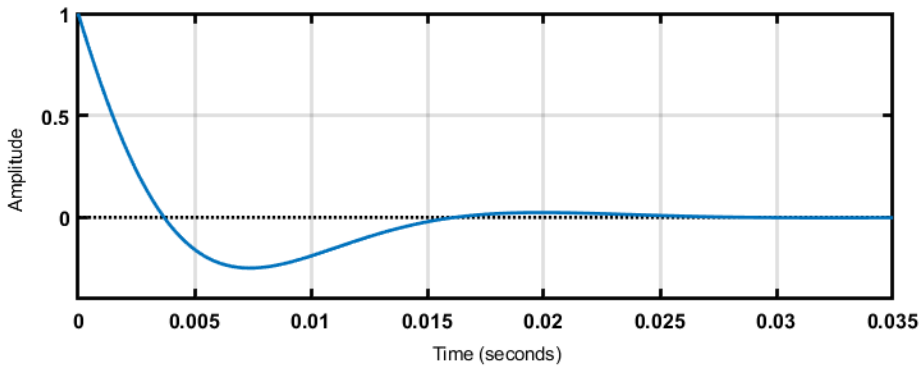

Figure 4.15: Second order HPF transient response

4.4.2.3 Second HPF Steady State performance

The steady-state response of second-order HPF is shown in Table 4.9 reveal that the error is highest at $\alpha = 60^0$ with THD = 5.70 and lowest at $\alpha = 0^0$ with THD = 2.89.

Table4.9: Second order HPF steady state error

Harmonics	$\alpha = 0^0$ (%)	$\alpha = 30^0$ (%)	$\alpha = 60^0$ (%)
5^{th}	2.67	2.66	5.25
7^{th}	0.89	0.89	1.64
11^{th}	0.22	0.21	0.77
13^{th}	0.10	0.10	0.24
17^{th}	0.06	0.06	0.25
THD	2.89	2.82	5.70

4.5 BSF Implementation

Band stop filter implementation block diagram is shown in Figure 4.16 (a) and (b). The transfer function of the BPF used in the APF extraction scheme is given as

$$\boldsymbol{T.F}_{(s)BSF} = \frac{s^2+{\omega_0}^2}{s^2+2\xi\omega_0 s+{\omega_0}^2} \qquad 4.3$$

The analysis of the data in section 4.1 reveals that the 5^{th}, 7^{th} 11^{th}, 13^{th} and 17^{th} current harmonics are the most significant in LMU LVD network that should be suppressed. To achieve this in the extraction unit of the APF, five BSF was cascaded in series with angular frequencies of 942.4rad/s, 1571 rad/s , 2199rad/s, 2827.4rad/s and 3456rad/s respectively as shown in Figure4.16 (b). The response of the extraction unit is represented by the Bode plot in Figure4.16 (c). The arrangement shows that selective

harmonics cancellation can be achieved depending on the harmonics contents prevalent on the network.

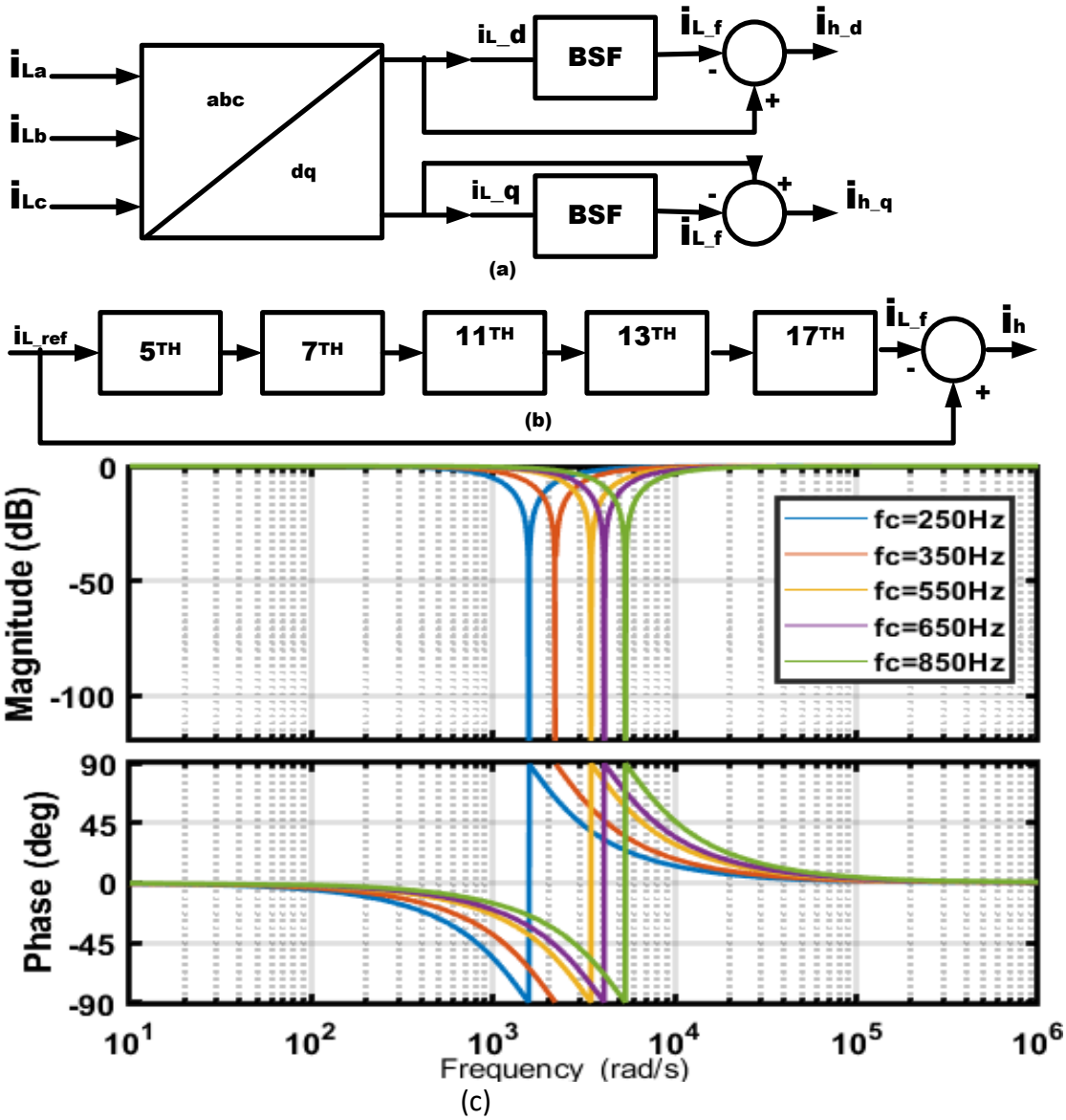

Figure 4.16: (a) BSF implementation block diagram, (b) cascaded BSP, (c) BSF Bode plot.

4.5.1 PCC Current with Compensation

Figure 4.17 (a)-(f) show the result of Band Stop Filter implemented in the extraction unit of APF scheme, with cutoff frequencies of 250Hz, 350Hz, 550Hz, 650Hz and 850Hz and damping ratio of 0.7071, when $\alpha =$ changes from 0^0 to 60^0 .

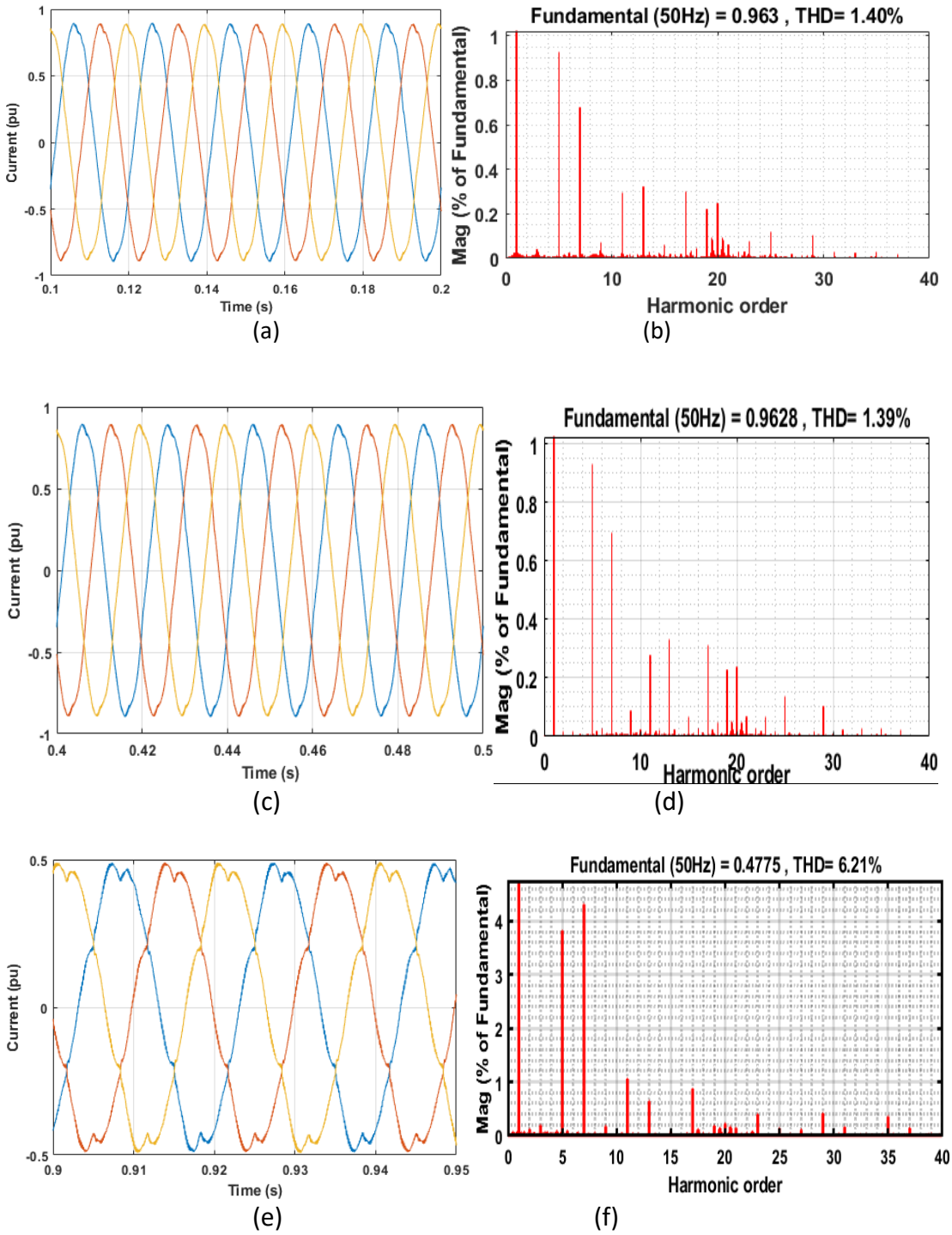

Figure 4.17: Second order BSF PCC current with compensation. (a) current waveform at $\alpha = 0°$, (b) current waveform spectrum $\alpha = 0°$, (c) current waveform at $\alpha = 30°$, (d) current waveform spectrum $\alpha = 30°$, (e) current waveform at $\alpha = 60°$ and (f) current waveform spectrum $\alpha = 60°$.

The distorted waveform and FFT spectrum shows that the harmonics level after extraction unit was minimal with THD within IEEE 519-1992 recommended limit except at $\alpha = 60°$.

Table 4.12 shows BSF PCC current before and after compensation. From the table, it is observed that after filtering and compensation, there was a significant decrease in the current harmonics and THD values.

Table4.10: PCC current before and after compensation for 2nd order BSF.

PCC Current Without compensation				PCC Current With compensation		
Harmonics	$\alpha = 0^0$ (%)	$\alpha = 30^0$ (%)	$\alpha = 60^0$ (%)	$\alpha = 0^0$ (%)	$\alpha = 30^0$ (%)	$\alpha = 60^0$ (%)
5th	18.88	19.60	37.89	0.93	0.93	3.82
7th	6.60	6.81	12.58	0.68	0.70	4.31
11th	3.30	3.34	11.86	0.29	0.28	1.06
13th	1.58	1.65	8.50	0.32	0.33	0.64
17th	1.35	1.38	5.58	0.30	0.31	0.87
THD	21.63	21.18	43.49	1.04	1.39	6.21

4.5.2 Transient Response of BSF

The transient Performance of the second-order BSF in the extraction unit of the APF shown in Figure 4.18 reveals that the system settling time occurs at time t =0.00014 while the rise time is 0.000317sec as shown in Figure 4.28. There was an overshoot of approximately 1.6%.

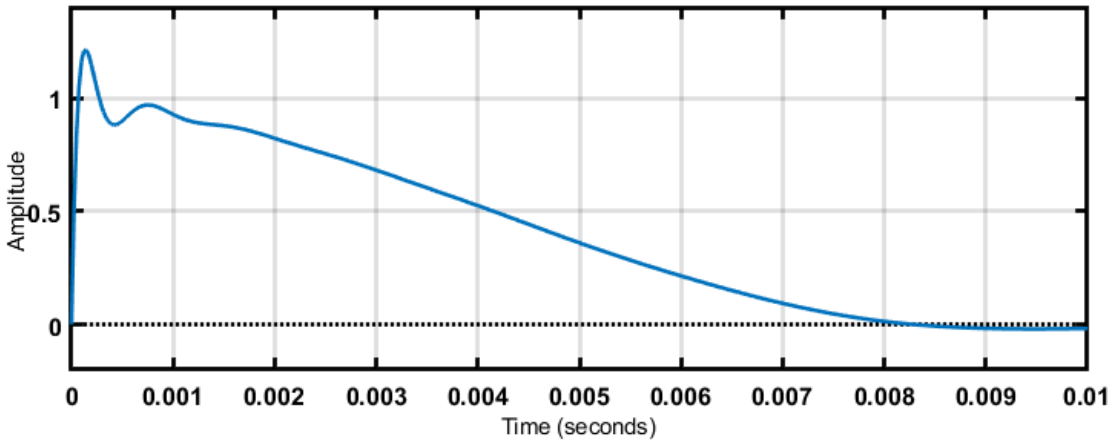

Figure 4.18: BSF Transient Response

4.5.3 BSF Steady State Performance

The steady-state error in current harmonics values for BSF is shown in Table 4.13; the steady-state is highest at $\alpha = 60^0$ with THD = 2.78% however the performance is better compare with the response of LPF and HPF.

Table 4.11: BSF steady-state Analysis

Harmonics order	$\alpha = 0^0$ (%)	$\alpha = 30^0$ (%)	$\alpha = 60^0$ (%)
5^{th}	0.19	0.22	0.50
7^{th}	0.02	0.04	0.20
11^{th}	0.06	0.05	0.13
13^{th}	0.02	0.03	0.02
17^{th}	0.01	0.00	0.03
THD	1.02	0.71	2.78

4.6 Comparative Analysis

Comparative analysis of the simulated LPF, HPF and BSF used in the current harmonics extraction unit of APF are based on the following:

4.6.1 Transient performance

Transient performance of the various extraction methods are expressed in terms of rise time, settling time and overshoot as shown in Table 4.12. The results show that the settling time of BSF is the smallest at 0.00014seconds, compared to other filters implemented in the extraction unit, this show that it attain steady-state faster than others as seen in Figure 4.19. The first order LPF, HPF responses do not have overshoot as shown in Table 4.12, this is because the overshoot is a function of the damping ratio. In terms of second order systems with overshoot, the settling time indicate the time it takes to attain steady-state.

Table 4.12: Transient performance

	Settling time(sec)	Rise time(sec)	Overshoot
1^{st} LPF	0.002	0.005	----
2^{ND} LPF	0.025	0.008	7.14%
1^{ST} HPF	0.018	0.006	-----
2^{ND} HPF	0.05	0.0070	9.5%
BSF	0.00014	0.000317	1.6%

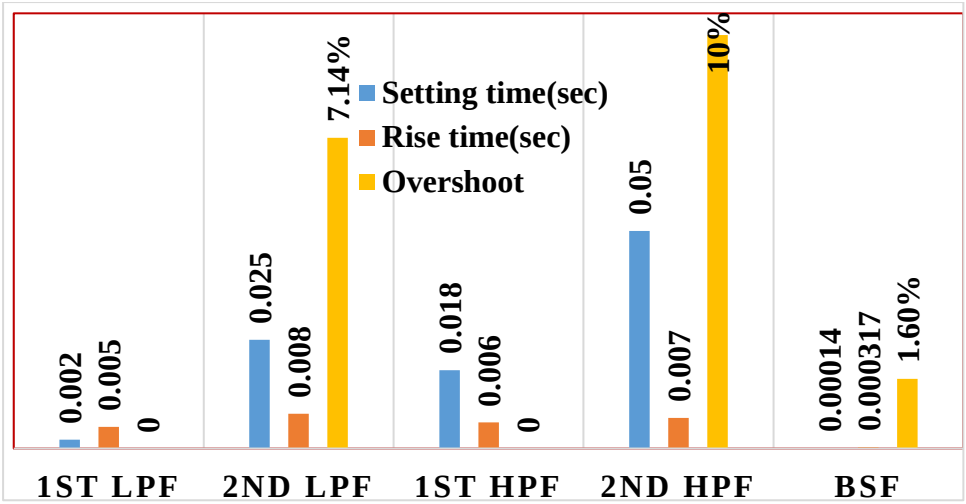

Figure 4.19: Transient performance of LPF, HPF and BSP

4.6.2 Steady State performance

The comparison of Steady-State performance of LPF, HPF and BSF implemented in the current extraction unit of APF are presented in Figure 4.20 (a)-(d). The performance of BSF and second order LPF give an excellent result because their respective percentage THD values (shown in appendix B1-B3) are within the less than 5% standard expected for current harmonics. Although the first and second order HPF performance could not sufficiently reduce the 5^{th} harmonics at $\alpha = 60°$ as shown in Figure 4.20 (a) and (d), this is due to the inherent delay in turning on the thyristor used as the load current, as the turn on delay increases, from at $\alpha = 0°$ to 60° the more the thyristor behave as an inductive load, the more the current lag the voltage.

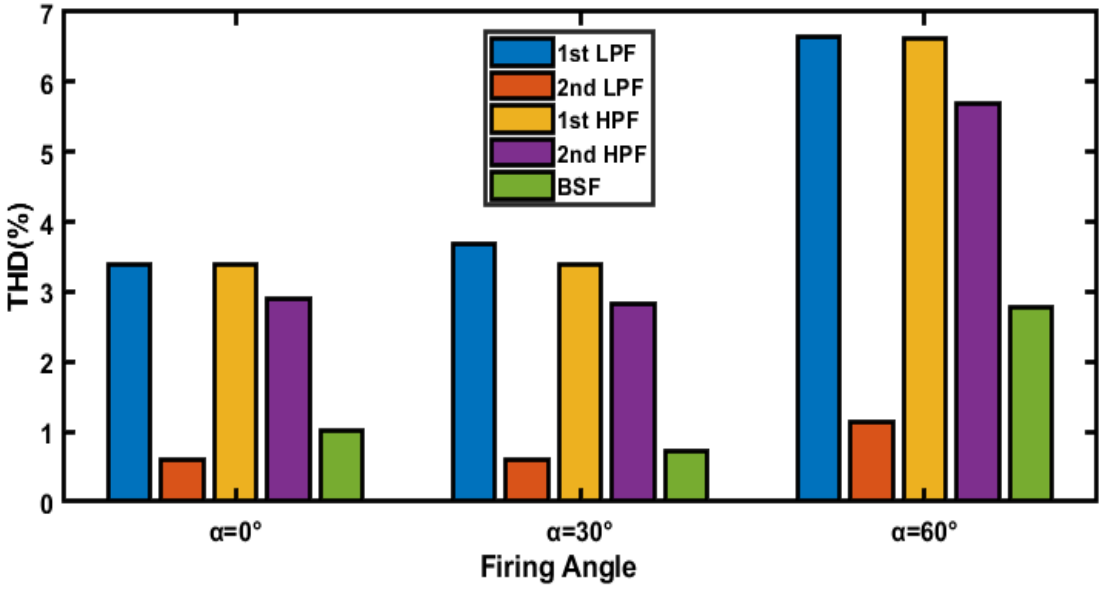

(a)

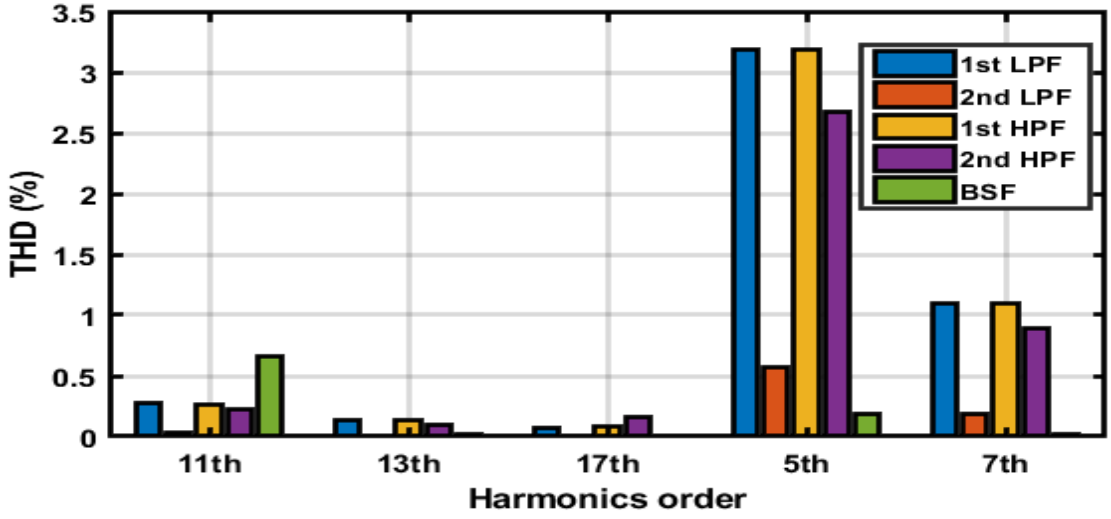

(b)

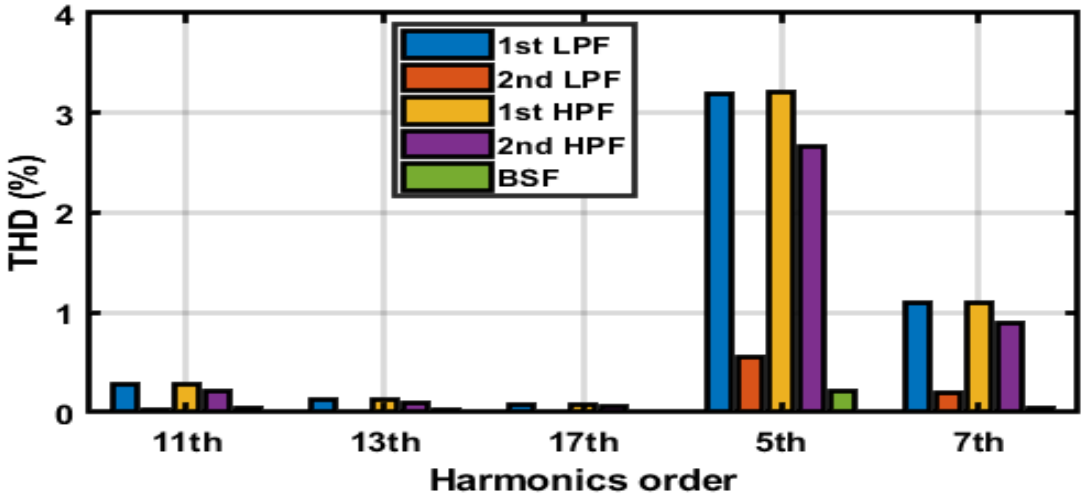

(c)

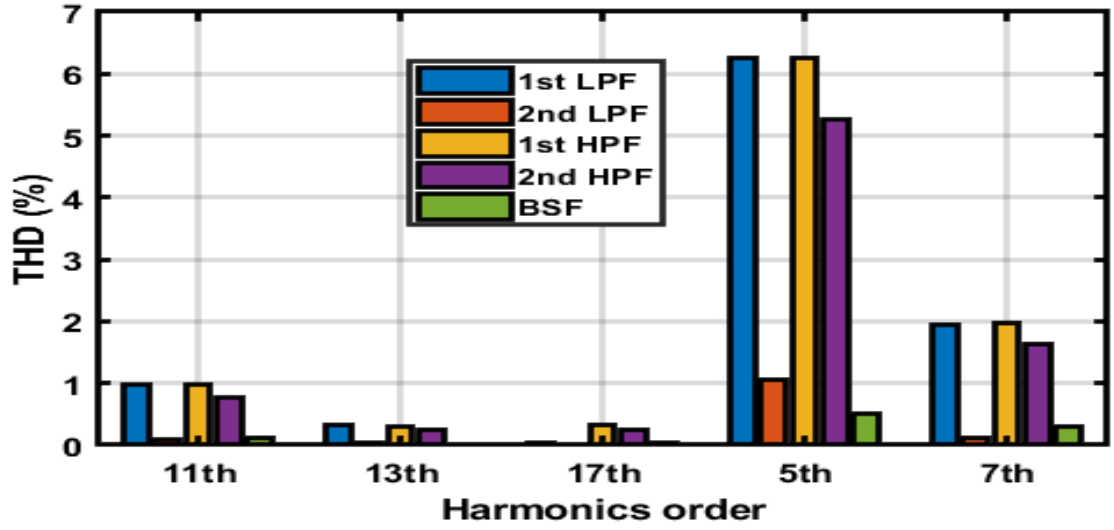

(d)

Figure 4.20: Steady State performance of LPF, HPF and BSF (a) percentage THD (b) at $\alpha = 0°$, (c) at $\alpha = 30°$ and (d) at $\alpha = 60°$.

4.6.3 Comparison of THD between Extraction Unit and PCC Current

THD error Analysis between the extraction unit and PCC current after Compensation is shown in Figure 4.21. From figure 4.21, it can be observed that there are tracking error as the firing angle (α) changes from 0° to 60°. This indicate imperfect tracking and cancellation of the harmonics current. This is due to the delay experience in the process of extraction and the current controller unit of the APF scheme. The corresponding dataset are presented in appendix B4.

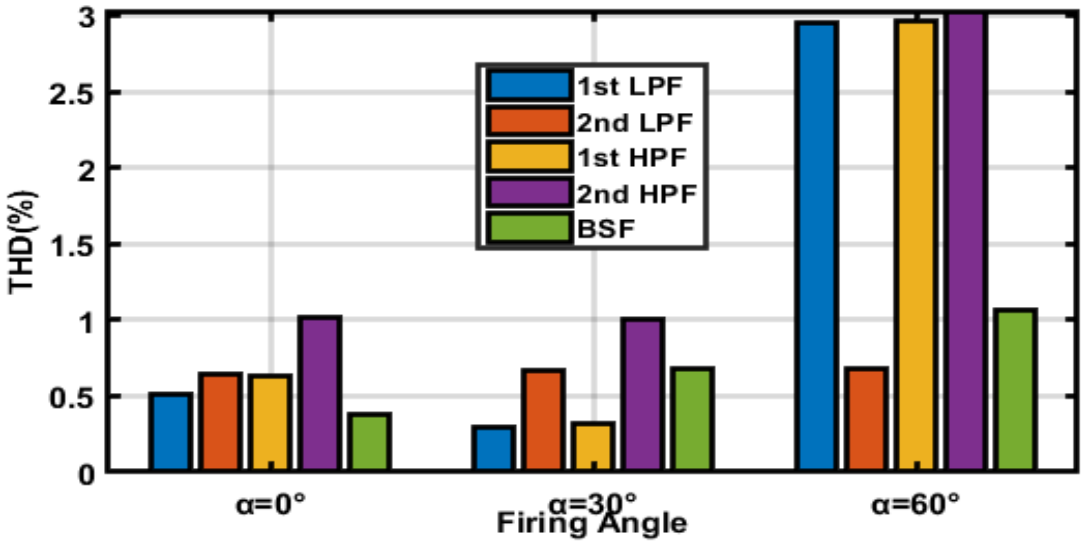

Figure 4.21: THD Analysis between extraction unit and PCC current after Compensation

4.6.4 Comparison of THD After compensation

The comparison of percentage THD of 1st and 2nd order LPF and HPF and BSF used in the current extraction unit are given in Table 4.13. The bar chart analysis of the percentage comparison of THD of 1st and 2nd order LPF and HPF; and BSF of the implemented extraction unit of APF are shown in Figure 4.22, it can be observed that the resultant THD of the first and second order LPF, HPF and BSF are within the recommended (less than 5%) limit at a firing angle of 0^0 and 30^0. However, the percentage THD at $\alpha = 60°$ is higher than 5% required limit for current harmonics values. This is attributed to the distorted waveform resulting from the harmonics contents above the 17th current harmonics considered at $\alpha = 60°$. The 23rd, 29th, 31st and 35th harmonics present at the load current are 3.51%, 2.13%, 0.58% and 1.72% respectively.

Table4.13: THD PCC current during Compensation

Firing angle (α)	1st LPF (%)	2nd LPF (%)	1st HPF (%)	2nd HPF (%)	BSF (%)
0^0	3.39	1.25	4.03	1.87	1.40
30^0	3.69	1.26	3.71	1.82	1.39
60^0	9.59	11.29	9.59	10.42	6.21

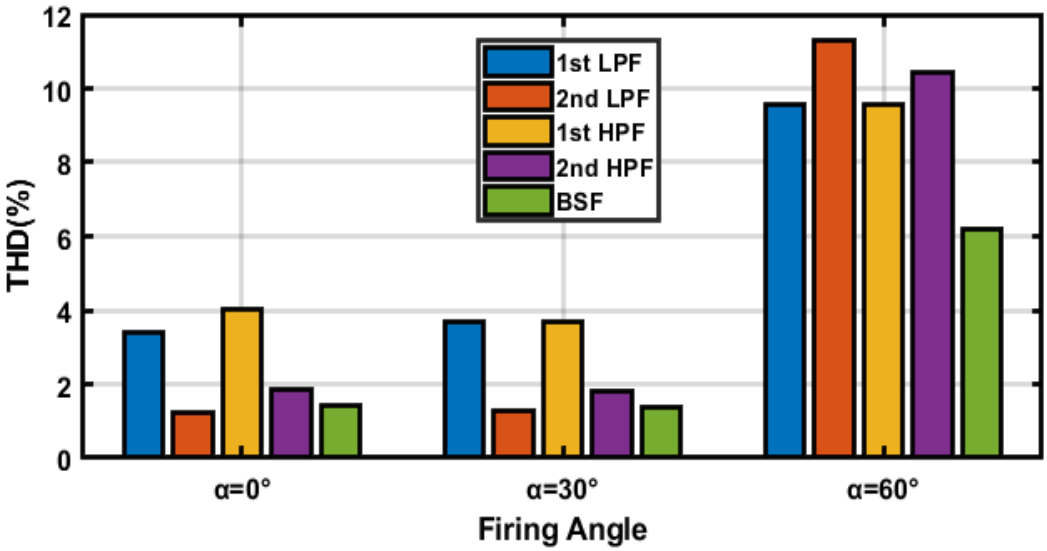

Figure 4.22: Comparison of THD after Compensation

To reduce the high percentage THD value associated with 60° firing angle, BSF implemented in the extraction unit was expanded to extract up to the 37th harmonics, the implemented circuit is shown in Figure 4.23.

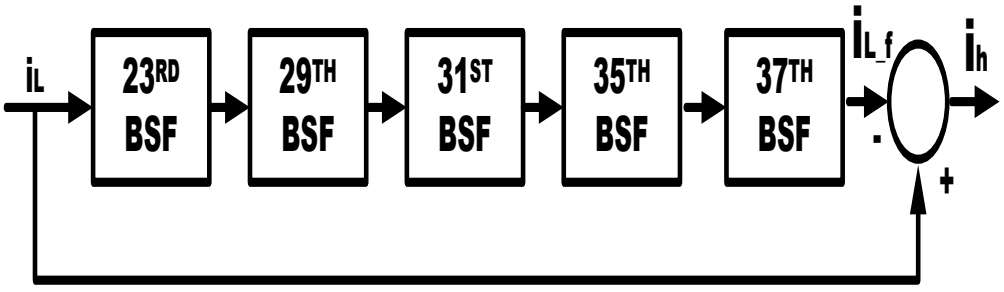

Figure 4:23: Cascaded Band Stop Filter

The results of the simulation reveal the superiority of the BSF over LPF and HPF in the extraction unit of active power filter scheme in removing specific harmonic from the network. The FFT plot and the sinusoidal waveform obtained are given in Figure 4.24 (a)-(b).

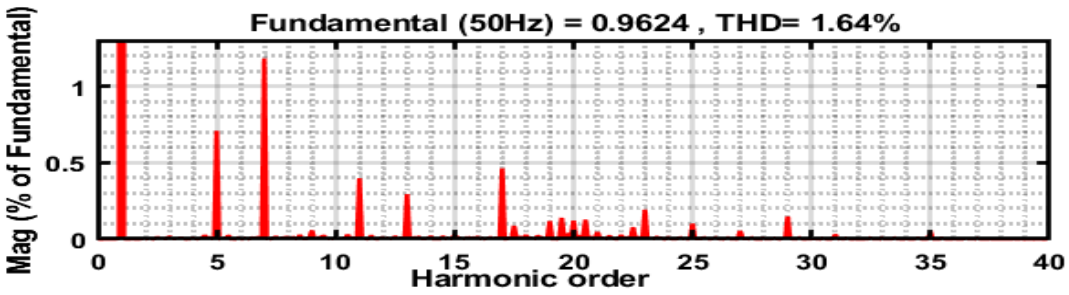

(a)

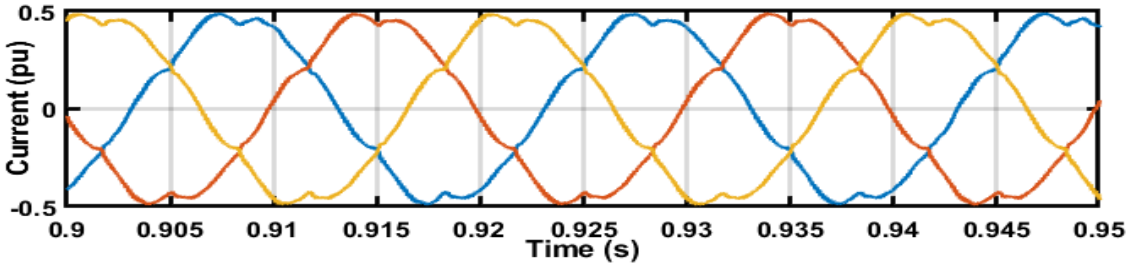

(b)

Figure 4.24: BSF response at $\alpha = 60°$ (a) FFT plot (b) waveform

The percentage THD has been reduced to 1.64% from the 43.49% with a better waveform.

CHAPTER FIVE

CONCLUSION AND RECOMMENDATIONS

5.1 Conclusion

In this research, current harmonics extraction unit of the active power filter (APF) was investigated. The performance of first and second LPF and HPF and BSF was studied under balanced condition of LVD network. The implementation was done by using a three phase thyristor rectifier load similar to the measured current harmonics data obtained in LMU LVD network. This investigation considered the transient and steady-state response of each filter implemented in the extraction unit of AFP. It was observed that the current harmonics present at PCC before compensation was significantly removed after compensation. The steady-state performance also revealed a low level of steady-state error after compensation with first and second LPF, HPF and BSF. The highest steady-state error was however observed with the 2nd order HPF filter as shown in figure4.21. The transient response of each of the filter circuit implemented in the extraction unit of the APF show that first-order LPF, HPF and BSF are satisfactory, it was noticed that first order LPF and HPF attain steady state faster because of the absence of overshoot. The difference between the FFT before and after implementation of the filter circuit in the extraction unit of APF shows that BSP is effective in stopping specific harmonics content across the implemented firing angle. The resultant THD of first and second-order LPF, HPF and BSF implemented in the extraction unit are within the recommended limit at a firing angle of 0^0 and 30^0. However, THD analysis between the extraction unit and PCC current after Compensation reveal a slight error, this is due to the effect of the delay in the extraction unit and the current controller unit of the APF scheme.

5.2 Recommendation for Further Work

Further study can be done to improve and enhance the quality of the extraction unit of the APF for harmonics mitigation.

The following are suggested for future work.

i. The use of series active power filter for voltage harmonics mitigation with the investigated filter in the extraction unit.
ii. The performance of LPF, HPF and BSF configuration in APF extraction unit in unbalanced network.

iii. Further research can also be done to improve the current control by selecting a suitable scale for a modified current prediction control technique.

iv. Finally, similar investigation can be carried out on LVD network line of the three phase four wire and unbalanced network.

5.3 Contribution to Existing Knowledge

The contribution to knowledge of this investigation are summarized below:

i. The research developed a cascaded band stop filter (BSF) extraction unit capable of extracting specific dominant harmonics up to the 37^{th} category.

ii. The research also established that the Landmark University Low voltage Distribution (LVD) network has harmonics above 5% Total harmonics distortion (THD).

REFERENCE

Agrawal, S., Kumar, P., and Palwalia, D. K. (2017). Artificial neural network based three phase shunt active power filter. *2016 IEEE 7th Power India International Conference, PIICON 2016*. https://doi.org/10.1109/POWERI.2016.8077153

Agrawal, S., Sharma, D., and Palwalia, D. K. (2018). Performance analysis of SAPF based on self tuned harmonic filter with fuzzy logic controller. *2017 Recent Developments in Control, Automation and Power Engineering, RDCAPE 2017*, 487–492. https://doi.org/10.1109/RDCAPE.2017.8358320

Akagi, H. (1999). A shunt active filter based on voltage detection for harmonic termination of a radial power distribution line. *IEEE Transactions on Industry Applications*, *35*(3). https://doi.org/10.1109/28.767015

Al-bakry, A. A. A., Wadday, A. G., Yasin, N. M., and Sultan, A. J. (2018). *A novel Technique for Electrical Power System Harmonics Identification Based on Blind Source Extraction (BSE). 13*(8), 6004–6008.

Al-Ogaili, A. S., Ramasamy, A., Hoon, Y., Verayiah, R., Marsadek, M., Juhana, T., and Rahmat, N. A. (2020). Time-domain harmonic extraction algorithms for three-level inverter-based shunt active power filter under steady-state and dynamic-state conditions-an evaluation study. In *International Journal of Electrical and Computer Engineering* (Vol. 10, Issue 6, pp. 5609–5620). https://doi.org /10.11591/ijece.v10i6.pp5609-5620

Amamra, S. A., Tripathy, Y., Barai, A., Moore, A. D., and Marco, J. (2020). Electric vehicle battery performance investigation based on real world current harmonics. *Energies*, *13*(2). https://doi.org/10.3390/en13020489

Anandh, N., D'Sa, P. A., Gautam, M. V, and Sandeep, V. S. (2017). Power quality estimation, analysis and improvement for uninterrupted power supply. *2016 International Conference on Control Instrumentation Communication and Computational Technologies, ICCICCT 2016*, *March*, 26–31. https://doi.org/ 10.1109/ICCICCT.2016.7987914

Annapoorani, I., and Samikannu, R. (2017). *Series Active Power Filter for Power Quality Improvement Based on Distributed Generation*. *12*(22), 12214–12218.

Baliyan, A., Jamil, M., Rizwan, M., Alsaidan, I., & Alaraj, M. (2021). *An Intelligent PI Controller-Based Hybrid Series Active Power Filter for Power Quality Improvement*. *2021*.

Büyük, M., İnci, M., Tan, A., and Tümay, M. (2019). Improved instantaneous power theory based current harmonic extraction for unbalanced electrical grid conditions. *ElectricPower Systems Research*, *177*. https://doi.org/10.1016/j.epsr.2019.106014

Chishti, F., Murshid, S., and Singh, B. (2021). Frequency Adaptive Multistage Harmonic Oscillator for Renewable-Based Microgrid under Nonideal Grid Conditions. *IEEE Transactions on Industrial Electronics*, *68*(1), 358–369. https://doi.org/10.1109/TIE.2020.2965474

Deokar, S. A., and Waghmare, L. M. (2011). Impact of power system harmonics on insulation failure of distribution transformer and its remedial measures. *ICECT 2011 - 2011 3rd International Conference on Electronics Computer Technology*, *3*, 136–140. https://doi.org/10.1109/ICECTECH.2011.5941817

Dubey, A. K., Mishra, J. P., and Kumar, A. (2021). Performance improvement of shunt active power filter under variable grid frequency condition using complex coefficient filter-frequency locked loop. *International Journal of Circuit Theory and Applications*, *49*(4), 1164–1181. https://doi.org/10.1002/cta.2920

Ebadian, M., Talebi, M., and Ghanizadeh, R. (2015). A New Approach Based on Instantaneous Power Theory for Improving the Performance of UPQC Under Unbalanced and Distortional Load Conditions. *Automatika – Journal for Control, Measurement, Electronics, Computing and Communications*, *56*(2). https://doi.org/10.7305/automatika.2015.07.750

G. Srinivas, P. Sai Kumar, K. Anuhya, and V. Hyndavi. (2020). Current Harmonic Reduction on Source Side by using ANN Controller. *International Journal of Engineering Research And*, *V9*(05), 871–877. https://doi.org/10.17577 /ijertv 9is050579

Gurguiatu, G., Vechiu, I., and Munteanu, T. (2011). Power quality improvement using renewable energy. *Renewable Energy and Power Quality Journal*, *March 2015*, 735–738. https://doi.org/10.24084/repqj09.437

He, J., and Li, Y. W. (2013). Hybrid voltage and current control approach for dg-grid interfacing converters with LCL filters. *IEEE Transactions on Industrial Electronics*, *60*(5), 1797–1809. https://doi.org/10.1109/TIE.2012.2190374

He, J., Li, Y. W., Blaabjerg, F., and Wang, X. (2014). Active harmonic filtering using current-controlled, grid-connected DG units with closed-loop power control. *IEEE Transactions on Power Electronics*, *29*(2), 642–653. https://doi.org/10.1109/ TPEL.2013.2255895

Hoon, Y., Amran, M., Radzi, M., Hassan, M. K., and Mailah, N. (2016). *Three-phase Three-level Shunt Active Power Filter with Simplified Synchronous Reference Frame*. *November*. https://doi.org/10.1109/IEACON.2016.8067346

Hoon, Y., Radzi, M. A. M., Hassan, M. K., and Mailah, N. F. (2017). Control algorithms of shunt active power filter for harmonics mitigation: A review. In *Energies* (Vol. 10, Issue 12). https://doi.org/10.3390/en10122038

Hoon, Y., Radzi, M. A. M., Zainuri, M. A. A. M., and Zawawi, M. A. M. (2019). Shunt active power filter: A review on phase synchronization control techniques. In *Electronics (Switzerland)* (Vol. 8, Issue 7). https://doi.org/10.3390/ electronics 8070791

Hu, J., Liang, J., Ding, Y., Ding, A., Yin, Z., and Li, Z. (2020). Research on three-phase four-wire active power filter based on LCLCL coupling structure. *Journal of Physics: Conference Series*, *1544*(1). https://doi.org/10.1088/1742-6596/ 1544 /1/012075

Huang, H. (2018). *Analysis and Control of Modular Multilevel Cascaded Converter-Based Flexible AC Transmission Systems*. *September*.

Huang, H., Oghorada, O. J. K., Zhang, L., and Chong, B. V. P. (2018). *Harmonics and unbalanced load compensation by a modular multilevel cascaded converter active power conditioner; Harmonics and unbalanced load compensation by a modular multilevel cascaded converter active power conditioner*. https://doi.org /10.1049/joe.2018.8144

Huang, H., Oghorada, O. J. K., Zhang, L., and Chong, B. V. P. (2019). Harmonics and unbalanced load compensation by a modular multilevel cascaded converter active

power conditioner. *The Journal of Engineering*, *2019*(17), 3778–3783. https://doi.org/10.1049/joe.2018.8144

Huang, H., Zhang, L., Oghorada, O., and Mao, M. (2021). Analysis and Control of a Modular Multilevel Cascaded Converter-Based Unified Power Flow Controller. *IEEE Transactions on Industry Applications*, *57*(3), 3202–3213. https://doi.org/10.1109/TIA.2020.3029546

Izadian, A. (2019). Fundamentals of modern electric circuit analysis and filter synthesis: A transfer function approach. In *Fundamentals of Modern Electric Circuit Analysis and Filter Synthesis: A Transfer Function Approach*. https://doi.org/10.1007/978-3-030-02484-0

Jacob, A., Abraham, B. T., Prakash, N., and Philip, R. (2014). *A Review of Active Power Filters In Power System Applications*. 10253–10261.

Kalair, A., Abas, N., Kalair, A. R., Saleem, Z., and Khan, N. (2017). *Review of harmonic analysis , modeling and mitigation techniques*. *78*(May), 1152–1187.

Kanjiya, P., Khadkikar, V., and Zeineldin, H. H. (2015). Optimal control of shunt active power filter to meet IEEE Std. 519 current harmonic constraints under nonideal supply condition. *IEEE Transactions on Industrial Electronics*, *62*(2), 724–734. https://doi.org/10.1109/TIE.2014.2341559

Karimi-Ghartemani, M., Mokhtari, H., Iravani, M. R., and Sedighy, M. (2004). A signal processing system for extraction of harmonics and reactive current of single-phase systems. *IEEE Transactions on Power Delivery*, *19*(3), 979–986. https://doi.org/10.1109/TPWRD.2004.829942

Kashif, M., Hossain, M. J., Fernandez, E., Taghizadeh, S., Sharma, V., Ali, S. M. N., and Irshad, U. Bin. (2020). A Fast Time-Domain Current Harmonic Extraction Algorithm for Power Quality Improvement Using Three-Phase Active Power Filter. *IEEE Access*, *8*, 103539–103549. https://doi.org/10.1109/ ACCESS. 2020.2999088

Khan, H., Fernandes, B. G., and Kulkarni, A. (2018). Decoupled controller for simultaneous harmonic and unbalance compensation in a multifunctional RES system connected to a LV Distribution Grid. *2018 20th European Conference on*

Power Electronics and Applications, EPE 2018 ECCE Europe.

Klaić, Z., Knežević, G., Primorac, M., and Topić, D. (2020). Impact of photovoltaic and biogas power plant on harmonics in distribution network. *IET Renewable Power Generation*, *14*(1), 110–117. https://doi.org/10.1049/iet-rpg.2019.0528

Kryltcov, S., Makhovikov, A., and Korobitcyna, M. (2021). Novel approach to collect and process power quality data in medium-voltage distribution grids. *Symmetry*, *13*(3). https://doi.org/10.3390/sym13030460

Kumar, A., and Kumar, P. (2019). Comparative power quality analysis of different dstatcom topologies. *Iranian Journal of Electrical and Electronic Engineering*, *15*(4), 516–523. https://doi.org/10.22068/IJEEE.15.4.516

Kumar, Ajay, Patel, N., Gupta, N., Gupta, V., and Chitti Babu, B. (2020). Active power coefficient control for grid-tied photovoltaic system under voltage distortions. *Energy Sources, Part A: Recovery, Utilization and Environmental Effects*, 1–24. https://doi.org/10.1080/15567036.2020.1788674

Kumar, Ajay, Patel, N., Gupta, N., Gupta, V., and Davari, P. (2020). Performance enhancement of photovoltaic system under grid voltage distortion utilising total least-square control scheme. *IET Power Electronics*, *13*(14), 3204–3208. https://doi.org/10.1049/iet-pel.2020.0298

Kumar, M., Memon, Z. A., and Uqaili, M. A. (2020). Design and Implementation of Hybrid Active Power Filter (Hapf) for UPS System. *International Journal of ntegrated Engineering*, *12*(6), 229–238.https://doi.org/10.30880/IJIE.2020. 12.06 .026

Kumarpandey, M. (2017). *Current Harmonics Reduction Technique in a BLDC motor Drive application*. *July*. https://doi.org/10.21817/ijet/2017/v9i3/170903S068

Lahare, V. K., Rao, B. C., and Sahu, V. K. (2020). *A Novel Optimization based Hybrid Power Filter for Current Harmonic Mitigation*. *9*(08), 469–473.

Li, H., and Klontz, K. W. (2017). An investigation of current harmonic influence on induction motor in hybrid electric vehicle application. *2017 IEEE International Electric Machines and Drives Conference, IEMDC 2017*. https://doi.org/10.1109/IEMDC.2017.8002201

Li, P., Jin, W., Li, R., and Guan, M. (2020). Harmonics detection via input observer with grid frequency fluctuation. *International Journal of Electrical Power and Energy Systems*, *115*. https://doi.org/10.1016/j.ijepes.2019.105461

Liu, H., Member, S., Hu, H., Chen, H., and Zhang, L. (2017). *Fast and Flexible Selective Harmonic Extraction Methods Based on the Generalized Discrete Fourier Transform*. *8993*(c). https://doi.org/10.1109/TPEL.2017.2703138

Mahanty, R. (2014). Indirect current controlled shunt active power filter for power quality improvement. *International Journal of Electrical Power and Energy Systems*, *62*, 441–449. https://doi.org/10.1016/j.ijepes.2014.05.002

Mai, A. (2020). *Elimination of Current Harmonics in Electrical Machines with Iterative Learning Control*. *December*.

Mamdouh, M. M., Mansour, A. A., Nashed, M. N. F., Zobaa, A. F., and Abou Elzahab, E. E. (2014). Comparison between hysteresis and space vector PWM of shunt active power filter based on prediction harmonic current extraction. *Journal of Next Generation Information Technology*, *5*(2), 9–19.

Merabet, L., Saad, S., Abdeslam, D. O., and Omeiri, A. (2013). A comparative study of harmonic currents extraction by simulation and implementation. *International Journal of Electrical Power and Energy Systems*, *53*(1), 507–514. https://doi.org/10.1016/j.ijepes.2013.05.003

Mikkili, S., and Panda, A. K. (2018). *Power Quality Issues : Current Harmonics* (Issue October 2020). https://doi.org/10.1201/9781315222479

Mishra, A., Tripathi, P. M., and Chatterjee, K. (2018). A review of harmonic elimination techniques in grid connected doubly fed induction generator based wind energy system. *Renewable and Sustainable Energy Reviews*, *89*(February), 1–15. https://doi.org/10.1016/j.rser.2018.02.039

Moeini, A., Wang, S., Zhang, B., and Yang, L. (2020). A Hybrid Phase Shift-Pulsewidth Modulation and Asymmetric Selective Harmonic Current Mitigation-Pulsewidth Modulation Technique to Reduce Harmonics and Inductance of Single-Phase Grid-Tied Cascaded Multilevel Converters. *IEEE Transactions on IndustrialElectronics*,*67*(12),10388–10398.

https://doi.org/10.1109/TIE.2019.2959499

Moeini, A., Zhao, H., and Wang, S. (2018). A Current-Reference-Based Selective Harmonic Current Mitigation PWM Technique to Improve the Performance of Cascaded H-Bridge Multilevel Active Rectifiers. *IEEE Transactions on Industrial Electronics*, *65*(1), 727–737. https://doi.org/10.1109/TIE.2016.2630664

Mohammad, S., Gazafrudi, M., Langerudy, A. T., Fuchs, E. F., and Al-haddad, K. (2015). *Power Quality Issues in Railway Electrification : A Comprehensive Perspective*. *62*(5), 3081–3090.

Musa, S., and Radzi, M. A. M. (2017). Synchronous reference frame fundamental method in shunt active power filter for mitigation of current harmonics. *Pertanika Journal of Science and Technology*, *25*(S), 249–256.

Musa, Suleiman, Radzi, M. A. M., Hizam, H., Wahab, N. I. A., Hoon, Y., and Zainuri, M. A. A. M. (2017). Modified synchronous reference frame based shunt active power filter with fuzzy logic control pulse width modulation inverter. *Energies*, *10*(6). https://doi.org/10.3390/en10060758

N. S. da Silva, M., S. Salles, R., Degan, A., A. Duque, C., and F. Ribeiro, P. (2020). *Investigation of Harmonic Current Aggregation in the TBE/Eletronorte Transmission System*. https://doi.org/10.48011/asba.v2i1.1725

Neelima, K., Sastry, A. A. S., Kshithija, B., Goutam, K., and Chandra, G. H. (2020). *Mitigation of Harmonics in Power Transmission Network using Filters*. *1*, 1283–1288. https://doi.org/10.35940/ijrte.A2290.059120

Ni, F., Wo, S., and Li, Z. (2020). A Harmonic Detection Method of UPQC Based on LSL Algorithm in Photovoltaic Microgrids. *Journal of Control, Automation and Electrical Systems*, *31*(6), 1567–1575. https://doi.org/10.1007/s40313-020-00627-3

Nivetha, D., and Karunakaran, M. (2016). A Review on Power Quality Analysis , Techniques , Methods and Controlling. *International Journal of Advanced Research in Electrical, Electronics and Instrumentation Engineering*, *5*(3), 2049–2054. https://doi.org/10.15662/IJAREEIE.2015.0503143

Nowak, D. J., and Schmid, P. E. (1968). Introduction to Digital Filters. *IEEE*

Transactions on Electromagnetic Compatibility, *EMC-10*(2), 210–220. https://doi.org/10.1109/TEMC.1968.302947

Nwobu, C. J., Efika, I. B., Oghorada, O. J. K., and Zhang, L. (2015). A modular multilevel flying capacitor converter-based STATCOM for reactive power control in distribution systems. *2015 17th European Conference on Power Electronics andApplications,EPE-ECCEEurope2015*.https://doi.org/10.1109/EPE.2015.7309085

Ogheneovo Johnson, D. (2016). Issues of Power Quality in Electrical Systems. *International Journal of Energy and Power Engineering*, *5*(4), 148. https://doi.org/10.11648/j.ijepe.20160504.12

Oghorada, O. J. K., and Zhang, L. (2019). Unbalanced and Reactive Load Compensation Using MMCC-Based SATCOMs with Third-Harmonic Injection. *IEEE Transactions on Industrial Electronics*, *66*(4), 2891–2902. https://doi.org/10.1109/TIE.2018.2849962

Oghorada, O. J. K., Zhang, L., Han, H., Esan, A. B., and Mao, M. (2021). Inter-cluster voltage balancing control of a delta connected modular multilevel cascaded converter under unbalanced grid voltage. *Protection and Control of Modern Power Systems*, *6*(1). https://doi.org/10.1186/s41601-021-00203-0

Oghorada, O., Zhang, L., Esan, B., Egbune, D., and Uwagboe, J. (2020). Inter-Cluster Voltage Balancing Control of Star Connected Modular Multilevel Cascaded Converter under Unbalanced Grid Voltages. *Journal of Modern Power Systems and Clean Energy*.

Osman, D. A. A., Baharom, R., Johari, D., Hidayat, M. N., and Muhammad, K. S. (2019). Development of active power filter using rectifier boost technique. *International Journal of Power Electronics and Drive Systems (IJPEDS)*, *10*(3), 1446. https://doi.org/10.11591/ijpeds.v10.i3.pp1446-1453

Pandurangan, R., Kaliannan, P., and Shanmugam, P. (2021). Effects of Current Distortion on DC Link Inductor and Capacitor Lifetime in Variable Frequency Drive Connected to Grid with Active Harmonic Filter. *IEEE Transactions on Industry Applications*,*57*(1), 492–505. https://doi.org/10.1109/TIA.2020.3028555

Patel, K. S., and Makwana, V. H. (2020). Performance Investigation of Grid-Connected

DFIG using Integrated Shunt Active Filtering Capabilities. *E3S Web of Conferences*, *184*. https://doi.org/10.1051/e3sconf/202018401041

Rajput, V. N., Boteler, D. H., Rana, N., Saiyed, M., Anjana, S., and Shah, M. (2021). Insight into impact of geomagnetically induced currents on power systems: Overview, challenges and mitigation. In *Electric Power Systems Research* (Vol. 192). https://doi.org/10.1016/j.epsr.2020.106927

Rameshkumar, K., and Indragandhi, V. (2020). Overview of reference current extraction techniques in single phase shunt active power filter. *International Journal on Emerging Technologies*, *11*(2), 689–698.

Rusinaru, D., and Merfu, M. (2014). *Power Quality General Levels in Distribution Networks*. 58–62.

Salam, Z., Tan, P. C., and Jusoh, A. (2006). Harmonics mitigation using active power filter: a technological review. *Elektrika*, *8*(2), 17–26. http://eprints.utm.my/46/1/paper4dec06.pdf

Sanjan, P. S., Gowtham, N., Bhaskar, M. S., Subramaniam, U., Almakhles, D. J., Padmanaban, S., and Yamini, N. G. (2020). Enhancement of power quality in domestic loads using harmonic filters. *IEEE Access*, *8*, 197730–197744. https://doi.org/10.1109/ACCESS.2020.3034734

Schwanz, D., Bagheri, A., Bollen, M., and Larsson, A. (2016). *Active Harmonic Filters : control techniques review*. 36–41.

Sengar, K., and Kumar, A. (2019). Fractional Order Capacitor in First-Order and Second-Order Filter. *Micro and Nanosystems*, *12*(1), 75–78. https://doi.org/10.2174/1876402911666190821100400

Serrhini, M. (2019). *Learning and Analytics in Intelligent Systems 7 Innovation in Information Systems and Technologies to Support Learning*.

Shembekar, S. M., and Deshmukh, K. L. (2015). *Analysis of Reference Current Generation for Shunt Active Power Filter Using SRF Algorithm to Compensate Harmonic Current*. *3*(2), 93–97.

Singh, B., and Jain, V. (2020). TOCF Based Control for Optimum Operation of a Grid Tied Solar PV System. *IEEE Transactions on Energy Conversion*, *35*(3), 1171–

1181. https://doi.org/10.1109/TEC.2020.2990907

Somasundaram, B. (2016). *An Introduction to Harmonics , its Causes , Effects & Mitigation Techniques with case studies*. *February*. https://doi.org/10.13140/RG.2.1.3904.8724

Subramaniam, U., Bhaskar, S. M., Almakhles, D. J., Padmanaban, S., and Leonowicz, Z. (2019). Investigations on EMI mitigation techniques: Intent to reduce grid-tied PV inverter common mode current and voltage. *Energies*, *12*(17). https://doi.org/10.3390/en12173395

Sundaram, E., and Venugopal, M. (2016). On design and implementation of three phase three level shunt active power filter for harmonic reduction using synchronous reference frame theory. *International Journal of Electrical Power and Energy Systems*, *81*, 40–47. https://doi.org/10.1016/j.ijepes.2016.02.008

Suslov, K., and Stepanov, V. (2015). *A Principle of Power Quality Control in the Intelligent Distribution Networks*, 260–264.

Taiwo, O. P., Tiako, R., and Davidson, I. (2017). *Application of Dynamic Voltage Restorer for Power Quality Improvement in Low Voltage Electrical Power Distribution Network : An Overview*.*28*, 142–156. https://doi.org/10.4028/www.scientific.net/JERA.28.142

Tandekar, J., Ojha, A., and Jain, S. (2019). Five-level cascaded h-bridge mlc-based shunt active power filter for active harmonics mitigation in distributed network. *Journal of Circuits, Systems and Computers*, *28*(2). https://doi.org/10.1142/S021812661950035X

Tiwari, S. P., and Sharma, P. K. (2017). *Synchronous Reference Frame Theory for Active Power Filter*. *7*(10), 15178–15180.

Vadirajacharya, K., Agarwal, P., and Gupta, H. O. (2007). A simple control strategy for unified power quality conditioner using current source inverter. *8th International Power Engineering Conference, IPEC 2007*, 1219–1223.

Vardar, K., and Akpinar, E. (2011). Comparing ADALINE and IRPT methods based on shunt active power filters. *European Transactions on Electrical Power*, *21*(1), 924–936. https://doi.org/10.1002/etep.486

Varshney, G., Pandey, N., and Pandey, R. (2021). Electronically Tunable Multifunction Transadmittance-Mode Fractional-Order Filter. *Arabian Journal for Science and Engineering*, *46*(2), 1067–1078. https://doi.org/10.1007/s13369-020-04841-8

Verma, A. K., Jain, C., Singh, B., and Shahani, D. T. (2016). *Adaptive noise cancellation based harmonic elimination in grid integrated photovoltaic system*. https://doi.org/10.1049/iet-rpg.2015.0505

Wang, S., and Kang, J. (2019). Harmonic Extraction and Suppression Method of Permanent Magnet Synchronous Motor Based on Adaptive Linear Neural Network. *Diangong Jishu Xuebao/Transactions of China Electrotechnical Society*, *34*(4), 654–663. https://doi.org/10.19595/j.cnki.1000-6753.tces.181080

Wu, W., Liang, Z., Zhang, L., Zhao, R., and Kong, M. (2020). Numerical Simulation of Second-Order Microfluidic Filter. *Proceedings of the National Academy of Sciences India Section A-Physical Sciences*,*90*(3). https://doi.org/10.1007/s40010-018-0574-7

Xie, C., Li, K., and Zou, J. (2019). Multiple Second-Order Generalized Integrators Based Comb Filter for Fast Selective Harmonic Extraction. *2019 IEEE Applied Power Electronics Conference and Exposition (APEC)*, 2427–2432.

Yaghoobi, J., Alduraibi, A., and Zare, F. (2018). *Current Harmonic Estimation Techniques based on Voltage Measurements in Distribution Networks*. *July 2019*. https://doi.org/10.1109/AUPEC.2018.8757929

Yousfi, A., Allaoui, T., and Chaker, A. (2020). A new approach to extract reference currents for multilevel shunt active filter in three phase systems. *International Journal of Power Electronics and Drive Systems*, *11*(3), 1459–1467. https://doi.org/10.11591/ijpeds.v11.i3.pp1459-1467

Zainuri, M. A. A. M., Radzi, M. A. M., Soh, A. C., Mariun, N., Rahim, N. A., Teh, J., and Lai, C. M. (2018). Photovoltaic integrated shunt active power filter with simpler ADALINE algorithm for current harmonic extraction. *Energies*, *11*(5). https://doi.org/10.3390/en11051152

Zare, F., Soltani, H., Kumar, D., Davari, P., Delpino, H. A. M., and Blaabjerg, F. (2017). Harmonic emissions of three-phase diode rectifiers in distribution

networks. *IEEE Access*, *5*, 2819–2833. https://doi.org/10.1109/ACCESS. 2017 .2669578

Zhang, J., Geng, Z., Xu, S., and Chen, H. (2019). An Improved Adaptive Harmonic Detection Algorithm for Active Power Filter. *Diangong Jishu Xuebao/ Transactions of China Electrotechnical Society*, *34*(20). https://doi.org /10.19595 /j.cnki.1000-6753.tces.181217

Zhilin, E. V., and Prasol, D. A. (2020). Optimization approach to reduce the negative impact of high harmonic components of currents and voltages in high-voltage mine networks. *IOP Conference Series: Materials Science and Engineering*, *791*(1). https://doi.org/10.1088/1757-899X/791/1/012038

APPENDICES

Appendix A.1 Harmonics Data Obtained from LMU LVD Network.

CURRENT HARMONICS IN PHASE 1												
	rec_STD .Harm. current 3 L1 (%)	rec_STD .Harm. current 5 L1 (%)	rec_STD .Harm. current 7 L1 (%)	rec_STD .Harm. current 9 L1 (%)	rec_STD .Harm. current 11 L1 (%)	rec_STD .Harm. current 13 L1 (%)	rec_STD .Harm. current 15 L1 (%)	rec_STD .Harm. current 17 L1 (%)	rec_STD .Harm. current 19 L1 (%)	rec_STD .Harm. current 21 L1 (%)	rec_STD .Harm. current 23 L1 (%)	rec_STD .Harm. current 25 L1 (%)
2/27/2019 17:30	0	0	3.5	0	0	0	0	0	0	0	0	0
2/27/2019 18:00	0	0	3.1	0	0	0	0	0	0	0	0	0
2/27/2019 18:30	0.4	1.1	1.9	0	0	0	0	0	0	0	0	0
2/27/2019 19:00	1	1.3	1.5	0.4	0	0	0	0	0	0	0	0
2/27/2019 19:30	1.4	1.4	1.1	0.5	0	0.4	0	0	0	0	0	0
2/28/2019 16:00	0	0	0	0	0	0	0	0	0	0	0	0
2/28/2019 16:30	0	0	1.6	0	0	0	0	0	0	0	0	0
2/28/2019 17:00	0	0	2.4	0	0	0	0	0	0	0	0	0
2/28/2019 17:30	5.6	3.2	0	0	0	0	0	0	0	0	0	0
2/28/2019 18:00	88.7	62.7	34.8	17.4	0	0	0	0	0	0	17.4	24.6
2/28/2019 18:30	37.3	28.4	13.4	6.7	0	0	0	0	0	6.7	11.6	11.6
2/28/2019 19:00	6.9	6.6	2.9	0	0	0	0	0	0	0	0	0
2/28/2019 19:30	87.7	57.7	35.8	16	0	0	0	0	0	0	0	16
2/28/2019 20:00	87.7	59.9	35.8	16	0	0	0	0	0	0	0	16
2/28/2019 20:30	85.5	58.4	34.8	15.6	0	0	0	0	0	0	0	15.6
2/28/2019 21:00	26.1	17.5	10.5	4.6	0	0	0	0	0	0	4.6	4.6
2/28/2019 21:30	14.7	8.3	4.8	3.9	2.7	0	0	0	0	0	0	0
3/1/2019 9:30	4.2	3.9	0	1.1	1.6	0	0	0	0	0	1.6	0
3/1/2019 10:00	4.2	3.9	0	1.6	1.6	0	0	0	0	0	1.6	1.1
3/1/2019 10:30	1.4	1.4	1.9	0	0	0	0	0	0	0	0	0
3/1/2019 11:00	0	0	0	0	0	0	0	0	0	0	0	0
3/1/2019 11:30	0	0	0	0	0	0	0	0	0	0	0	0
3/1/2019 12:00	0.3	0.8	0.9	0	0.8	0	0	0	0	0	0.7	1.4
3/1/2019 12:30	0.3	0.9	1	0	0.8	0.2	0	0	0	0	0.9	2
3/1/2019 13:00	0.3	0.9	1	0.2	0.8	0	0	0	0	0	0.9	2.1
3/1/2019 14:00	0.6	0.4	1.2	0	0.4	0	0	0	0	0	0	0
3/1/2019 14:30	0.2	0.7	0.9	0	0.8	0	0	0	0	0	1	2.1
3/1/2019 15:00	0	0	1.7	0	0	0	0	0	0	0	0	0
3/1/2019 15:30	1.2	0	0	0	0	0	0	0	0	0	0	0
3/1/2019 16:00	1.7	0	1	0	0	0	0	0	0	0	0	0
3/1/2019 16:30	1.8	0	0	0	0	0	0	0	0	0	0	0
3/1/2019 17:00	0	0	1.7	0	0	0	0	0	0	0	0	0
3/1/2019 17:30	0	1.9	2.7	0	0	0	0	0	0	0	0	0
3/1/2019 18:00	0	2.5	2.3	0	0	0	0	0	0	0	0	0
3/1/2019 18:30	2.1	2.4	1.7	0	0.6	0	0	0	0	0	0	0
3/1/2019 19:00	1.5	2.2	1.5	0	0	0	0	0	0	0	0	0
3/1/2019 19:30	1.7	1.9	0.4	0.6	0	0	0	0	0	0	0	0
3/1/2019 20:00	1	1.3	0.5	0.6	0.3	0	0	0	0	0	0	0
3/1/2019 20:30	1.1	1.1	0.3	0.5	0	0	0	0	0	0	0	0
3/1/2019 21:00	1.2	1.1	0.4	0.7	0.2	0	0	0	0	0	0	0
3/1/2019 21:30	2.2	1	0.7	0.8	1	0	0	0	0	0	0.5	0.4
3/1/2019 22:00	7.9	4.1	1.4	2.5	2	0	0	0	0	0	0	0
3/1/2019 22:30	11	6.7	2.8	3.5	2.8	0	0	0	0	0	0	0
3/1/2019 23:00	11	6.8	2.9	3.5	2.9	0	0	0	0	0	0	0
3/1/2019 23:30	8.7	4.5	1.5	2.7	2.2	0	0	0	0	0	0	0
3/2/2019 0:00	8	4.1	1.4	2.5	2	0	0	0	0	0	0	0
3/2/2019 0:30	8	4.1	1.4	2.5	2	0	0	0	0	0	0	0
3/2/2019 1:00	8.7	4.6	1.6	2.8	2.3	0	0	0	0	0	0	0
3/2/2019 1:30	15.5	10.1	6.7	4.8	3.3	0	0	0	0	0	0	0
3/2/2019 2:00	0.1	0.1	0.1	0.1	0.1	0.1	0.1	0.1	0.1	0.1	0.1	0.1
3/2/2019 2:30	0.1	0.1	0.1	0.1	0.1	0.1	0.1	0.1	0.1	0.1	0.1	0.1
3/2/2019 3:00	0.1	0.1	0.1	0.1	0.1	0.1	0.1	0.1	0.1	0.1	0.1	0.1
3/2/2019 3:30	0.1	0.1	0.1	0.1	0.1	0.1	0.1	0.1	0.1	0.1	0.1	0.1

3/2/2019 4:00	0.1	0.1	0.1	0.1	0.1	0.1	0.1	0.1	0.1	0.1	0.1	0.1
3/2/2019 4:30	0.1	0.1	0.1	0.1	0.1	0.1	0.1	0.1	0.1	0.1	0.1	0.1
3/2/2019 5:00	0.1	0.1	0.1	0.1	0.1	0.1	0.1	0.1	0.1	0.1	0.1	0.1
3/2/2019 5:30	83.6	54.7	31.6	0	0	0	0	0	0	0	0	0
3/2/2019 6:00	84.8	60	40	20	0	0	0	0	0	0	0	0
3/2/2019 6:30	92.9	63.9	47.6	30.1	0	0	0	0	0	0	0	0
3/2/2019 7:00	6.3	4.1	2.3	1.9	1.9	0	0	0	0	0	0	0
3/2/2019 7:30	0.2	0.6	1	0	0.9	0	0	0	0	0	0.5	1.9
3/2/2019 8:00	0	0.7	0.9	0.2	0.9	0	0	0	0	0	0.5	1.9
3/2/2019 8:30	1.9	1.6	1.3	0.5	1	0	0	0	0	0.5	0.7	2.1
3/2/2019 9:00	4.1	3.7	1.2	1.7	1.2	0	0	0	0	1.2	1.7	1.2
3/2/2019 9:30	0	0	1.7	0	0	0	0	0	0	0	0	0
3/2/2019 10:00	0	0	2	0	0	0	0	0	0	0	0	0
3/2/2019 10:30	0	0	2.1	0	0	0	0	0	0	0	0	0
3/2/2019 11:00	0	0	2	0	0	0	0	0	0	0	0	0
3/2/2019 11:30	0	2.7	3.2	0	0	0	0	0	0	0	0	0
3/2/2019 13:30	0	3.3	4.5	0	0	0	0	0	0	0	0	0
3/2/2019 14:00	0	3.6	4.2	0	0	0	0	0	0	0	0	0
3/2/2019 14:30	0	3.7	3.7	0	0	0	0	0	0	0	0	0
3/2/2019 15:00	1.3	4.1	4.2	0	0	0	0	0	0	0	0	0
3/2/2019 15:30	1.1	3	3.8	0	0	0	0	0	0	0	0	0
3/2/2019 16:00	0	3.3	3.5	0	0	0	0	0	0	0	0	0
3/2/2019 16:30	0	4.2	3	0	0	0	0	0	0	0	0	0
3/2/2019 17:00	0	5.1	3.2	0	0	0	0	0	0	0	0	0
3/2/2019 17:30	0	5.2	3.3	0	0	0	0	0	0	0	0	0
3/2/2019 18:00	1.3	2.6	2	0	0	0	0	0	0	0	0	0
3/2/2019 18:30	0.6	1.5	1.5	0	0.3	0	0	0	0	0	0	0
3/2/2019 19:00	0.3	1	1.8	0.4	0.3	0	0	0	0	0	0	0
3/2/2019 19:30	1.7	1	1	0.4	0.8	0	0	0	0	0	0.5	1
3/2/2019 20:00	2.2	0.9	0.8	0.5	0.9	0	0	0	0	0	0.8	0.6
3/2/2019 20:30	5.7	4.4	0	1.1	0	0	0	0	0	0	0	0
3/2/2019 21:00	8.8	7.1	0	1.6	0	0	0	0	0	0	0	0
3/2/2019 21:30	1.2	0.7	2	0.5	0.2	0.3	0.2	0	0	0	0	0
3/2/2019 22:00	1.4	0.8	2	0.6	0.2	0.2	0.2	0	0	0	0	0
3/2/2019 22:30	1.3	1	2	0.6	0.5	0	0.2	0	0	0	0	0.3
3/2/2019 23:00	1.1	0.8	2.2	0.6	0.6	0.2	0.2	0	0	0	0	0.4
3/2/2019 23:30	1.2	0.7	2.2	0.6	0.4	0.2	0.2	0	0	0	0	0
3/3/2019 0:00	1.2	0.3	1.6	0.6	0.4	0.2	0	0	0	0	0	0
3/3/2019 0:30	1.2	0.4	1.7	0.6	0.4	0.3	0.2	0	0	0	0	0
3/3/2019 1:00	1.2	0.4	1.7	0.5	0.2	0.2	0.2	0	0	0	0	0
3/3/2019 1:30	1.1	0.5	1.6	0.5	0.4	0	0	0	0	0	0	0
3/3/2019 2:00	0.1	0.1	0.1	0.1	0.1	0.1	0.1	0.1	0.1	0.1	0.1	0.1
3/3/2019 2:30	0.1	0.1	0.1	0.1	0.1	0.1	0.1	0.1	0.1	0.1	0.1	0.1
3/3/2019 3:00	0.1	0.1	0.1	0.1	0.1	0.1	0.1	0.1	0.1	0.1	0.1	0.1
3/3/2019 3:30	0.1	0.1	0.1	0.1	0.1	0.1	0.1	0.1	0.1	0.1	0.1	0.1
3/3/2019 4:00	0.1	0.1	0.1	0.1	0.1	0.1	0.1	0.1	0.1	0.1	0.1	0.1
3/3/2019 4:30	0.1	0.1	0.1	0.1	0.1	0.1	0.1	0.1	0.1	0.1	0.1	0.1
3/3/2019 5:00	0.1	0.1	0.1	0.1	0.1	0.1	0.1	0.1	0.1	0.1	0.1	0.1
3/3/2019 5:30	0.7	0.9	1.2	0	0.9	0	0	0	0	0	0.3	0.8
3/3/2019 6:00	0.7	0.9	1.2	0	0.9	0	0	0	0	0	0.3	0.8
3/3/2019 6:30	0.6	0.9	1.1	0	0.8	0	0	0	0	0	0.4	0.8
3/3/2019 7:00	0.7	0.9	1.2	0	0.9	0	0	0	0	0	0.3	0.8
3/3/2019 7:30	0.3	0.3	0.7	0	0.6	0	0	0	0.3	0	0.6	1.9
3/3/2019 8:00	0.2	0.3	0.7	0	0.5	0	0	0	0.3	0	0.6	2
3/3/2019 8:30	0.2	0.3	0.7	0	0.6	0	0	0	0.2	0	0.6	1.7

3/3/2019 9:00	0.2	0.4	0.6	0	0.5	0	0	0	0.2	0	0.6	1.5
3/3/2019 9:30	0.3	0.4	0.6	0	0.5	0	0	0	0.2	0	0.7	1.5
3/3/2019 10:00	0.4	0.4	0.6	0	0.5	0	0	0	0.2	0	0.8	1.5
3/3/2019 10:30	0	0.4	0.6	0	0.4	0	0	0	0.2	0	0.8	1.5
3/3/2019 11:00	0	0.4	0.6	0	0.5	0	0	0	0.2	0	0.7	1.5
3/3/2019 11:30	0.2	0.4	0.6	0	0.5	0	0	0	0.2	0	0.7	1.5
3/3/2019 12:00	0.5	0.4	0.6	0	0.6	0	0	0	0.2	0	0.6	1.4
3/3/2019 12:30	0.6	0.5	0.6	0	0.7	0	0	0	0	0	0.4	1.2
3/3/2019 13:00	0.5	0.4	0.6	0	0.7	0	0	0	0	0	0.5	1.2
3/3/2019 13:30	0.5	0.5	0.7	0	0.7	0	0	0	0	0	0.5	1.3
3/3/2019 14:00	0.4	0.4	0.6	0	0.8	0	0	0	0	0	0.5	1.3
3/3/2019 14:30	0.3	0.3	0.5	0	0.8	0	0	0	0	0	0.4	1.4
3/3/2019 15:00	0.2	0.3	0.7	0	0.7	0	0	0	0	0	0.3	1.3
3/3/2019 15:30	0.2	0.4	0.6	0	0.7	0	0	0	0	0	0.4	1.3
3/3/2019 16:00	0.3	0.5	0.7	0	0.7	0	0	0	0	0	0.4	1.3
3/3/2019 16:30	0.2	0.5	0.7	0	0.7	0	0	0	0	0	0.4	1.3
3/3/2019 17:00	0.2	0.5	0.7	0	0.7	0	0	0	0	0	0.3	1.2
3/3/2019 17:30	0	0.5	0.7	0	0.7	0	0	0	0	0	0.3	1.2
3/3/2019 18:00	0.2	0.5	0.7	0	0.7	0	0	0	0	0	0.3	1.3
3/3/2019 18:30	0	0.7	0.9	0	0.8	0	0	0	0	0	0.3	1.3
3/3/2019 19:00	0.4	0.5	2.1	0.2	0.6	0.5	0.5	0.2	0	0.3	0.4	0.4
3/3/2019 19:30	0.4	0.9	2.1	0.2	0.7	0.4	0.4	0.2	0	0.2	0.3	0.4
3/3/2019 20:00	0.5	0.4	1.3	0	0.5	0.3	0	0	0	0	0	0
3/3/2019 20:30	0.3	0	1.2	0	0.4	0	0	0	0	0	0	0
3/3/2019 21:00	0.3	0.2	1	0	0.4	0	0	0	0	0	0	0
3/3/2019 21:30	0.2	0	1.1	0	0.5	0	0	0	0	0	0	0
3/3/2019 22:00	0.2	0.5	1	0	0.4	0	0	0	0	0	0	0
3/3/2019 22:30	0	0.3	1	0	0.3	0	0	0	0	0	0	0
3/3/2019 23:00	0	0	1.2	0	0.3	0	0	0	0	0	0	0
3/3/2019 23:30	0.2	0	1.3	0	0.5	0.2	0	0	0	0	0	0
3/4/2019 0:00	0.3	0	1.6	0	0.4	0.2	0	0	0	0	0	0
3/4/2019 0:30	0.2	0	1.6	0	0.3	0	0	0	0	0	0	0
3/4/2019 1:00	0.2	0	1.7	0	0.4	0	0	0	0	0	0	0
3/4/2019 1:30	0.2	0.4	1.8	0	0.5	0.2	0	0	0	0	0	0
3/4/2019 2:00	0.3	0.9	2.2	0	0.6	0.3	0	0	0	0	0	0
3/4/2019 2:30	0	0.9	2.3	0	0.6	0	0	0	0	0	0	0
3/4/2019 3:00	0.1	0.1	0.1	0.1	0.1	0.1	0.1	0.1	0.1	0.1	0.1	0.1
3/4/2019 3:30	0.1	0.1	0.1	0.1	0.1	0.1	0.1	0.1	0.1	0.1	0.1	0.1
3/4/2019 4:00	0.1	0.1	0.1	0.1	0.1	0.1	0.1	0.1	0.1	0.1	0.1	0.1
3/4/2019 4:30	0.1	0.1	0.1	0.1	0.1	0.1	0.1	0.1	0.1	0.1	0.1	0.1
3/4/2019 5:00	0.1	0.1	0.1	0.1	0.1	0.1	0.1	0.1	0.1	0.1	0.1	0.1
3/4/2019 5:30	0.1	0.1	0.1	0.1	0.1	0.1	0.1	0.1	0.1	0.1	0.1	0.1
3/4/2019 6:00	0.3	0.8	1.3	0	0.9	0	0	0	0	0	0	0.7
3/4/2019 6:30	0.2	0.9	1.3	0	0.9	0	0	0	0	0	0	0.7
3/4/2019 7:00	0.3	0.8	1.3	0	0.9	0.2	0	0	0	0	0.2	1.2
3/4/2019 7:30	0.4	0.8	1.2	0	0.9	0.2	0	0	0	0	0.4	1.8
3/4/2019 8:00	0.3	0.9	1.3	0	0.8	0	0	0	0	0	0.5	2
3/4/2019 8:30	0.3	0.8	1.3	0	0.7	0	0	0	0	0	0.6	1.9
3/4/2019 9:00	2.1	0	0	0	0	0	0	0	0	0	0	0
3/4/2019 9:30	2.8	0	1.2	0	0	0	0	0	0	0	0	0
3/4/2019 10:00	2.6	1.3	0	0	0	0	0	0	0	0	0	0
3/4/2019 10:30	2.8	1.1	0	0	0	0	0	0	0	0	0	0
3/4/2019 11:00	3.8	2.3	1.8	0	0	0	0	0	0	0	0	0
3/5/2019 10:00	2.1	1.7	0	0	0	0	0	0	0	0	0	0

CURRENT HARMONICS IN PHASE 2												
	rec_STD .Harm. current 3 L2 (%)	rec_STD .Harm. current 5 L2 (%)	rec_STD .Harm. current 7 L2 (%)	rec_STD .Harm. current 9 L2 (%)	rec_STD .Harm. current 11 L2 (%)	rec_STD .Harm. current 13 L2 (%)	rec_STD .Harm. current 15 L2 (%)	rec_STD .Harm. current 17 L2 (%)	rec_STD .Harm. current 19 L2 (%)	rec_STD .Harm. current 21 L2 (%)	rec_STD .Harm. current 23 L2 (%)	rec_STD .Harm. current 25 L2 (%)
2/27/2019 17:30	4.9	5.6	2.8	0	0	0	0	0	0	0	0	0
2/27/2019 18:00	7.5	5.9	3	0	0	0	0	0	0	0	0	0
2/27/2019 18:30	10	2.3	3.6	2.1	1.6	1.6	0.9	0.9	0.6	0.6	0.6	0.5
2/27/2019 19:00	4.1	1.7	1.5	0.7	0.5	0.6	0.3	0.3	0	0	0	0
2/27/2019 19:30	1.7	0.8	2.7	0.8	0.3	0.7	0.3	0.3	0	0	0	0
2/28/2019 16:00	4.7	5.4	0	0	0	0	0	0	0	0	0	0
2/28/2019 16:30	3.9	4.5	0	0	0	0	0	0	0	0	0	0
2/28/2019 17:00	3.7	5.9	0	0	0	0	0	0	0	0	0	0
2/28/2019 17:30	2.9	2.9	0	0	0	0	0	0	0	0	0	0
2/28/2019 18:00	3.1	0	0	0	0	0	0	0	0	0	0	0
2/28/2019 18:30	4.7	5.5	0	0	0	0	0	0	0	0	0	0
2/28/2019 19:00	17.1	5	7.6	3.4	5.4	2.4	1.9	1.8	1.3	0.9	3.2	3
2/28/2019 19:30	9.3	5.7	11	3.4	9.6	2.6	0	1.9	1.7	0	6.5	6
2/28/2019 20:00	9.3	5.8	11.5	3.4	9.7	2.8	0	1.9	1.7	0	6.5	5.8
2/28/2019 20:30	9.3	6.9	12.6	3.5	11.1	2.9	0	2.2	1.9	0	7.3	6.7
2/28/2019 21:00	9.3	7.3	11.8	3.2	10.4	2.5	1	2.3	1.8	0	6.5	5.6
2/28/2019 21:30	8.2	6	9.4	2	9	2	0.8	2	1.7	0.8	5.2	4.8
3/1/2019 9:30	1.3	1.7	0	0	0	0	0	0	0	0	0	0
3/1/2019 10:00	2.1	2.1	0	0	0	0	0	0	0	0	0	0
3/1/2019 10:30	3.6	3.1	0	0	0	0	0	0	0	0	0	0
3/1/2019 11:00	9.3	4.6	0	0	0	0	0	0	0	0	0	0
3/1/2019 11:30	9.4	4.7	0	0	0	0	0	0	0	0	0	0
3/1/2019 12:00	13.4	6.7	0	0	0	0	0	0	0	0	0	0
3/1/2019 12:30	53.4	26.7	0	0	0	0	0	0	0	0	0	26.7
3/1/2019 13:00	39.7	22.9	0	0	0	0	0	0	0	0	0	22.9
3/1/2019 14:00	11.7	5.8	0	0	0	0	0	0	0	0	0	0
3/1/2019 14:30	40.8	0	0	0	0	0	0	0	0	0	0	23.5
3/1/2019 15:00	4.2	4.2	0	0	0	0	0	0	0	0	0	0
3/1/2019 15:30	2.1	1.8	0	0	0	0	0	0	0	0	0	0
3/1/2019 16:00	1.7	1.2	0	0	0	0	0	0	0	0	0.8	0
3/1/2019 16:30	3.5	2.4	0	0	0	0	0	0	0	0	0	0
3/1/2019 17:00	3.5	2.9	0	0	0	0	0	0	0	0	0	0
3/1/2019 17:30	3.4	4.2	0	0	0	0	0	0	0	0	0	0
3/1/2019 18:00	2.8	4.1	1	0	0	0	0	0	0	0	0	0
3/1/2019 18:30	12.1	3.5	3.9	2.6	1.9	1.8	1.3	1.1	0.9	0.8	0.5	0.5
3/1/2019 19:00	11.5	2.8	4.1	2.4	1.8	1.4	1.2	1	0.8	0.7	0.5	0.5
3/1/2019 19:30	6.2	1.6	1.9	0.9	0.6	0.7	0.4	0.4	0.2	0.3	0.2	0
3/1/2019 20:00	5.6	1.1	1.6	0.6	0.5	0.4	0.3	0.4	0	0.3	0	0
3/1/2019 20:30	5	0.9	1	0.5	0.5	0.2	0.3	0.3	0	0.2	0	0
3/1/2019 21:00	5	0.8	1.4	0.5	0.4	0.3	0.4	0.3	0	0.2	0	0
3/1/2019 21:30	3.3	1.2	2.7	0.5	3.1	0.7	0	0.4	0.5	0	2.1	1.6
3/1/2019 22:00	5.2	2.8	4.1	0.8	5.5	1	0.5	1.1	1.1	0	3	2.8
3/1/2019 22:30	5.9	2.9	4.7	0.6	6.8	1	0.8	1.5	1.5	0	3.3	3.2
3/1/2019 23:00	7	3.6	5.8	0.7	8	1.2	1	1.7	1.6	0	3.7	3.7
3/1/2019 23:30	5.1	2.4	4	0.5	5.9	0.9	0.5	1.2	1.3	0	3	2.9
3/2/2019 0:00	4.6	2.1	3.5	0	5.4	0.8	0.5	1.2	1.2	0	2.7	2.6
3/2/2019 0:30	4.6	2.1	3.5	0.5	5.3	0.8	0.5	1.1	1.2	0	2.7	2.7
3/2/2019 1:00	5.1	2.5	4.2	0.5	5.9	1.1	0.5	1.2	1.2	0	2.9	2.9
3/2/2019 1:30	8.4	4	7.5	0.9	9.5	1.8	1.2	2	2	0	4.1	4.2
3/2/2019 2:00	0.1	0.1	0.1	0.1	0.1	0.1	0.1	0.1	0.1	0.1	0.1	0.1
3/2/2019 2:30	0.1	0.1	0.1	0.1	0.1	0.1	0.1	0.1	0.1	0.1	0.1	0.1
3/2/2019 3:00	0.1	0.1	0.1	0.1	0.1	0.1	0.1	0.1	0.1	0.1	0.1	0.1
3/2/2019 3:30	0.1	0.1	0.1	0.1	0.1	0.1	0.1	0.1	0.1	0.1	0.1	0.1

3/2/2019 4:00	0.1	0.1	0.1	0.1	0.1	0.1	0.1	0.1	0.1	0.1	0.1	0.1
3/2/2019 4:30	0.1	0.1	0.1	0.1	0.1	0.1	0.1	0.1	0.1	0.1	0.1	0.1
3/2/2019 5:00	0.1	0.1	0.1	0.1	0.1	0.1	0.1	0.1	0.1	0.1	0.1	0.1
3/2/2019 5:30	10.5	4.5	9.4	0	10.8	1.6	0	2.2	2.2	0	5.3	6
3/2/2019 6:00	9.8	4	9	1.4	11.3	2.2	1	2.4	2.4	0	5.4	5.2
3/2/2019 6:30	9.7	4.2	9.2	1.4	11.5	2.4	1	2.4	2.2	0	4.8	4.9
3/2/2019 7:00	5.2	2.7	4.7	0.5	5.8	1	0.5	1.3	1.3	0	3.1	2.8
3/2/2019 7:30	0.2	0.6	1	0	0.9	0	0	0	0	0	0.5	1.9
3/2/2019 8:00	0	0.7	0.9	0.2	0.9	0	0	0	0	0	0.5	1.9
3/2/2019 8:30	1.4	1.3	1.2	0.5	1	0	0	0	0	0	0	2
3/2/2019 9:00	3.4	2.6	0	0	1	0	0	0	0	0	0	0
3/2/2019 9:30	3.3	2.5	0	0	0.9	0	0	0	0	0	0	0
3/2/2019 10:00	3.3	3.1	0	0	0	0	0	0	0	0	0	0
3/2/2019 10:30	4.6	4.1	0	0	0	0	0	0	0	0	0	0
3/2/2019 11:00	4.1	2.9	0	0	0	0	0	0	0	0	0	0
3/2/2019 11:30	3.5	5.6	0	0	0	0	0	0	0	0	0	0
3/2/2019 13:30	6	7.8	1.9	0	0	0	0	0	0	0	0	0
3/2/2019 14:00	5.6	7.7	1.7	0	0	0	0	0	0	0	0	0
3/2/2019 14:30	3.3	6	1.6	0	0	0	0	0	0	0	0	0
3/2/2019 15:00	6.1	8.7	2.9	0	0	0	0	0	0	0	0	0
3/2/2019 15:30	3	5.5	1.5	0	0	0	0	0	0	0	0	0
3/2/2019 16:00	2.2	5.2	1.3	0	0	0	0	0	0	0	0	0
3/2/2019 16:30	3	6.3	1.2	0	0	0	0	0	0	0	0	0
3/2/2019 17:00	6.2	9.5	2	0	0	0	0	0	0	0	0	0
3/2/2019 17:30	5.8	9.2	2.9	0	0	0	0	0	0	0	0	0
3/2/2019 18:00	2.2	4.5	1.4	0	0	0	0	0	0	0	0	0
3/2/2019 18:30	7.7	1.8	2.8	1.4	1	1.3	0.8	0.8	0.4	0.4	0.4	0.2
3/2/2019 19:00	6.1	1.3	2.3	1	0.7	0.8	0.6	0.6	0.4	0.4	0.3	0.2
3/2/2019 19:30	2.7	1	1.8	0.3	2	0	0	0.3	0.4	0	1.8	1.3
3/2/2019 20:00	3.4	1.1	2.7	0.8	3	0.5	0	0.4	0.7	0	2.5	1.7
3/2/2019 20:30	3.2	2.4	6.5	1.5	2.8	1.7	0.6	0.6	0.4	0	1.6	1.1
3/2/2019 21:00	3.4	1.8	6.9	1.8	1.7	2.8	1	0.5	0	0	0	0
3/2/2019 21:30	6.3	6.9	17.9	3.5	3	6.4	2.1	1	0	0	0	0
3/2/2019 22:00	6.8	8.8	20.4	6.1	2.9	4.2	2	1.2	0	0	0	0
3/2/2019 22:30	7.3	9	20.4	5.2	5.6	3.7	2.1	1.7	0	0	1.7	2.4
3/2/2019 23:00	7.1	9.2	20.7	3.8	5.9	4.2	1.5	1.5	1.1	0	2.7	2.7
3/2/2019 23:30	6.3	9.4	22.7	5.1	2.6	4.4	2	1.6	0	0	0	0
3/3/2019 0:00	6.8	6.7	17.4	5	3.1	3.5	2	2	0	0	0	0
3/3/2019 0:30	7.1	7.2	17.5	5	3.7	3.7	1.6	1.6	0	0	0	0
3/3/2019 1:00	7.1	7.5	17.4	5	2.8	4	1.6	1.6	0	0	0	0
3/3/2019 1:30	7.1	7.9	18	5.4	2.7	3.1	1.9	1.9	0	0	0	0
3/3/2019 2:00	0.1	0.1	0.1	0.1	0.1	0.1	0.1	0.1	0.1	0.1	0.1	0.1
3/3/2019 2:30	0.1	0.1	0.1	0.1	0.1	0.1	0.1	0.1	0.1	0.1	0.1	0.1
3/3/2019 3:00	0.1	0.1	0.1	0.1	0.1	0.1	0.1	0.1	0.1	0.1	0.1	0.1
3/3/2019 3:30	0.1	0.1	0.1	0.1	0.1	0.1	0.1	0.1	0.1	0.1	0.1	0.1
3/3/2019 4:00	0.1	0.1	0.1	0.1	0.1	0.1	0.1	0.1	0.1	0.1	0.1	0.1
3/3/2019 4:30	0.1	0.1	0.1	0.1	0.1	0.1	0.1	0.1	0.1	0.1	0.1	0.1
3/3/2019 5:00	0.1	0.1	0.1	0.1	0.1	0.1	0.1	0.1	0.1	0.1	0.1	0.1
3/3/2019 5:30	8.3	3.9	9	1.9	10.2	2.4	0	2.4	2.4	0	4.8	5.9
3/3/2019 6:00	7.6	3.2	9.3	1.7	10.6	2.5	1	2.3	2.3	0	5.4	6.1
3/3/2019 6:30	7.4	2.5	8.5	1.4	11.2	2.9	1.4	2	2.3	1	6.4	6.6
3/3/2019 7:00	7.9	3.2	8.7	1.4	11.1	2.5	1.4	1.8	2	1	5.5	5.8
3/3/2019 7:30	0.3	0.3	0.8	0	0.7	0	0	0	0.3	0	0.6	1.9
3/3/2019 8:00	0.2	0.3	0.7	0	0.5	0	0	0	0.3	0	0.6	2
3/3/2019 8:30	0.2	0.3	0.7	0	0.6	0	0	0	0.2	0	0.6	1.7

3/3/2019 9:00	0.2	0.4	0.6	0	0.5	0	0	0	0.2	0	0.6	1.5
3/3/2019 9:30	0.3	0.4	0.6	0	0.5	0	0	0	0.2	0	0.7	1.5
3/3/2019 10:00	0.4	0.4	0.6	0	0.5	0	0	0	0.2	0	0.8	1.5
3/3/2019 10:30	0	0.4	0.6	0	0.4	0	0	0	0.2	0	0.8	1.5
3/3/2019 11:00	0	0.4	0.6	0	0.4	0	0	0	0.2	0	0.7	1.5
3/3/2019 11:30	0.2	0.4	0.5	0	0.4	0	0	0	0.2	0	0.7	1.5
3/3/2019 12:00	0.5	0.4	0.6	0	0.6	0	0	0	0.2	0	0.6	1.4
3/3/2019 12:30	0.6	0.5	0.6	0	0.7	0	0	0	0	0	0.4	1.2
3/3/2019 13:00	0.5	0.4	0.6	0	0.7	0	0	0	0	0	0.5	1.2
3/3/2019 13:30	0.5	0.5	0.7	0	0.7	0	0	0	0	0	0.5	1.3
3/3/2019 14:00	0.4	0.4	0.6	0	0.8	0	0	0	0	0	0.5	1.3
3/3/2019 14:30	0.3	0.3	0.5	0	0.8	0	0	0	0	0	0.4	1.4
3/3/2019 15:00	0.2	0.3	0.7	0	0.7	0	0	0	0	0	0.3	1.3
3/3/2019 15:30	0.2	0.4	0.6	0	0.7	0	0	0	0	0	0.4	1.3
3/3/2019 16:00	0.3	0.5	0.7	0	0.7	0	0	0	0	0	0.4	1.3
3/3/2019 16:30	0.2	0.5	0.7	0	0.7	0	0	0	0	0	0.4	1.3
3/3/2019 17:00	0.2	0.5	0.7	0	0.7	0	0	0	0	0	0.3	1.2
3/3/2019 17:30	0	0.5	0.7	0	0.7	0	0	0	0	0	0.3	1.2
3/3/2019 18:00	0.2	0.5	0.7	0	0.7	0	0	0	0	0	0.3	1.3
3/3/2019 18:30	0	0.7	0.9	0	0.8	0	0	0	0	0	0.3	1.3
3/3/2019 19:00	1.7	3.3	2	0	0	0	0	0	0	0	0	1
3/3/2019 19:30	8.5	7.8	11	1.3	7	1.3	0	0	1.3	0	3.9	3.6
3/3/2019 20:00	4.4	6.5	16.5	1.8	3.8	2.6	1.5	0	0	0	0	0
3/3/2019 20:30	4.7	6.3	16.1	3	3.7	4.9	1.1	0	0	0	0	0
3/3/2019 21:00	6	5.4	16.1	3.4	4	4.8	1.2	0	0	0	0	0
3/3/2019 21:30	6.7	6	16.4	4	3.2	4.9	1.7	0	0	0	0	0
3/3/2019 22:00	6.9	7.5	15.4	4.2	1.2	4.6	1.2	0	0	0	0	0
3/3/2019 22:30	6.7	7.8	15.3	3.8	0	4.8	1.7	0	0	0	0	0
3/3/2019 23:00	6.4	6.7	16	3.6	1.2	4.9	1.2	0	0	0	0	0
3/3/2019 23:30	6.1	4.9	18.8	3.4	2.6	5.5	1.2	0	0	0	0	0
3/4/2019 0:00	6.1	4.4	19.8	2.4	1.6	6	1.6	0	0	0	0	0
3/4/2019 0:30	6.1	4.2	17.6	2.9	1.7	5.5	1.2	0	0	0	0	0
3/4/2019 1:00	6.2	3.6	17.9	2.6	2	4.2	1.2	0	0	0	0	0
3/4/2019 1:30	6.3	4.6	20.6	2.6	2.9	4.2	1.6	0	0	0	0	0
3/4/2019 2:00	6.3	6.9	27.6	1.1	2.9	5.8	1.6	0	0	0	0	0
3/4/2019 2:30	6.2	7.4	28.6	0	2.8	5.9	0	0	0	0	0	0
3/4/2019 3:00	0.1	0.1	0.1	0.1	0.1	0.1	0.1	0.1	0.1	0.1	0.1	0.1
3/4/2019 3:30	0.1	0.1	0.1	0.1	0.1	0.1	0.1	0.1	0.1	0.1	0.1	0.1
3/4/2019 4:00	0.1	0.1	0.1	0.1	0.1	0.1	0.1	0.1	0.1	0.1	0.1	0.1
3/4/2019 4:30	0.1	0.1	0.1	0.1	0.1	0.1	0.1	0.1	0.1	0.1	0.1	0.1
3/4/2019 5:00	0.1	0.1	0.1	0.1	0.1	0.1	0.1	0.1	0.1	0.1	0.1	0.1
3/4/2019 5:30	0.1	0.1	0.1	0.1	0.1	0.1	0.1	0.1	0.1	0.1	0.1	0.1
3/4/2019 6:00	8.5	5.2	10.9	2.9	9.9	2.2	1.3	2.2	2.2	0	5.7	6.2
3/4/2019 6:30	7.9	5	11.3	2	10.2	2	1	1.7	2	1	5.9	6
3/4/2019 7:00	2.1	1.5	3.2	0.5	2.8	0.6	0.3	0.3	0.5	0.3	1.6	2.3
3/4/2019 7:30	0.4	0.8	1.2	0	0.9	0.2	0	0	0	0	0.4	1.8
3/4/2019 8:00	0.5	0.9	1.2	0	0.8	0	0	0	0	0	0.5	2.1
3/4/2019 8:30	4.7	2.1	0	0	0	0	0	0	0	0	0	0
3/4/2019 9:00	5	1.9	0	0	0	0	0	0	0	0	0	0
3/4/2019 9:30	4.6	3	0	0	0	0	0	0	0	0	1.5	0
3/4/2019 10:00	5.5	3.9	0	0	0	0	0	0	0	0	1.7	0
3/4/2019 10:30	2.5	2	0	0	0	0	0	0	0	0	0	0
3/4/2019 11:00	2	2.7	1.2	0	0	0	0	0	0	0	0	0
3/5/2019 10:00	1.4	1.7	0	0	0	0	0	0	0	0	0	0

CURRENT HARMONICS IN PHASE 3												
	rec_STD .Harm. current 3 L3 (%)	rec_STD .Harm. current 5 L3 (%)	rec_STD .Harm. current 7 L3 (%)	rec_STD .Harm. current 9 L3 (%)	rec_STD .Harm. current 11 L3 (%)	rec_STD .Harm. current 13 L3 (%)	rec_STD .Harm. current 15 L3 (%)	rec_STD .Harm. current 17 L3 (%)	rec_STD .Harm. current 19 L3 (%)	rec_STD .Harm. current 21 L3 (%)	rec_STD .Harm. current 23 L3 (%)	rec_STD .Harm. current 25 L3 (%)
2/27/2019 17:30	5.5	7.6	0	2.1	2.9	0	0	0	0	0	0	0
2/27/2019 18:00	5.1	6.5	0	1.8	1.8	0	0	0	0	0	0	0
2/27/2019 18:30	2	1	0.9	0	0.7	0	0.4	0	0	0	0	0
2/27/2019 19:00	0.7	0.9	0.7	0.6	0.6	0.3	0	0	0	0	0	0
2/27/2019 19:30	3.1	0.5	1.2	0.6	0.3	0.5	0	0	0	0	0	0
2/28/2019 16:00	5.7	7.7	3.6	2.5	3.6	0	0	0	0	0	0	0
2/28/2019 16:30	3.9	4.5	2.2	1.6	2.2	0	0	0	0	0	0	0
2/28/2019 17:00	4.9	4.4	2.1	2.1	2.5	0	0	0	0	0	0	0
2/28/2019 17:30	8.9	9.9	5.4	4.4	4.4	0	0	0	0	0	0	0
2/28/2019 18:00	51.6	60.5	40.8	31.6	18.1	0	0	0	0	0	0	0
2/28/2019 18:30	15.3	21.6	11.5	10	8	5.7	0	0	0	0	0	0
2/28/2019 19:00	9	5.9	7.2	1.2	3.8	0.9	0	0	0.4	0	1.3	3.5
2/28/2019 19:30	9.7	7	8.2	1	4.1	1	0	0	0.3	0	1.6	4.1
2/28/2019 20:00	9.6	7.1	8.2	0.9	4.2	1	0	0	0	0	1.6	4.1
2/28/2019 20:30	9.4	7.3	8	0.8	4.2	0.9	0	0	0	0	1.6	4.2
2/28/2019 21:00	9.4	6.5	8	1.1	4.2	0.8	0	0	0.3	0.3	1.2	4
2/28/2019 21:30	9	5.4	6.7	0.9	3.9	0.8	0	0	0.3	0.3	1	3.7
3/1/2019 9:30	4.8	3.5	1.2	1.2	1.7	0	0	0	0	0	0	0
3/1/2019 10:00	5.5	4.8	1.6	1.6	2.7	0	0	0	0	0	0	0
3/1/2019 10:30	7.2	7.6	3.4	3.4	3.4	0	0	0	0	0	0	0
3/1/2019 11:00	49.9	58.6	35.3	24.9	17.6	0	0	0	0	0	0	0
3/1/2019 11:30	53	61.2	39.5	30.6	24.9	17.6	0	0	0	0	0	0
3/1/2019 12:00	51.6	60.5	36.5	25.8	18.1	0	0	0	0	0	0	0
3/1/2019 12:30	49.9	58.6	39.5	30.6	17.6	17.6	0	0	0	0	0	0
3/1/2019 13:00	52.5	61.5	41.5	32.1	18.5	18.5	0	0	0	0	0	0
3/1/2019 14:00	44.1	49.3	34.8	22	15.6	0	0	0	0	0	0	0
3/1/2019 14:30	45.3	51.4	34.2	24.2	17.1	0	0	0	0	0	0	0
3/1/2019 15:00	5.1	5.5	1.9	1.9	2.7	0	0	0	0	0	0	0
3/1/2019 15:30	4.5	4.5	1.6	1.6	2.7	0	0	0	0	0	0	0
3/1/2019 16:00	5	4.6	2	2	2.9	1.4	0	0	0	0	0	0
3/1/2019 16:30	5.7	6.6	2.6	1.9	3.3	0	0	0	0	0	0	0
3/1/2019 17:00	4.7	6.4	1.9	1.9	2.7	0	0	0	0	0	0	0
3/1/2019 17:30	4.6	7.4	1.9	1.9	2.7	0	0	0	0	0	0	0
3/1/2019 18:00	2.5	5.6	1.1	1.6	1.6	0	0	0	0	0	0	0
3/1/2019 18:30	3	2.2	0.5	0.8	1.2	0.5	0.8	0	0	0	0	0
3/1/2019 19:00	2.4	2.2	0.8	0.7	1.2	0.8	0.8	0.5	0	0	0	0
3/1/2019 19:30	2.4	1.7	1	0.8	0.5	0.4	0.4	0	0	0	0	0
3/1/2019 20:00	2.8	1.9	1.2	0.9	0.5	0.3	0.3	0	0	0	0	0
3/1/2019 20:30	2.9	1.7	1	0.9	0.3	0.4	0.2	0	0	0	0	0
3/1/2019 21:00	2.8	1.5	1.3	1	0.5	0.4	0.2	0	0	0	0	0
3/1/2019 21:30	4.2	2.3	2.9	0.4	1.9	0.5	0	0.2	0.3	0	1	2.2
3/1/2019 22:00	7.8	3.9	5.1	0.7	3.5	0.7	0	0	0.4	0	1.2	3.9
3/1/2019 22:30	8.3	4.2	5.3	0.7	3.8	0.8	0.3	0	0.3	0	1.2	4
3/1/2019 23:00	8.3	4.2	5.3	0.6	3.8	0.9	0.3	0	0.3	0	1.1	4
3/1/2019 23:30	7.9	3.9	5	0.8	3.6	0.8	0	0	0.3	0	1.2	3.9
3/2/2019 0:00	7.8	3.8	4.9	0.7	3.6	0.7	0.3	0	0.3	0.3	1.2	3.9
3/2/2019 0:30	7.8	3.9	4.9	0.7	3.6	0.7	0	0	0.3	0	1.2	3.8
3/2/2019 1:00	8	4	5.1	0.7	3.6	0.8	0.3	0	0.3	0	1.1	3.7
3/2/2019 1:30	9	4.9	5.9	0.8	4.2	0.9	0.3	0	0	0	1.1	4.2
3/2/2019 2:00	0.1	0.1	0.1	0.1	0.1	0.1	0.1	0.1	0.1	0.1	0.1	0.1
3/2/2019 2:30	0.1	0.1	0.1	0.1	0.1	0.1	0.1	0.1	0.1	0.1	0.1	0.1
3/2/2019 3:00	0.1	0.1	0.1	0.1	0.1	0.1	0.1	0.1	0.1	0.1	0.1	0.1
3/2/2019 3:30	0.1	0.1	0.1	0.1	0.1	0.1	0.1	0.1	0.1	0.1	0.1	0.1

3/2/2019 4:00	0.1	0.1	0.1	0.1	0.1	0.1	0.1	0.1	0.1	0.1	0.1	0.1
3/2/2019 4:30	0.1	0.1	0.1	0.1	0.1	0.1	0.1	0.1	0.1	0.1	0.1	0.1
3/2/2019 5:00	0.1	0.1	0.1	0.1	0.1	0.1	0.1	0.1	0.1	0.1	0.1	0.1
3/2/2019 5:30	9.5	5.4	6	0.8	4.2	0.8	0	0	0	0	1.5	4.6
3/2/2019 6:00	9.7	4.8	6.2	0.9	4.2	1	0	0.3	0.5	0	1.5	4.6
3/2/2019 6:30	9.7	5.1	6.3	1	4.2	1	0	0	0.3	0	1.2	4.2
3/2/2019 7:00	8.3	4	5.4	0.6	3.6	0.8	0	0.3	0.5	0	1.2	3.9
3/2/2019 7:30	0.2	0.6	1	0	0.9	0	0	0	0	0	0.5	1.9
3/2/2019 8:00	0	0.7	0.9	0.2	0.9	0	0	0	0	0	0.5	1.9
3/2/2019 8:30	1.3	1.8	1.5	0.8	1.1	0.5	0	0	0	0	0	2
3/2/2019 9:00	4.2	3.8	1.8	1.8	2.2	0	0	0	0	0	0	0
3/2/2019 9:30	3.9	3.5	1.1	1.6	2	0	0	0	0	0	0	0
3/2/2019 10:00	4.2	3.6	1.2	1.7	2.4	0	0	0	0	0	0	0
3/2/2019 10:30	3.7	3.7	1.2	1.7	2.5	1.2	0	0	0	0	0	1.2
3/2/2019 11:00	3.1	2.9	1	1.4	2.3	1	0	0	0	0	0	0
3/2/2019 11:30	3.2	5.3	1.2	1.7	2.1	1.2	0	0	0	0	0	0
3/2/2019 13:30	3.2	6.1	0	1.3	1.3	0	0	0	0	0	0	0
3/2/2019 14:00	3.7	6.4	0	1.5	1.5	0	0	0	0	0	0	0
3/2/2019 14:30	3	5.3	0	0	1.1	0	0	0	0	0	0	0
3/2/2019 15:00	3.6	6.1	0	0	1.3	0	0	0	0	0	0	0
3/2/2019 15:30	2.8	5.1	0	1.1	1.1	0	0	0	0	0	0	0
3/2/2019 16:00	2.7	5	0	1.1	1.1	0	0	0	0	0	0	0
3/2/2019 16:30	4.6	8.5	2	2	2	0	0	0	0	0	0	0
3/2/2019 17:00	4.9	9.8	2.2	2.2	2.2	0	0	0	0	0	0	0
3/2/2019 17:30	5.4	10	2.2	2.2	2.2	0	0	0	0	0	0	0
3/2/2019 18:00	1.9	3.8	0	0	1.1	0	0	0	0	0	0	0
3/2/2019 18:30	0.5	1.7	0.3	0	0.6	0	0	0	0	0	0	0
3/2/2019 19:00	0.2	1.3	0.6	0.2	0.5	0	0	0	0	0	0	0
3/2/2019 19:30	3.1	2.5	2.8	0.4	1.6	0.3	0	0	0	0	1	2
3/2/2019 20:00	3.8	2.6	3.4	0.6	1.9	0.5	0	0.2	0.2	0	1.2	2.4
3/2/2019 20:30	7	2.3	4.7	1	1.8	0.8	0	0	0	0	0.8	1.8
3/2/2019 21:00	7.3	1	3.7	1.2	1	0.9	0	0	0	0	0	0
3/2/2019 21:30	9.6	2.9	4.7	1.3	1.3	1.2	0.4	0	0	0	0	0
3/2/2019 22:00	10.5	3.5	6	1.6	1.3	0.4	0	0	0	0	0	0
3/2/2019 22:30	10.7	4.2	6.9	1.5	2.6	0.4	0.4	0	0	0	0.4	1.9
3/2/2019 23:00	10.4	3.9	7.1	1.6	3.1	0.7	0.6	0	0	0	0.6	2.3
3/2/2019 23:30	10.3	3.5	6.8	1.8	2	0.7	0.6	0	0	0	0	0
3/3/2019 0:00	10.6	3.3	4.6	2	1.9	0.4	0.4	0	0	0	0	0
3/3/2019 0:30	10.7	3.4	4.7	2	1.7	0.6	0.6	0	0	0	0	0
3/3/2019 1:00	10.5	3.4	4.6	1.8	1.3	0.7	0.6	0	0	0	0	0
3/3/2019 1:30	10.4	3.5	4.5	1.8	1.5	0	0.7	0	0	0	0	0
3/3/2019 2:00	0.1	0.1	0.1	0.1	0.1	0.1	0.1	0.1	0.1	0.1	0.1	0.1
3/3/2019 2:30	0.1	0.1	0.1	0.1	0.1	0.1	0.1	0.1	0.1	0.1	0.1	0.1
3/3/2019 3:00	0.1	0.1	0.1	0.1	0.1	0.1	0.1	0.1	0.1	0.1	0.1	0.1
3/3/2019 3:30	0.1	0.1	0.1	0.1	0.1	0.1	0.1	0.1	0.1	0.1	0.1	0.1
3/3/2019 4:00	0.1	0.1	0.1	0.1	0.1	0.1	0.1	0.1	0.1	0.1	0.1	0.1
3/3/2019 4:30	0.1	0.1	0.1	0.1	0.1	0.1	0.1	0.1	0.1	0.1	0.1	0.1
3/3/2019 5:00	0.1	0.1	0.1	0.1	0.1	0.1	0.1	0.1	0.1	0.1	0.1	0.1
3/3/2019 5:30	9.3	4.2	5.8	0.9	4.7	0.5	0	0	0	0.5	1.2	4.5
3/3/2019 6:00	9.6	3.9	5.9	0.8	4.7	0.8	0.4	0	0	0.4	1.3	4.5
3/3/2019 6:30	9.5	3.8	5.9	0.4	4.4	0.9	0	0.4	0.4	0	1.5	4.7
3/3/2019 7:00	9.4	4	6.2	0.5	4.5	0.8	0	0	0	0.4	1.2	4.4
3/3/2019 7:30	0.9	0.4	0.9	0	0.7	0	0	0	0.2	0	0.6	1.9
3/3/2019 8:00	0.2	0.3	0.7	0	0.5	0	0	0	0.3	0	0.6	2
3/3/2019 8:30	0.2	0.3	0.7	0	0.6	0	0	0	0.2	0	0.6	1.7

3/3/2019 9:00	0.2	0.4	0.6	0	0.5	0	0	0	0.2	0	0.6	1.5
3/3/2019 9:30	0.3	0.4	0.6	0	0.5	0	0	0	0.2	0	0.7	1.5
3/3/2019 10:00	0.4	0.4	0.6	0	0.5	0	0	0	0.2	0	0.8	1.5
3/3/2019 10:30	0	0.4	0.6	0	0.4	0	0	0	0.2	0	0.8	1.5
3/3/2019 11:00	0	0.4	0.6	0	0.4	0	0	0	0.2	0	0.7	1.5
3/3/2019 11:30	0.2	0.4	0.5	0	0.4	0	0	0	0.2	0	0.7	1.5
3/3/2019 12:00	0.5	0.4	0.6	0	0.6	0	0	0	0.2	0	0.6	1.4
3/3/2019 12:30	0.6	0.5	0.6	0	0.7	0	0	0	0	0	0.4	1.2
3/3/2019 13:00	0.5	0.4	0.6	0	0.7	0	0	0	0	0	0.5	1.2
3/3/2019 13:30	0.5	0.5	0.7	0	0.7	0	0	0	0	0	0.5	1.3
3/3/2019 14:00	0.4	0.4	0.6	0	0.8	0	0	0	0	0	0.5	1.3
3/3/2019 14:30	0.3	0.3	0.5	0	0.8	0	0	0	0	0	0.4	1.4
3/3/2019 15:00	0.2	0.3	0.7	0	0.7	0	0	0	0	0	0.3	1.3
3/3/2019 15:30	0.2	0.4	0.6	0	0.7	0	0	0	0	0	0.4	1.3
3/3/2019 16:00	0.3	0.5	0.7	0	0.7	0	0	0	0	0	0.4	1.3
3/3/2019 16:30	0.2	0.5	0.7	0	0.7	0	0	0	0	0	0.4	1.3
3/3/2019 17:00	0.2	0.5	0.7	0	0.7	0	0	0	0	0	0.3	1.2
3/3/2019 17:30	0	0.5	0.7	0	0.7	0	0	0	0	0	0.3	1.2
3/3/2019 18:00	0.2	0.5	0.7	0	0.7	0	0	0	0	0	0.3	1.3
3/3/2019 18:30	0	0.7	0.9	0	0.8	0	0	0	0	0	0.3	1.3
3/3/2019 19:00	2.1	2.6	2.2	0	0	0	0	0	0	0	0	1.1
3/3/2019 19:30	8.4	6.3	7.9	1.5	3.9	1.1	0.9	0	0	0	0.6	3.5
3/3/2019 20:00	6.5	6.2	6.8	2.9	1.3	1.1	1.1	0.7	0	0	0	0
3/3/2019 20:30	6.1	5.7	6.3	2.7	1	0.6	1.1	0.7	0	0	0	0
3/3/2019 21:00	6.4	5.7	6.1	2.8	1	0.4	1.1	0.7	0	0	0	0
3/3/2019 21:30	7.2	5.5	6.1	2.6	1.4	0.4	0.8	0.7	0	0	0	0
3/3/2019 22:00	7.7	5.9	5.7	2.6	1	0	0.8	0.6	0	0	0	0
3/3/2019 22:30	7.8	5.7	5.9	2.8	0.7	0	0.8	0.6	0	0	0	0
3/3/2019 23:00	7.8	5.6	5.9	2.9	0.4	0	0.8	0.6	0	0	0	0
3/3/2019 23:30	8	5.6	6.2	3.3	0.9	0.6	0.9	0.6	0	0	0	0
3/4/2019 0:00	7.9	5.3	7.3	3.1	1.3	1	1	0.6	0	0	0	0
3/4/2019 0:30	7.8	5.2	8	3.4	0.6	0.9	1	0.7	0	0	0	0
3/4/2019 1:00	7.7	5.2	8.3	3.4	0.9	0.9	1	0.7	0	0	0	0
3/4/2019 1:30	7.8	4.7	8.7	3.2	1.4	0.8	1	0.8	0	0	0	0
3/4/2019 2:00	8.2	3.8	10.4	3.1	2.1	1.2	1.1	0.8	0	0	0	0
3/4/2019 2:30	8.2	3.6	10.6	3	2.4	1.1	1.1	0.7	0	0	0	0
3/4/2019 3:00	0.1	0.1	0.1	0.1	0.1	0.1	0.1	0.1	0.1	0.1	0.1	0.1
3/4/2019 3:30	0.1	0.1	0.1	0.1	0.1	0.1	0.1	0.1	0.1	0.1	0.1	0.1
3/4/2019 4:00	0.1	0.1	0.1	0.1	0.1	0.1	0.1	0.1	0.1	0.1	0.1	0.1
3/4/2019 4:30	0.1	0.1	0.1	0.1	0.1	0.1	0.1	0.1	0.1	0.1	0.1	0.1
3/4/2019 5:00	0.1	0.1	0.1	0.1	0.1	0.1	0.1	0.1	0.1	0.1	0.1	0.1
3/4/2019 5:30	0.1	0.1	0.1	0.1	0.1	0.1	0.1	0.1	0.1	0.1	0.1	0.1
3/4/2019 6:00	8.8	4.7	6.5	1.5	4.8	1.2	0.9	0	0.5	0	0.5	4.1
3/4/2019 6:30	8.7	4.6	6.8	1.8	4.7	1.2	0.9	0	0.5	0.4	0.7	4.1
3/4/2019 7:00	5	2.6	3.9	1	2.7	0.7	0.5	0	0.3	0.3	0.5	2.7
3/4/2019 7:30	0.4	0.8	1.2	0	0.9	0.2	0	0	0	0	0.4	1.8
3/4/2019 8:00	0.5	1	1.3	0.2	0.9	0	0	0	0	0	0.5	2.1
3/4/2019 8:30	7.8	7.1	3	3	3	0	0	0	0	0	0	0
3/4/2019 9:00	5.4	4.5	0	2.1	2.1	0	0	0	0	0	0	0
3/4/2019 9:30	7.2	5.8	1.9	2.7	3.3	0	0	0	0	0	0	0
3/4/2019 10:00	6.8	5.9	1.8	2.6	3.2	0	0	0	0	0	0	0
3/4/2019 10:30	6.5	5.5	1.7	2.4	3	0	0	0	0	0	0	0
3/4/2019 11:00	5.6	4.7	0	2	2	0	0	0	0	0	0	0
3/5/2019 10:00	5.5	3.7	1.2	1.2	1.2	0	0	0	0	0	0	0

Appendix A2 SIMULINK block model

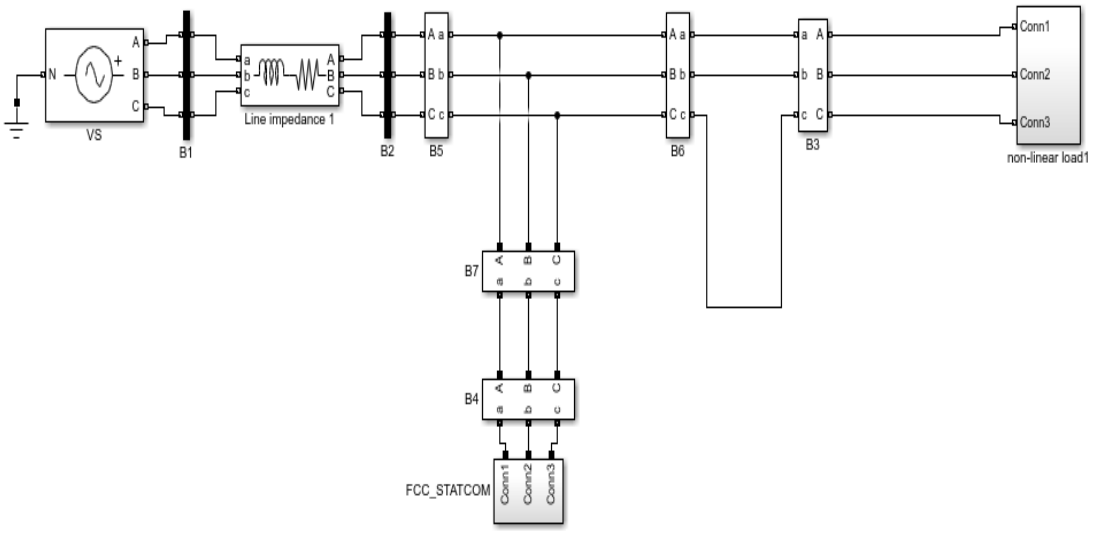

Appendix B1 Steady State performance of LPF, HPF and BSF at $\alpha = 0°$

THD (%)	1st LPF	2nd LPF	1st HPF	2nd HPF	BSF
5th	3.19	0.57	3.19	2.67	0.19
7th	1.09	0.18	1.09	0.89	0.02
11th	0.27	0.03	0.26	0.22	0.06
13th	0.14	0.01	0.13	0.10	0.02
17th	0.07	0.01	0.08	0.16	0.01

Appendix B2 Steady – State Performance of LPF, HPF and BSF at $\alpha = 30^0$

Harmonics	1st LPF (%)	2nd LPF (%)	1st HPF (%)	2nd HPF (%)	BSF (%)
5th	3.19	0.56	3.20	4.65	0.22
7th	1.09	0.19	1.09	1.62	0.04
11th	0.28	0.03	0.28	0.39	0.05
13th	0.13	0.01	0.13	0.19	0.03
17th	0.07	0.01	0.07	0.10	0.00

Appendix B3 Steady – State Performance of LPF, HPF and BSF at $\alpha = 60^0$

Harmonics	1st LPF (%)	2nd LPF (%)	1st HPF (%)	2nd HPF (%)	BSF (%)
5th	6.25	1.07	6.25	9.12	0.50
7th	1.94	0.13	1.97	2.88	0.30
11th	0.97	0.09	0.97	1.40	0.13
13th	0.32	0.03	0.31	0.44	0.02
17th	0.032	0.01	0.32	0.46	0.03

Appendix B4 THD Error Analysis between Extraction Unit and PCC Current after Compensation

Firing angle (α)	1st LPF (%)	2nd LPF (%)	1st HPF (%)	2nd HPF (%)	BSF (%)
0^0	0.51	0.64	0.63	1.02	0.38
30^0	0.30	0.67	0.32	1.00	0.68
60^0	2.95	0.68	2.97	3.03	1.06